AD NUMBER

AD902042

NEW LIMITATION CHANGE

TO

Approved for public release, distribution unlimited

FROM

Distribution authorized to U.S. Gov't. agencies only; Test and Evaluation; Aug 1972. Other requests shall be referred to U.S. Army Frankford Arsenal ATTN: SMUFA-L3300, Tacony and Bridge Streets, Philadelphia, PA, 19137.

AUTHORITY

FA ltr, 14 Nov 1974

Third Annual Technical Progress Report

"Environmental Sensitivity of Structural Metals : Liquid Metal Embrittlement"

Illinois Institute of Technology, Chicago, Illinois

Period Covered

June 1, 1971 - May 31, 1972

Submitted by:

Paul Gordon, Department of Metallurgical and Materials Engineering, Program Manager

Norman N. Breyer
James W. Dally
Darryl L. Albright
Lawrence J. Broutman
William R. Warke
Earl Zwicker
Russell D. Larsen

Contract Number:
DAAA-25-69-C0608

Submitted June 1972 to:

U. S. Army
Frankford Arsenal
Tacony and Bridge Streets
Philadelphia, Pennsylvania 19137

Attn: SMUFA-L3300

THIRD ANNUAL TECHNICAL PROGRESS REPORT

PROJECT THEMIS

"ENVIRONMENTAL SENSITIVITY OF STRUCTURAL METALS: LIQUID METAL EMBRITTLEMENT"

Period Covered

June 1, 1971 - May 31, 1972

Submitted by:

Paul Gordon, Department of Metallurgical and Materials Engineering, Program Manager

Norman N. Breyer

James W. Dally

Darryl L. Albright

Lawrence J. Broutman

William R. Warke

Earl Zwicker

Russell D. Larsen

Contract Number:

DAAA-25-69-C0608

Submitted June 1972 to:

U. S. Army
Frankford Arsenal
Tacony and Bridge Streets
Philadelphia, Pennsylvania 19137

CONTENTS

Abstract and Summary of Accomplishments to Date

The phenomenon of liquid metal embrittlement is being investigated on levels from the atomic through bulk specimen and structural properties, and is being considered from both experimental and theoretical viewpoints. The research is aimed at elucidating the three important aspects of LME, namely, the mechanism by which embrittlement takes place at a crack, or potential crack, site, the mechanism by which the embrittling species is transported to this site, and various metallurgical, physical, and mechanical factors which have a significant influence on the severity of the embrittlement.

This THEMIS program got underway in July of 1969; the major accomplishments to date are summarized below:

The Specificity of Embrittling Systems in LME

The literature of LME customarily describes the phenomenon as specific, i.e., that only certain environments embrittle certain metals. A critical literature survey carried out here has shown that invariably the claims for non-embrittlement of specific couples are based either on insufficient evidence, unpublished research, or tests at a single temperature. Since LME is found characteristically to show an embrittlement "trough" between a ductile-to-brittle and brittle-to-ductile transition temperature, a single test temperature could well lie in the trough region. Thus, we tentatively propose that LME may well be quite general, and we are now carrying out extensive tests on reportedly non-embrittling systems as a check on this proposal. We are also examining the same problem from a theoretical point of view.

Embrittlement by Solid Metals

Contrary to the standard description that liquid metal embrittlement is observed over a temperature range extending from the melting point of the embrittling species

up to a brittle-to-ductile transition temperature, work by Mostovoy and Breyer showed that the lead embrittlement of high strength steels occurred as much as 200°F below the melting point of lead. Additional research carried out in the present program has demonstrated that Zn, Cd, Sn, and In, as well as Pb, each embrittles quenched and tempered 4140 steel well below the melting points of the embrittler. In each case, embrittlement, as indicated by a loss in reduction of area and in true fracture stress, was observed down to a homologous temperature (ratio of absolute temperature to melting temperature) of about 0.75. With respect to the possibility as proposed by Mostovoy and Breyer, that this embrittlement depends upon vapor transport of the embrittler to the propagating crack tip, it has been observed that the severities of embrittlement by these solid embrittlers do not correlate with the wide variation in vapor pressures of the embrittlers in the temperature range.

Some preliminary work on embrittlement of copper by mercury has shown that Hg will embrittle the copper at temperatures as low as -80°C, about 40°C below the melting point of mercury.

The Vapor Embrittlement of Metals

To test the Mostovoy-Breyer proposal of vapor transport as the general transport mechanism in LME, high strength E-4130 steel strips were stressed by bending at appropriate temperatures in a vacuum chamber with their tensile surfaces exposed to vapors from a molten lead -2% antimony alloy. The selected specimen temperatures were somewhat above the melting point of lead and well below that of antimony. The following significant observations were made: (a) the lead deposited on the steel crack surfaces was present as tiny droplets, despite attempts to produce good wetting; (b) nevertheless, embrittlement, and failure, of the samples took place; (c) the lead droplets were observed not to be present immediately adjacent to the crack tip, but instead hexagonally shaped crystal whiskers were found here - presumably crystals of

antimony which is both solid at the specimen temperature, and of hexagonal - rhombohedral - symmetry (lead in f.c.c.). These observations are interpreted as strong evidence that the embrittlement in this case was produced largely by the antimony and that it was transported in the vapor state. (It seems possible, but less likely on various grounds, that the antimony was transported by solid state diffusion).

The Effect of Structural Metal Purity on LME

In this research, LME studies are being carried out on specially prepared high purity steels containing controlled trace additions of elements known to segregate to prior austenite grain boundaries. The steels have been heat treated in ways known either to promote, on the one hand, or minimize on the other, this grain boundary segregation. The susceptibility of the steel to LME by high purity lead is then compared for these two conditions. Since LME fractures in the lead-steel couple are known to be intergranular, an effect was expected and indeed, in the cases of Sb and Sn as dopants in the steel, has been observed. The steels were more brittle in lead when the Sb and Sn were segregated than when they were not. However, in the cases of the P or As bearing steel, no difference in embrittlement was seen between the segregated and unsegregated states. These results indicate that a temper brittle steel (segregated) may be more sensitive to the effects of an aggressive environment than a non-temper brittle one, depending on the natures of the segregate and the environment, and suggest the existence of common underlying principles in the two types of embrittlement.

To test whether these conclusions are of more general applicability than in steel systems, additional work on copper-based and nickel-based systems have been undertaken. So far, results on copper plus .01% Bi embrittled by mercury has revealed a similar effect of segregation, ie, segregation of the bismuth in the copper enhances the embrittlement by mercury.

The Effect of Purity of the Embrittling Metal

The effect of Sb or Sn additions to the embrittling lead on the embrittlement of 4145 steel surface-wetted with the lead alloys has been studied in detail. The following relationship was found between the Sb or Sn addition and the ductile-to-brittle recovery temperature, T_R

$$\frac{1}{T_R} = A \log (\% \text{ Sn or } \% \text{ Sb}) + B$$

where A and B are constants specific to the additive. Assuming this results from some thermally activated process, the apparent activation energy for thePb-Sn embrittler was found to be 47 kcal/mol, a value intermediate between the heats of vaporization of Pb (42.5 kcal/mol) and Sn (55 kcal/mol). That for the Pb-Sb embrittler was 38 kcal/mol, somewhat below the vaporization energy for both Sb (46.7) and Pb. The possible significance of these values is under consideration.

It is interesting to note that the relative effects of the Sb or Sn on the severity of the embrittlement by the lead are of the same order of magnitude here where the addition is made to the liquid embrittler as it is when the Sb or Sn is added to the solid steel and segregated to the grain boundaries (see above). Again, the possible significance of this observation to mechanism is under consideration.

Effect of Cold Work on Lead Embrittlement of Alloy Steels

Prior cold deformation of internally leaded 4145 steel by die drawing various percentages (10%, 20%, 30%, 50% R.A.) to a common final strength level of 200 ksi has resulted in a decrease in subsequent LME susceptibility. This work has revealed that the embrittlement susceptibility may be essentially eliminated by the 50% R.A. deformation. In order to determine if the decrease in the severity of embrittlement by prior cold work is an effect unique to an internally leaded steel, e.g., because the Pb inclusions may act as incipient cracks, bars from the non-leaded ingot of the same 4145 heat were processed with the same deformation-heat treatment

schedule that had been used for the leaded bar stock. In this case, the lead was supplied externally by soldering a Pb-4.0 w/o Sn alloy to the surface of the specimen. As had been found in the internally lead steel specimens, the severity of embrittlement for the externally wetted steel specimens decreased as the amount of cold work increased and was drastically reduced for 50% deformation. We have concluded from these data that the effect of cold work on lead embrittlement is not controlled by the location of the lead, but rather by an intrinsic effect of deformation as it influences the fracture path in the steel matrix.

Macrographic and electron fractographic examination of fracture surfaces has revealed considerable evidence that the effect of cold work manifests itself through:

(a) changing the fracture path; in undeformed samples, it is along prior austenite grain boundaries, whereas as the deformation is increased the path tends to follow more and more along Fe-Fe_3C boundaries, and;

(b) changing the fracture mode from intergranular in the undeformed samples to more and more transgranular as the deformation is increased; at 50% deformation the mode is entirely transgranular.

The Effect of Combined Stresses on Liquid Metal Embrittlement

Using the time to failure in delayed failure tests on two embrittlement couples, Be-Cu in Hg and 2024 Al in Hg-Ga alloy, the effect of stress state on LME was investigated. The solid alloy in each case was in the precipitation hardened condition. Three different stress states were employed - tension, torsion, and biaxial tension.

For the Be-Cu in (Hg) couple it was found that the severity of embrittlement followed a maximum tensile stress criterion, with failure times for tension and torsion being identical for the same applied or resolved tensile stress. The severity of embrittlement of 2024 Al in (Hg-Ga), however, did not follow a maximum tensile

stress, maximum shear stress, or maximum energy criterion. These experiments suggest, therefore, that even for materials possessing similar strengthening mechanisms, LME may not be simply attributable to a single embrittlement mechanism.

Crystallographic Aspects of Liquid Metal Embrittlement

The effect of relative crystal orientation on the fracture behavior of Hg-Ga embrittled aluminum bicrystals is being studied. Two sets of bicrystals of 99.99+% pure aluminum were grown with a controlled variation in the crystallographic planes parallel to the grain boundary. One set had a common growth direction of [110] for both crystals, while the other set had different growth directions [110] and [100] for the two crystals. The fracture load was then determined for each bicrystal boundary, using double cantilever beam samples. Although a fracture load variation with crystallographic orientation was clearly observed, sufficient plastic deformation accompanied the fracture to prevent an accurate determination of this trend and of fracture surface energies. Additional bicrystals are currently being prepared to provide samples for a refined fracture test procedure known to reduce plastic deformation to inconsequential levels.

Dynamic Aspects of Liquid Metal Embrittlement

Dynamic aspects of LME were studied by making high speed photographic recordings of liquid mercury-induced failure of polycrystalline 2024-T3 aluminum sheet specimens. The failure phenomenon consisted of 3 distinct phases: a) an initiation period -- the time interval between application of the liquid mercury to the specimen edge and the first indication of a crack, b) a period of discontinuous LME crack growth, and c) a period of high velocity shear rupture which was essentially independent of the embrittling agent.

Both the initiation time and the rate of discontinuous LME crack growth were found to be exponential functions of the magnitude of the tensile stress applied to the aluminum specimen.

It was observed that a propagating LME crack, when deprived of its mercury supply, will become arrested until the crack is resupplied with mercury whereupon crack propagation will resume. This indicates the crack propagation rate is limited by the rate of supply of mercury to the crack front region.

The strong dependence of LME crack propagation rate upon the magnitude of applied tensile stress, indicates that the controlling mechanism of mercury supply to the crack front is on the atomic level and is not bulk fluid flow since the latter cannot be significantly affected by a tensile stress on the fluid's conduit. Further study of the experimental data is currently underway to determine which of several possible atomic transport mechanisms is the most likely one controlling the LME-induced crack propagation rate.

Surface Energy Studies

The purpose of this work is to determine the force-distance curve when atomically clean and smooth surfaces are brought together, and so obtain a direct measurement of true surface energy. The effects of environment may then also be studied, to observe effects on surface energy.

In order to maintain and produce atomically clean surfaces, it is necessary to conduct the experiments in an ultra-high vacuum system (UHV). Such a system is now functional in the laboratory. In addition, an electronic microbalance capable of operation in UHV is required to measure the attractive force between surface, and such a balance is now operational. Mounted on a vibration isolation table, it has measured mass differences of a few micrograms. Work has progressed to the point of attempting measurement of attractive forces between surfaces separated by a few thousand Angstroms in air. This has not yet been successful because of residual vibration and surface preparation problems.

Statistical Mechanics of Fracture and Embrittlement

The purpose of this work was to develop the statistical mechanics associated with the concept that fracture, embrittlement, and related materials phenomena can be treated as many-body, cooperative events, i.e., geometric catastrophies arising from unstable lattice configurations with the concomitant propagation of such instabilities through a lattice.

To date we have developed a classical geometric model for fracture and embrittlement and have submitted to THEMIS five special technical reports outlining the model itself, the statistical mechanical approach applied, and numerous consequences of the model and its variants. These encompassed two of the major goals of the program. First, we are now able to carry out the difficult and tedious cell-cluster analysis of the imperfect anharmonic solid (we are working within what we now call the "anharmonic approximation" in contrast to the conventional harmonic approximation of lattice dynamics) by computer assistance using a polytope-bound analytic integration algorithm. Second, we have modelled a two-dimensional lattice containing a grain boundary of the coincidence-site variety and have carried out a cell-cluster analysis of this system. We are thus able to provide a measure of the stability of a lattice containing a grain boundary in relation to a perfect lattice without such a defect.

This overall concept visualizes the phenomenon of liquid-metal embrittlement as a local lattice destabilization along a grain boundary; with our anharmonic lattices, embrittlement manifests itself as a local Kirkwood melting. A liquid metal provides the crucial additional lattice destabilization which allows for catastrophic failure when the lattice is subjected to stress. If this is in fact the case, such embrittlement effects are predicted to be non-specific, i.e., to exist generally in liquid metal-solid metal couples and other materials containing grain boundaries or their equivalent.

Consequently, we plan to develop independently a general phenomenological description of materials failure phenomena in terms of the relative lattice destabilization effects which are cause by (a) defects, (b) lattice configuration, (c) modes of deformation, and (d) interatomic forces. We believe that our work with the imperfect anharmonic solid has provided us with considerable insight into the structure of such a phenomenology.

Papers Presented or Published

"Effect of Test Variables on the Lead-Embrittlement of Steels" and "The Effect of Composition on the Lead-Embrittlement of Steel," presented by W. R. Warke at the TMS Fall Meeting and ASM Materials Engineering Congress in Philadelphia, October, 1969.

W. R. Warke, K. L. Johnson and N. N. Breyer, "Liquid Metal Embrittlement of Steel by Lead and Lead Alloys," Corrosion by Liquid Metals, 1970, p. 417.

"Effect of Cold Work on Lead Embrittlement of 4145 Steel" and "Liquid Metal Embrittlement of Steel Externally Applied Lead and Lead Alloys," presented by N. N. Breyer at the TMS Spring Meeting in Atlanta, May 1970.

"The Role of Crystal Orientation in the Energy of Embrittled Grain Boundaries," presented by D. L. Albright at the TMS Fall Meeting and ASM Materials Engineering Congress in Cleveland, October 1970.

W. R. Warke and N. N. Breyer, "Effect of Steel Composition on Lead Embrittlement," JISI, 209 (1971), 779.

"Liquid Metal Embrittlement," presented by P. Gordon to the Department of Mechanical Engineering at the University of Houston, November 1971.

C. G. Miller and R. D. Larsen, "Relative Stabilities of a Family of Plastically-Deformed Lattice Close Packings of Rigid," J. Comput. Phys., 7, (1971) 465.

C. G. Miller and R. D. Larsen, "The Salsburg Polytope Bound Algorithm: Application to the Imperfect Anharmonic Solid," Proc. Conf. on Computers in Chemical Education and Research (DeKalb, Aug. 1971), pp. 5-35.

C. G. Miller and R. D. Larsen, "Local Stability of Imperfect Rigid Disk Lattice Systems: Cell-Cluster Analysis of Coincidence-Site Grain Boundary Models," submitted to Phys. Rev.

C. G. Miller and R. D. Larsen, "Lattice Destabilization in Imperfect Crystals," IUPAP Conference on Statistical Mechanics," University of Chicago, (March 1971).

R. D. Larsen, "Statistical Mechanics of the Imperfect Anharmonic Solid," AUA-ANL Materials Science Conference: Defects in Solids, Argonne National Laboratory (May 1971).

First Quarterly Technical Progress Report on "Environmental Sensitivity of Structural Metals: Liquid Metal Embrittlement" covering period June 25, 1969 to September 30, 1969.

Second Quarterly Technical Progress Report on "Environmental Sensitivity of Structural Metals: Liquid Metal Embrittlement," covering period October 1, 1969 to December 31, 1969.

First Annual Technical Progress Report on "Environmental Sensitivity of Structural Metals: Liquid Metal Embrittlement," covering period June 25, 1969 to June 24,1970.

First Semi-Annual Technical Progress Report on "Environmental Sensitivity of Structural Metals: Liquid Metal Embrittlement," covering period June 25, 1970 to December 31, 1970.

Second Annual Technical Progress Report on "Environmental Sensitivity of Structural Metals: Liquid Metal Embrittlement," covering period June 25, 1970 to May 31,1971.

Second Semi-Annual Technical Progress Report on "Environmental Sensitivity of Structural Metals: Liquid Metal Embrittlement," covering period June 1, 1971 to November 30, 1971.

C. G. Miller and R. D. Larsen, "Exact Cell and Correlated-Cell Model Molecular Pair Distribution Functions," THEMIS STR No. 1.

C. G. Miller and R. D. Larsen, "Statistical Mechanics of Fracture and Embrittlement. 1. A Hard-Core Lattice Model," THEMIS STR No. 2.

C. G. Miller and R. D. Larsen, "Relative Stabilities of a Family of Plastically-Deformed Lattice Close Packings of Rigid Disks," THEMIS STR No. 3.

C. G. Miller and R. D. Larsen, "The Salsburg Polytope Bound Algorithm: Application to the Imperfect Anharmonic Solid," THEMIS STR No. 4.

C. G. Miller and R. D. Larsen, "Local Stability of Imperfect Rigid Disk Lattice Systems: Cell-Cluster Analysis of Coincidence-Site Grain Boundary Models," THEMIS STR No. 5.

1. Embrittlement by Solid Metals

Chief Investigator: W. R. Warke
Associate Investigator: P. Gordon
Graduate Student: J. C. Lynn

Purpose: To investigate "liquid" metal embrittlement below the melting point of the embrittler.

Progress: Part A: Dynamic Tensile Tests

A special technical report based on the previously reported results obtained from dynamic tensile tests of AISI 4140 steel has been prepared and will be available in the near future.

As pointed out in the last annual report, the non-uniformity of deformation around the circumference in the necked region is presumably a cause of error in measuring the reduction of area and the true fracture strength. This problem was avoided by applying the embrittler completely around the gage section of the tensile specimen (AISI 4140 steel) rather than at a single spot on one side as had been done previously. Five specimens prepared by this ring soldering technique and embrittled by Zn, Pb, Cd, Sn, and In, respectively, were tested at 0.95 of their respective melting points in degrees absolute, H.T. = 0.95. The data points are shown in Fig. 1; the solid curves are those shown in Fig. 5 in the last annual report. The specimens surface wetted with lead and cadmium circumferentially showed a higher degree of necking while the true fracture stress remained about the same when compared to the ones obtained by spot soldering and indicated by the solid curves. The degree of severity of embrittlement with respect to homologous temperature remained basically the same. The fracture appearances indicated that one or several unstable primary microcracks initiated around the specimen under the soldered region, and propagated toward the center of the bar until the final fast (catastrophic)

fracture took place. Secondary stable microcracks parallel to the primary fracture surface were observed in most of the soldered regions. Fig. 2 shows the fracture of the specimen ring soldered with cadmium: stable secondary microcracks as well as the unstable primary crack are visible in (a) and (b). A ring of brittle fracture (consisted of several unstable primary microcracks) on the fracture surface, Fig. 2(c), emanated from the soldered region and propagated concentrically toward the center of the bar until the final fast shear (catastrophic) fracture took place.

A zinc electroplating solution having the composition shown in Table 1[1] was prepared following standard procedures.

Table 1. Composition of Zinc Electroplating Solution

Component	oz/gal	gm/l
Total NaCN	12.3	92
Zinc as Metal	4.5	34
Caustic Soda (NaOH)	10.5	79
Current Density (C.D.)	10-70 amp/ft^2	1-8 amp/dm^2

The solution was then purified by plating out zinc at a current density of 1 amp/ft^2, for 24 hours by using pure zinc (99.999% Zn) for both cathode and anode. A tensile specimen coated with waterproof Duco Cement (made by Du Pont) except for a 1/4 inch wide band at the minimum gage diameter region, was then degreased, cleaned in 20% HCl acid solution, and electroplated. After plating at 50 amp/ft^2 C.D. for 4 hours, a 5.4 mil thick zinc layer was deposited on the tensile specimen, C-18. Another specimen, C-19, was plated for 45 minutes at 50 amp/ft^2 C.D. to produce a thinner coating (0.5 mil). The specimens were then heated in a furnace at 390°F for 24 hours in order to bake out any hydrogen which might have been introduced during plating. Hydrogen embrittlement which might confuse the LME

results is thus eliminated[2], although hydrogen embrittlement is generally not observable at temperature higher than 150°C.[3] Two other specimens (C-20 and C-21) of 1 mil and 2.3 mil thick zinc coating obtained after 30 minutes and 200 minutes, respectively, at 25 amp/ft^2 C.D., were not baked prior to testing. Elevated temperature tensile properties of these specimens are listed in Table 2. The baked specimens (C-18 and C-19) showed a lesser degree of embrittlement than the specimen (C-21) without baking. Also the zinc embrittlement of steel obtained by electroplating was found to be milder than that obtained by soldering.

A cadmium electroplating solution having the composition shown in Table 3[1] was also prepared. The solution was again purified by plating out cadmium at 1 amp/ft^2 C.D. for 24 hours by using pure cadmium (99.9999% Cd) for both cathode and anode. A specimen was then degreased, cleaned, and kept in a sodium cyanide solution prior to electroplating. Difficulty was encountered in obtaining good adhesion of the electroplated cadmium and consistent results in the subsequent tensile test results. This variability was attributed to problems in cleaning the steel and keeping it clean prior to plating. A variety of cleaning processes have been employed in this study. Among them were anodic cleaning in H_2SO_4 (50% by vol.), 65% H_3PO_4 (by vol.) + 35% H_2SO_4 + 10 ml chromic acid, and 15% sodium cyanide (by wt.), as well as simple cleaning in HCl acid solution (ranging from 20% to 50% by wt.). Various current densities (10 - 50 amp/ft^2) and plating times, giving a range of thicknesses of the deposit (0.5 ~ 4 mil), have also been tried. A very adhesive deposit was obtained by applying a cadmium strike from a solution having a low cadmium content. This thin coating applied prior to deposition in the regular solution assists in breaking down any film that might still be present on the surface. The clean steel surface is then sealed from being contaminated between cleaning and plating.

Table 2. Elevated Temperature Tensile Properties of Specimens Coated with Zinc by Various Methods

Sample No.	Coating Method	Coating Thickness	Baking Process	Test Temperature, °F	Homologous Temperature, T/T_m	RA, % (Normalized RA)	$\bar{\sigma}_f$, ksi (Normalized $\bar{\sigma}_f$)
C-15	Spot Soldered	N.A.*	N.A.	742-757	0.964	27.7 (0.38)	151 (0.55)
C-17	Ring Soldered	N.A.	N.A.	725-730	0.95	50 (0.685)	160 (0.57)
C-18	Electroplated	5.4 mil (@ 50 asf** C.D) for 4 hours	Yes	731-747	0.958	71.5 (0.98)	251 (0.9)
C-19	Electroplated	0.5 mil (@ 50 asf C.D.) for 45 min.	Yes	725	0.95	68.6 (0.94)	243 (0.865)
C-20	Electroplated	1 mil (@ 25 asf C.D.) for 90 min.	No	777	0.99	59.2 (0.8)	169 (0.635)
C-21	Electroplated	2.3 mil (@ 25 asf C.D.) for 200 min.	No	730	0.958	66.7 (0.914)	221 (0.792)

* Not Applicable

** amp/ft^2

Table 3. Composition of Cadmium Electroplating Solution

Component	oz/gal	gm/l
Cd O	4	30
Na CN	16	120
Cadmium as Metal	3.5	26
Free Cyanide	9	67.5
Current Density	15 - 45 amp/ft^2	1.7 - 5 amp/dm^2

Eight specimens were electroplated* in the laboratory. Four of these bars were heated to 650°F for 3 minutes in order to melt the cadmium deposit. Another eight specimens were plated (0.1 mil) commercially; four were retained in the as-plated condition and four were heated to 650°F prior to testing. One specimen from each group was then tested at each of four sub-melting point temperatures and the tensile properties are shown in Fig. 3. In spite of the relatively large degree of scatter, it seems evident that the soldered cadmium degraded the tensile properties more than the electroplated cadmium. The results are also presented in the form of a bar chart in Fig. 4 for comparison of various coating methods at the same test temperature. Furthermore, the embrittlement, or the degradation of the properties, caused by cadmium is shown in Fig. 5, where normalized true fracture strength and normalized

---

* 1. Anodic cleaned in H_2SO_4, 50% by vol, at 100 asf C.D. for 1 min. and water rinsed.

2. Anodic cleaned in 15% sodium cyanide at 25 asf C.D. for 1 min.

3. Cadmium strike at 10 asf C.D. for 1 min.; strike solution contained 12 oz/gal of Na CN and 1 oz/gal of Cd O

4. Plated at 15 asf C. D. for 20 min. to get about 0.5 mil thick deposit.

reduction of area are used. A normalized value of unity means no embrittlement. It is appropriate to mention that there were twenty seven other specimens, electroplated under various conditions as mentioned earlier. When tensile tested in this temperature range, inconsistent results were obtained and the reproducibility was very poor. Nonetheless, the properties obtained by spot soldering seem to serve as lower bound; any electroplated specimen was found to be more ductile.

As far as the fracture appearance was concerned, secondary microcracks were observed in all the specimens coated with cadmium regardless of the coating method. There were differences in the size of the microcracks; the higher the reduction of area (or the higher the true fracture strength), the finer and shallower the stable secondary microcracks were. A typical fracture of a sample coated with electroplated cadmium is shown in Fig. 6. Regardless of the fact that many secondary microcracks were formed within the plated region, the specimen exhibited a large amount of plastic deformation (necking) prior to fracturing. Several secondary microcracks were observed even in a region, Fig. 6(d), where the steel surface was not completely covered while plating and consequently a very thin cadmium film had deposited. The reason why none of these easily-initiated microcracks propagated to a large enough size to dominate the fracture before a large amount of plastic deformation (necking) occurred under the presumably "suitable" condition, is not understood.

In spite of the good reproducibility reported in the literature[4], the difficulty of using electroplated embrittler was also encountered by other researchers. Fuger and Spurr used a clamp to press electroplated cadmium onto titanium[5] and steel[6] specimens in order to observe solid cadmium embrittlement. In view of the difficulties and inconsistencies experienced with electroplated cadmium and zinc, it was decided, to use the soldering technique to apply the embrittler throughout the duration of this program. This decision applies primarily to the notch specimens to be used in the static fatigue (delayed failure) testing.

Part B: Static Fatigue Tests

Some preliminary results have been obtained on the delayed failure of notched specimens of AISI 4140 steel under static fatigue conditions. The geometry of the notch tensile specimens being employed was shown in Fig. 17 of the last annual report. The notched specimens were heat treated prior to grinding the notches using the same austenitizing, quenching and tempering conditions as had been used for the smooth tensile specimens. This heat treatment, which had given a nominal tensile strength of 200 ksi at room temperature, gave notch tensile strength of 293 ksi at room temperature and 281 ksi at 610°F. Two specimens were tested in air under static loading at 630°F: one failed in 31 hours at 240 ksi and the other did not fail after 336.4 hours at 200 ksi.

In order to apply the embrittlers to the notch roots, a fine wire of each metal was produced from the high purity metals used previously. A piece of this wire, together with a little soldering salt, was wound around the notch root and the sample was heated about 60°F over the respective melting point. Subsequent examination of broken samples indicated that this technique gave good wetting and symmetrical crack growth.

The wetted notched bars were mounted in the stress rupture machines and heated to the preselected test temperature. After heating to the test temperature, the tensile bar was loaded with a dead weight, the applied stress having been calculated based on the minor diameter at the notch root. The time to failure was recorded. Delayed failures of steel inthe presence of cadmium (M.P. = 610°F) was observed from 570°F, down to 370°F. The data available at the time this report was prepared are shown in Fig. 7. The applied stress ranged from 200 ksi to 80 ksi, while the delayed failure time ranged from minutes to 10 days. The lower the temperature or the lower the applied stress, the longer the time required for the specimen to break. The data collected to date seem to indicate the static fatigue limit of about 86 ksi for the steel-cadmium couple at 570°F. In addition to cadmium, steel embrittled by zinc and indium were also observed and the results are tabulated in Table 4.

Table 4. Delayed Failures of 4140 Steel by Various Embrittlers as Indicated

Embrittler	Specimen No.	Test Temperature, °F	Applied Stress, ksi	Time to Failure, min.	Remarks
Zn (m.p. 787°F)	NC - 5	740	200	294	
	NC - 1	740	120	4,000	
	NC - 3	740	120	4,476	
	NC - 4	740	80	3,996	
	NC - 2	670	120	13,848	
In (m.p. 313°F)	NE - 1	290	200	30	
	NE - 2	290	160	47	
	NE - 3	290	120	132	
Pb (m.p. 620°F)	NA - 7	600	240	N.F.* after 2,592	
	NA - 1	600	120	N.F. after 24,042	
Sn (m.p. 449°F)	ND - 1	440	240	N.F. after 7,194	See Fig. 9

* No Failure

A typical steel specimen which had experienced delayed failure in the presence of cadmium is shown in Fig. 8. Slow brittle fracture emanated from the notch root and propagated toward the center of the bar until fast shear (catastrophic) fracture took place. The slow cracked region can be differentiated from the fast fracture region by differences in color and roughness of the fracture. It is also apparent that more than one crack were initiated from the notch root at the same place. Furthermore, the cracks that led to the final fracture were in many cases ones that were inclined to the transverse direction. This is different from what was observed in smooth tensile samples where both primary and secondary microcracks were approximately perpendicular to the loading direction.

Also listed in Table 4 are several specimens which had been wetted with tin and lead and which did not fail. One of them (ND-1) was sectioned longitudinally after having been statically loaded at 240 ksi for 7,194 min. (119.9 hours) at 440°F (9 degree below the melting point of tin). A photomicrograph at the notch root is shown in Fig. 9(a). Four cracks were initiated in different directions from the root of the notch. This agrees with the observation on the fracture surface of the cadmium wetted bars that more than one crack had emanated from the notch root at the same place. It will be noted that intimate contact between the embrittler (tin) and the steel substrate had been obtained by soldering, as shown in Fig. 9(b), a higher magnification photomicrograph of Area A in Fig. 9(a).

Future Plan: Stress rupture tests will be continued for the five embrittlers zinc, lead, cadmium, tin and indium. Quantitative studies of the embrittlement will be possible once delayed failure times are obtained as a function of stress and temperature. Hopefully, activation energies will be obtained and will fall into a pattern consistent with one of the embrittlement theories. Fractographic and metallographic studies will be continued in conjunction with the stress rupture testing.

2. Combined Influences of Strain Rate and Temperature on LME

Chief Investigator: J. W. Dally
Associate Investigator: N. N. Breyer
Graduate Student: K. Johnson

This investigation has been terminated as a result of Dr. Dally accepting a position at the University of Maryland.

3. The Effect of Structural Metal Purity on LME

Chief Investigator: W. R. Warke
Associate Investigators: P. Gordon and N. N. Breyer
Graduate Student: S. Dinda

Purpose: To study the effect of the segregation of trace impurities to grain boundaries in LME.

Progress: The behavior of "pure" steel and antimony-doped steel in a liquid metal environment and the attendant changes on mechanical properties were reported in the Second Annual Progress Report. The elevated temperature tensile tests of tin, phosphorous or arsenic doped (500 ppm) alloy specimens (AISI 3340) have since been carried out under four different conditions. The conditions were: unsegregated with no liquid metal, unsegregated with liquid metal environment, segregated with no liquid metal and segregated with liquid metal environment. The liquid metal employed in this experiment was pure lead. The unsegregated condition was produced by water quenching after tempering while the segregated condition was obtained through the extended step-cooling treatment described in earlier reports.

Tensile Properties of Tin-Doped Steel:

Elevated temperature tensile properties of tin-doped steel for the four different conditions referred to above are shown in Figs. 10 through 13. It may be seen in

Figs. 10 and 12 that in the absence of the liquid metal the properties of segregated specimens were almost the same as those of unsegregated specimens. On the other hand, the severity of the liquid metal embrittlement at 650°F was much higher for segregated specimens (14 percent reduction of area) than for unsegregated ones (32 percent reduction of area) when both were wetted with lead. There was also a difference of about 100°F in the LME transition temperature (return of ductility at the higher temperature) between the unsegregated and segregated states (Figs. 11 and 13). To compare the properties of tin-doped steel with those of "pure" steel reported previously, the reduction of area, which is the most sensitive parameter in liquid metal embrittlement, was plotted for both unsegregated (Fig. 14) and segregated (Fig. 15) conditions in the presence of lead. It is interesting to note that there was very little difference between the pure steel and the tin bearing steel in the unsegregated condition (Fig. 14), but a higher severity of embrittlement was observed for tin doped specimens as compared to "pure" ones when both were in the segregated state (Fig. 15). Again, there was also a shift in transition temperature. This greater severity of embrittlement and the shift in transition temperature are believed to be due to the segregation of tin to the grain boundaries in the tin-doped steel.

De-embrittlement Study of Tin-Doped Steel:

It is well accepted that temper embrittlement is another phenomenon which is a reflection of grain boundary segregation of trace impurities. It has been known for some time that temper embrittleness is reversible[7-9]; that is, the segregated impurities can be dispersed away from the grain boundaries and the mechanical properties are restored. This dispersion of impurities can be accomplished by heating a segregated specimen to a temperature above the range where segregation and embrittlement occur and then quenching in water. Low, et al.[7] suggested that the de-embrittling treatment be 1200°F for one hour followed by a water quench. In this

study, the de-embrittling temperature was kept at 1157°F in order to avoid further loss in strength level and so that the results could be compared with o. er specimens. In an effort to evaluate the sensitivity of this de-embrittling treatment, five segregated tin specimens were heated at 1157°F for 0 (quenched upon reaching temperature) 5, 10, 15 and 20 minutes respectively. The above mentioned times were at temperature (1157°F) and the specimens reached that temperature in about 3 minutes. A thermocouple was tied to each specimen during heating. The specimens were subsequently tested at 650°F with lead on the surface. The r lts of this experiment are tabulated in Table 1. The percentage reduction of area was plotted against the de-embrittling time in Fig. 16. It is very interesting to note that for a segregated specimen, it took a week in the temperature range from 1100°F down to 600°F for the step-cooling treatment, but after heating at 1157°F for 15 minutes, the specimen was more ductile than the unsegregated specimen for the same test conditions. It is also observed that the specimen which was de-embrittled for 20 minutes at 1157°F was much more ductile than was the unsegregated one (Table 1). It has correspondingly been found from temper brittleness studies[7-9] that the transition temperature is lower for de-embrittled specimens than that of unsegregated ones. Viswanathan[9] concluded in his study that some segregation occurs inadvertently in unsegregated samples. Our results tend to confirm this.

Table 1. Tensile Properties of Tin-Doped Steel Specimens with Pure Lead Soldered On the Surface in the De-embrittled Condition Tested at 650°F.

Heat Treatment Condition	De-embrittling Time	Yield Strength ksi	Ultimate Tensile Strength ksi	True Fracture Strength ksi	Reduction of Area %
As Step-Cooled	-	103.0	118.0	137.0	14.0
De-embrittled	0	99.5	120.0	135.0	18.0
"	5	98.0	121.0	137.0	27.6
"	10	100.0	122.0	146.0	32.0
"	15	99.0	120.0	158.0	37.6
"	20	101.0	121.0	164.0	40.7
Unsegregated	-	102.0	125.0	143.0	32.5

A special technical report about the effect of the segregation of tin on liquid metal embrittlement is being written and will be distributed in the near future.

Tensile Properties of Phosphorous-Doped Steel:

Turning now to consideration of the elevated temperature tensile properties of steels doped with phosphorous (Figs. 17 through 20), it can be seen that the properties of the segregated specimens were almost the same as those of the unsegregated specimens. Also, the properties were comparable with the pure material under the same test conditions. This apparent insensitivity of LME to phosphorous-doped steel prompted us to investigate whether phosphorous was completely dispersed away from the grain boundaries in the unsegregated state. This was investigated metallographically using a temper-brittleness reagent which contains picric acid, ethyl ether, zephrine chloride, and water. It has been shown[10] that if phosphorous is present in the grain boundaries, then dark etching grain boundaries are revealed by the above reagent. First, two phosphorous-doped samples, one in the unsegregated state and the other in the segregated state, were etched with the above reagent and both samples showed dark grain boundaries (Fig. 21). This indicated that phosphorous was still present in the grain boundaries in the unsegregated condition. In an attempt to find out at what stage phosphorous segregated to grain boundaries, one austenitized (1600°F, 1 hour, oil quenched) specimen was etched with the above solution and dark grain boundaries were revealed (Fig. 22). This indicated that the segregation of phosphorous could have occurred during austenitization. This is in agreement with McMahon's postulate[8] that the impurities segregate to the grain boundaries during austenitization. A further attempt to disperse the phosphorous from grain boundaries by tempering at higher temperatures (higher than 1157°F) was made. Three austenitize (1600°F, 1 hour, oil quenched) phosphorous-doped samples were tempered at 1200°F for 20 minutes, 1250°F for 5 minutes and 1300°F for 5 minutes, respectively

and then water quenched. The shortened tempering time was used to maintain the same strength level. The specimens were etched with the temper-brittleness reagent and all of them exhibited dark grain boundaries. Photomicrographs of these specimens are shown in Fig. 23. This indicated that dispersion of the phosphorous was not feasible by tempering at higher temperatures. As was pointed out earlier, it has been hypothesized that de-embrittled specimens have less segregation than unsegregated samples[9]. So one step-cooled specimen was de-embrittled at 1157°F for 1 hour, then it was etched with the above solution. This specimen also showed dark grain boundaries (Fig. 24). Although the results are purely qualitative, the above metallographic study indicated that phosphorous was present at grain boundaries both in the unsegregated and segregated states.

By comparing the elevated temperature tensile test results of pure steel and phosphorous-doped steel, it was observed that there was not much difference between the properties of the two steels. If phosphorous had any effect on liquid metal embrittlement, then properties of phosphorous-doped steel would be different than those of the pure one. It would, therefore, appear that the liquid metal embrittlement of steel by lead is insensitive to the segregation of phosphorous in the phosphorous-doped steel.

Tensile Properties of Arsenic-Doped Steel:

The elevated temperature tensile tests of arsenic-doped steel have been completed. It was again found that there was little difference between the properties of the unsegregated and segregated conditions both for tests with and without lead (Fig. 25 through 28). It was also observed that the properties of the arsenic-doped steel and the pure steel were almost identical. It has been reported by many investigators[7,8,10] in temper embrittlement studies that arsenic is a mild embrittler and it increases the Charpy V-notch transition temperature by about 40°F in AISI 3340

steel (antimony increases the transition temperature by about 700°F in the same steel). Joshi and Stein[11] recently reported, in a temper-embrittlement study, that they did not observe any segregation of arsenic in an arsenic-doped AISI 3340 steel by Auger-electron spectroscopic analysis. They also showed that there was only a very small shift in transition temperature upon step-cooling. So it seems reasonable to suggest that arsenic segregation had a negligible effect on liquid metal embrittlement.

Tensile Properties of Furnace-Cooled Specimen Doped with Antimony:

As reported in the Second Annual Progress Report, the embrittlement produced by segregation of antimony alone was so severe as to mask the effect of the liquid metal environment. To evaluate the role of the liquid metal, it was decided that the step-cooling treatment would be replaced by a short tempering time, that is, less antimony would be segregated to the grain boundaries. After experimenting with different tempering times, it has been found that the segregation of antimony in a specimen furnace-cooled from 1100°F to room temperature was sufficient to produce an effect in liquid metal environment. The unsegregated specimens doped with antimony were introduced into the furnace at 1100°F, then furnace-cooled to room temperature. The specimens were tested at elevated temperatures both with and without a liquid metal environment. The test results are shown in Figs. 29 and 30. The furnace-cooled specimen showed 46 percent reduction of area when tested at room temperature, whereas the step-cooled specimen had zero percent reduction of area[12] at the same test temperature. The unsegregated antimony-doped sample had 25 percent[12] reduction of area while the furnace-cooled specimen (Fig. 30) showed 12 percent reduction of area when both were tested with lead at 650°F. The furnace-cooled specimen also had about 75°F higher transition temperature (recovery at higher temperature) than that of the unsegregated one. It is noteworthy that segregation of antimony by merely furnace-cooling from 1100°F to room temperature had such

a significant effect on liquid metal embrittlement. It may be concluded that antimony is a severe embrittler and has a pronounced effect on liquid metal embrittlement.

Future Plans: Fracture surfaces will be analyzed by both light microscopy and scanning electron microscopy. A liquid metal other than Pb may be used as an embrittling liquid on phosphorous-doped steel.

4. The Effect of Purity of the Embrittling Liquid Metal

Chief Investigator: N. N. Breyer
Associate Investigators: J.W. Dally, W.R. Warke
Graduate Student: A. Harsolia

Purpose: To study the effect of lead composition on the fracture behavior of externally wetted 4140 steel.

Introduction: The presence of alloying elements in the lead, whether applied to the surface of steel specimens or dispersed internally in leaded steel, has been found to greatly increase the severity of lead embrittlement. The elements antimony, zinc and tin have been found capable of raising the brittle-to-ductile transition temperature of 4145 steel wetted by pure lead by as much as 300°F. The binary systems Pb-Sn and Pb-Sb on 4145 steel have also been completely characterized for second element (i.e. Sn or Sb) of varying compositions. The effect of Sn or Sb in the Pb on the brittle-to-ductile transition temperature has been found to follow the following relationship:

$$1/T_R = A \log (\% \text{ Sn or } \% \text{ Sb}) + B$$

where A and B are constants, and T_R is the absolute transition temperature.

The straight line relationship from this equation permits the determination of an apparent activation energy for each of the second alloy elements, Sn or Sb. In the case of the Pb-Sn alloys the relationship yielded a value of about 47 kcal/mol, which value is between the heats of vaporization of Pb and Sn (42.5 and 55 kcal/mol respectively). Similar calcuations for the Pb-Sb alloys yielded an activation energy of about 38 kcal/mol, which is somewhat below the heats of vaporization of both Pb and Sb. Although the determination of an activation energy may yield values more apparent than real, the values obtained are consistent with a vapor transport model proposed by Mostovoy and Breyer[13].

The present investigation is a continuation of the study of the effect of varying compositions. In the present work the addition of Zn or Bi to pure Pb is being examined to determine the fracture behaviour of 4140 steel externally wetted.

Progress and Plans: The systems Pb-Zn and Pb-Bi have been chosen for complete characterization for decreasing second element composition down to trace element percentages. The binary alloys of Pb-Zn containing zinc additions of 1, 0.5, 0.2, 0.1 and 0.05 weight percent are to be studied. Similarly, Pb-Bi alloys containing bismuth additions of 10, 5, 2, 1, and 0.5 weight percent will be prepared to study their effect on the elevated temperature tensile properties of 200 ksi nominal UTS non-leaded 4140 steel. Base line, ETT properties of the above steel with pure Pb will also be determined.

Pb-10% Bi and Pb-5% Bi alloys have been made and during the present period testing of these alloys is underway.

5. The Specificity of Embrittling Systems

Chief Investigator: W. R. Warke
Graduate Student: F. A. Shunk

Purpose: To re-evaluate the present knowledge of this aspect of liquid metal embrittlement (LME), to develop additional experimental evidence needed to complement the evaluation, and to review and/or generate theoretical and phenomenological models in terms of the experimental data.

Progress: Concurrent with the experimental investigation, existing models of LME have been examined in terms of how they may be used to account for specificity in LME. It is generally accepted that the liquid metal influences both crack initiation and crack propagation. Thus, an inquiry into specificity is concerned with both aspects of the fracture process. In the following discussion, that aspect of the fracture process to which any given model is most applicable has been considered. Because of our previous conclusion that the available experimental data are, at best, inconclusive with regard to the existence of specificity, no consideration has been given here to the phenomenological criteria which have been proposed for the selection of embrittlement couples; these were commented on in previous reports.

There are, effectively, three models for LME which need to be considered. In historical order, these are (a) the "surface energy" model (1960), (b) the "bond breaking" model (1963), and (c) the "strain hardening" model (1967). Each of these models has started with the assumption of a pre-existing crack; only (b) has been extended to consider crack initiation and is discussed below following a brief discussion of the other two models.

In the surface energy model as proposed by Rostoker et al.[14] it is argued that, when wetting occurs (a prerequisite for LME), the energy required to fracture the sol' is reduced due to changes in the interfacial energies and the stress required to propag-

a crack - - according to the Griffith criterion - - is correspondingly reduced. The claim for the existence of specificity is based on experiments in which LME was not observed although wetting by the liquid metal was achieved. Thus, the surface energy model does not provide a sufficiency criterion for the occurrence of LME. It may be that a further restriction, e.g. a critical contact angle must be obtained, would make this model more useful in considerations of specificity. (There are very few data in the literature for liquid metal - solid metal contact angles.)

In the strain hardening model, which was proposed by Ives and Hancock[15], it is argued that deformation of the material at the crack tip raises the shear stress to such a level that brittle fracture may occur (in accordance with the theory of Kelly et al.[16]). The model does not attribute any role to the liquid metal and therefore, by omission, seems to imply either that specificity is solely a function of the initiation process or that LME does not exhibit specificity.

In contrast to the surface energy and strain hardening models, the bond breaking model is an atomistic one (Stoloff and Johnston[17] and Westwood and Kamdar[18]). In this model, it is assumed that the interaction energy between two atoms at the crack tip is decreased as a result of the presence of the liquid (as compared to what it would be if no liquid were present) and therefore the force necessary to separate these two atoms is decreased. The theory then suggests that the decreased interaction force is reflected in the macroscopic results obtained in a standard tensile test. This is an attractive approach to LME; however, it is also an ad hoc approach and consequently has no predictive capability.

Specificity in the bond-breaking model may be inferred if any of three situations occurs: (a) the reduction of the interaction force is too small to be detectable in the macroscopic tensile test; (b) the liquid has no effect on the interaction force; or (c) the interaction force is increased by the liquid metal. In its present form, this model

does not indicate how any of these situations might occur nor has it been expanded to encompass any fundamental theories of the solid state.

The attractiveness of the bond breaking model is based solely on the fact that it is atomistic in character. As a direct result, the extensive formalism which has been developed in the course of attempting to unravel the many-body problem is available. In its simplest form, LME is observed in two-phase, two-component systems under stress and may be a non-equilibrium phenomenon. Accordingly, there are a number of potential approaches for refining the bond breaking model and possibly giving it a theoretical basis. In terms of the assumptions of this model, a quantum statistical mechanics determination of the significant parameters in separating a semi-infinite solid into two non-interacting parts would be needed (single-phase, single-component system under stress). The "significant" parameters referred to in the preceding sentence might be significant only when the results are compared with the congruent LME system (two-phase, two-component under stress). As an alternative to a detailed calculation of this type, which would include ion-ion, electron-electron, and electron-ion interactions across an interface, it is conceivable that a comparison of the free energy of a semi-infinite solid with that of an infinite liquid-solid system containing an interface would be instructive. There appears to be no basis for assuming, as has been done above, that a classical formulation would not be at least as satisfactory as a quantal formulation. These problems appear to be relevant to the suggestion of Cytron et al.[19] that the liquid-metal imposes a constraint on the plastic strain which is occurring in LME.

Experimental work during the past year has been concerned with the Fe-Hg test couple. Extensive efforts to obtain good, direct wetting of the Fe by Hg were only partially successful. The Hg adhered to the surface in globular form. Tensile tests of these specimens at -36°C and at strain rates of 10 in/in/min indicated that no embrittlement occurred. Because only partial wetting by the Hg was obtained, this

could not be taken as a definitive result. Accordingly, a hybrid system was devised to obtain wetting. In this latter system, Cu was deposited on the Fe specimen by cementation from an acidified $CuSO_4$ solution. After drying, the Cu was wetted with an HgCl solution and an excess of metallic Hg. Results obtained to date indicate that, at -36°C, the Hg-coated specimens exhibit less elongation than do those tested with no coating. Because these were survey tests, it is still necessary to establish what role the Cu may have in influencing the mechanical properties; although, published data[20] indicate that the solubility of Cu in Hg is 0.006 a/o at room temperature.

Plans: Characterization of various models will be continued with the objective of identifying suitable fundamental characteristics for correlation with LME phenomena. The experimental investigation will be continued concurrently.

6. Direct Measurement of Surface Energies

Chief Investigator: E. Zwicker
Post-Doctoral Research: H. Haukaas
Undergraduate Participant: two students, unsupported

Purpose: To measure surface energies by means of microbalance measurement of the force-distance curve when atomically clean surfaces are brought together.

Progress: During the summer of 1971, Dr. Harvey B. Haukaas, Physics Department, Northland College, Ashland, Wisconsin, worked on this problem with the support of the NSF Research Participation for College Teachers Program. After a review of the literature, he focused his attention on the measurement of force and distance.

In order to measure force, the Cahn electrobalance was isolated from the 200 to 400 microgram "noise" encountered on an ordinary bench. This was done by

mounting the balance on a three-legged platform (compatible with supports in the UHV system), and then placing this in a plexiglass box. The box, with balance inside, was then placed on a Lansing Research Corporation Vibration Isolation Table, with a resonant frequency of 1 or 2 hertz. This arrangement reduced the "noise" so that a mass difference of 3 to 5 micrograms could be measured.

A small (3mm cube) plexiglass sample was mounted on a holder attached to one end of the balance beam, and a large piece of plexiglass ($30 \times 30 \times 6 mm^3$), the lower sample, was placed on a carrier directly below the upper sample. The carrier is simply a flat aluminum plate ($4.25 \times 2 \times 0.125$ inches^3) supported on three, finely-adjustable legs. The attractive force between the upper and lower samples was to be measured as a function of their separation. The separation was measured by a Newton's rings optical system, consisting of a mercury arc lamp, condensing lens, green filter and collimator. This illuminated the region between the transparent samples. The resultant interference fringes were observed through a telescopic system.

The three legs of the carrier were adjusted until the lower sample was placed into contact with the upper sample, as indicated by a negative force response from the electrobalance (repulsion). The arm of the balance was then caused to move by careful adjustment of a very fine potentiometer control in the electrobalance circuitry. This caused the surfaces to move apart. As they parted, it became apparent that there was a relative vibration between them. Its amplitude was 1500 to 2000 Å as revealed by the fringes, and its frequency was judged to be about 20 hertz. The vibration appears to originate from sound waves, since the amplitude increases whenever the sound level in the room is increased by any means, even someone walking into the laboratory. Work will continue to solve this vibration problem.

The heating elements and controller for bakeout of the UHV system have been assembled and tested, and the Fiberfrax insulating wall has been completed. A support for the bottom insulating wall has just been completed, and when all electrical

leads have been brought through, the bottom insulation will be put into permanent position under the UHV system. The system will then be tested to maintain 212°F, and vacuum within the system should be improved by an order of magnitude, to about 10^{-11} torr.

Dr. Haukaas has conducted additional work during the academic year at Northland College, under an NSF extension of the Summer Program. His effort has been concentrated on developing a piezoelectric movement to control the position of the lower sample electronically with a high resolution and precision. A report on his progress is expected imminently.

Efforts will continue to solve these problems.

7. Crystallographic Aspects of Liquid Metal Embrittlement

Chief Investigator: D. L. Albright
Graduate Student: J. A. Kargol
Undergraduate Student: T. Garcia (Summer 1971, independently supported)

Purpose: To determine the effect of crystallographic orientation and grain boundary structure on the fracture behaviour of grain boundaries embrittled by a liquid metal and to obtain valid surface energy measurements for the fracture process.

Progress: During the summer of 1971, an undergraduate student (supported on an Olin Foundation grant) worked on atomic modeling of some of the grain boundary orientations which we have produced in pure aluminum bicrystals. This work provided information concerning atomic mismatch at the boundary, as well as a geometric model of the nature of the boundary. Subsequently, the chief investigator had several discussions with Prof. R. D. Larsen of IIT's Chemistry Department concerning the testing of the latter's geometric fracture model[21] by using the grain

boundary structures determined above. Since the subject bicrystals had known variations in fracture tendency, it was anticipated that the relative stability of various lattice configurations could be determined from theoretical calculations and then compared with the experimental measurements. However, as the theoretical approach unfolded, it became increasingly apparent that further refinement of the theory was desirable before calculations based on a reasonable variety of bicrystals could be undertaken. In particular, the assumptions encountered in treating other than two-dimensional, close-packed arrangements are the major deterrents to application of the theory.

Throughout the past year, effort has been concentrated on refining experimental techniques to the point where the fracture surface energies to be measured will be truly representative of the orientation effect in LME. One of the associated problems is the consistent production of bicrystals of sufficient perfection. Current experiments often control crystallographic and metallographic boundary orientations to $\pm 1^{\circ}$ of the ideal values sought. This control has resulted from a series of changes in seed crystal preparation, boat design, and solidification conditions. Bicrystals have been grown in which the grain boundary is held parallel to the growth direction and parallel to the bicrystal surface normal direction by the use of protrusions in the top and bottom of the graphite crucible into which the aluminum seed crystals grow. Except for stray grains which may grow into the charge, the bicrystal growing apparatus appears to consistently produce samples from which acceptable liquid metal embrittlement fracture specimens can be obtained.

Many times the occurrence of stray grains constitutes a significant problem, however, since these grains can dominate the resultant bicrystal due to more favorable growth conditions than the ideal orientation sought. It is clear that these stray grains arise due to recrystallization of portions of the seed crystals upon heating in the bicrystal growing apparatus. Although the seed crystals are chemically etched just

prior to bicrystal growth, there is enough deformation remaining from previous mechanical cutting and polishing to lead to the recrystallization. As a result of this lack of predictability in bicrystal orientation, other methods of seed production have been investigated, with the conclusion that strain-free cutting of seeds from larger crystals can best be performed by spark erosion cutting. This method allows seeds to be cut to precise dimensions with accurate control of crystallographic orientation, while it does not produce any appreciable deformation within the crystal, i.e., the crystal does not tend to recrystallize upon heating. Steps are presently being taken to acquire seed crystals produced in this manner, either by purchase of such seeds or by acquisition of a spark erosion cutter that would enable production of the seeds.

A second experimental problem which has received substantial attention is the elimination of plastic deformation during the fracture of bicrystal test specimens. In order to obtain valid surface energies for the intergranular fracture of aluminum under liquid metal embrittlement conditions, this deformation must be eliminated. The procedure now being used follows the method developed by Mostovoy, et al.[22] The method utilizes a double-cantilever beam specimen with the beams contoured so as to produce a compliance (reciprocal stiffness) which changes at a constant rate with crack length. This design "produces" a crack that propagates at a constant load. The specimen geometry is drawn to scale in Fig. 31, where the bicrystal sample is shown sandwiched between two cover plates.

This test enables the crack extension force, G, to be determined accurately for the fracture being produced, through the equation:

$$G = \frac{P^2}{2b_n} \frac{dC}{da}, \qquad \ldots\ldots\ldots\ldots\ldots (1)$$

where P = applied load,

b_n = crack width

a = crack length, and

C = specimen or structure compliance at crack length a.

The compliance, or ratio of deflection to load, has been found to be:

$$C = \frac{8}{Eb} \int_o^a \left(\frac{3x^2}{h^3} + \frac{1}{h} \right) dx \ , \qquad \text{..... (2)}$$

where E = elastic modulus of specimen material,

b = width of cantilever beams,

x = distance from loading point, and

h = beam height at distance x.

Differentiation of Eq. (2) with respect to crack length yields:

$$\frac{dC}{da} = \frac{8}{Eb} \left[\frac{3a^2}{h^3} + \frac{1}{h} \right] . \qquad \text{..... (3)}$$

Eq. (3) shows that a linear compliance change can be produced by designing the specimen so as to keep the right side of the equation constant. Since 8/Eb is a constant, the linear compliance change is achieved by machining the taper of the double cantilever beam sample such that:

$$\left[\frac{3a^2}{h^3} + \frac{1}{h} \right] = m = \text{a constant.} \qquad \text{..... (4)}$$

Eq. (1) can then be rewritten as:

$$G = \left[\frac{4P^2}{Eb_n^2 b} \right] m. \qquad \text{..... (5)}$$

The quantity m can have any value. Various values were chosen for m to determine a desirable taper (based on compatibility with the bicrystal samples grown and with the ease of machining) for the double-cantilever beam specimen. The value finally selected for m was 90, which resulted in the specimen contour previously referenced, Fig. 31.

Under an applied load, fracture occurs at a critical load, P_c, corresponding to a critical value for the crack extension force, G_c. If the specimen fails under plain strain conditions, the value G_{IC} is the quantity determined from the fracture test. Previous double cantilever beam fracture tests on liquid metal embrittled aluminum bicrystals resulted in some plastic deformation of the cantilever beams during crack extension[23]. Energy absorbed when this deformation was produced contributed to the value of G measured, thus rendering the results of the fracture tests less meaningful. This deformation will be prevented in future tests by machining cover plates from a high strength aluminum alloy (T351), which has about the same elastic modulus as pure aluminum, and adhering them with high strength adhesive to each side of the bicrystal sample, Fig. 31. The grooves cut into the cover plates are cut so as to avoid interference with the plastic zone ahead of the progressing crack tip. It has also been shown that with this specimen geometry, samples with the ratio b_n/b less than about 0.8 should fail by plane strain crack propagation.[21]

The fracture specimen described is presently being calibrated to determine the experimental value of m, which varies from the theoretical value due to the grooves cut in the cover plates. Subsequently, fracture tests performed on aluminum bicrystals should result in an accurate determination of the plain strain fracture toughness in a liquid metal environment, $K_{I\,LME}$, as a function of crystallographic orientation.

Plans: The graduate student involved in this work will devote all of his energies to the experimental aspects of LME fracture noted above. This effort should culminate in precise surface energy values and a proposed model for the orientation effects in this embrittlement couple. Determination of crystallographic substructure at the boundary will be pursued insofar as it affects the proposed model. As time permits, the chief investigator will devote a portion of his effort to establishing the merit of a geometric approach to fracture in this couple.

8. Effect of Cold Work on Lead Embrittlement of Alloy Steels

Chief Investigator: N. N. Breyer
Graduate Student: M. Watkins

Purpose: This investigation is intended to separate the individual effects of cold working, strain rate, and strength level on the embrittlement behavior of steel by lead.

Progress: It was reported in the Second Annual Technical Progress Report that die drawing internally leaded 4145 steel various percentages (10, 20, 30 and 50% deformation) to a final strength level of 200 ksi resulted in a decrease of embrittlement severity. It can be seen in Fig. 32 that the embrittlement trough was eliminated for 50% deformation. In order to determine if the decrease in the severity of embrittlement by cold work was an effect unique to an internally leaded steel, bars from the non-leaded ingot of the same 4145 heat were processed with the same heat treatment - deformation schedule used for the leaded bar stock. The heat treatment-deformation processing schedule is given in Table 1. For the non-leaded steel specimens, lead was supplied externally by soldering a Pb-4.0 w/o Sn alloy (M.P. 598°F) to the surface.

Fig. 33 shows the base line data of the non-leaded 4145 steel at 200 ksi nominal strength achieved by heat treatment alone. When specimens were externally wetted with the Pb-4.0 w/o Sn alloy, the LME trough was observed between 550-900°F as shown in Fig. 34. Both the reduction of area and the true fracture stress were severely degraded in this temperature range. Fig. 35 compares the RA values of the specimens processed to a final strength of 200 ksi by three different heat treatment - deformation combinations (Table 1). The transition temperature for the return to ductility shifted significantly to lower temperatures and the severity of LME decreased drastically as the amount of deformation increased. Several interesting

Table 1.

ROOM TEMPERATURE TENSILE PROPERTIES OF NON-LEADED 4145 STEEL AS ACHIEVED BY HEAT TREATMENT AND THE HEAT TREATMENT DEFORMATION PROCESSING

Thermal Processing	Room Temperature Tensile Properties Achieved by Thermal Processing Only		Deformation by Die Drawing at Room Temperature	Room Temperature Tensile Properties Achieved by Thermal Processing and Die Drawing	
1525°F Aus. Oil Quench plus 900°F Temp.	Y.S.	184.4 ksi	0%	Y.S.	184.4 ksi
	T.S.	192.7 ksi		T.S.	192.7 ksi
	T.F.S.	297.0 ksi		T.F.S.	297.0 ksi
	R. A.	55.7%		R. A.	55.7%
1525°F Aus. Oil Quench plus 1050°F Temp.	Y.S.	149.0 ksi	30%	Y.S.	190.0 ksi
	T.S.	160.5 ksi		T.S.	191.5 ksi
	T.F.S.	267.8 ksi		T.F.S.	268.0 ksi
	R. A.	58.6%		R. A.	50.3%
1525°F Aus. Oil Quench plus 1080°F Temp.	Y.S.	146.5 ksi	50%	Y.S.	205.0 ksi
	T.S.	158.0 ksi		T.S.	207.5 ksi
	T.F.S.	266.5 ksi		T.F.S.	264.0 ksi
	R. A.	59.7%		R. A.	43.4%

Y.S. = Yield Strength 0.2% Offset
T.S. = Tensile Strength
T.F.S. = True Fracture Stress (uncorrected)
R. A. = Reduction in Area at Fracture

features of this figure bear closer examination. For example, the lowering of ductility at room temperature must be considered. It is well documented in the literature that cold working normally reduces ductility. This trend was found at temperatures between RT and 600°F where the RA values decreased with increasing amounts of cold work. In order to separate the opposing effects of cold work on LME and ductility exhaustion as measured by RA in the embrittlement trough, it was necessary to compare four groups of specimens. Fig. 40 summarizes the RA properties for the 30% cold work series shown in Figs. 36 through 39 while Fig. 45 summarizes the RA properties for the 50% cold work series shown in Figs. 41 through 44. All of the specimens in the 30% cold work series were initially heat treated to 162 ksi. One group at 162 ksi (Groups 1) received no further processing after heat treatment (Fig. 36). The second group with this same treatment was surface wetted with the Pb-Sn alloy (Fig. 37). This group showed the expected LME trough. The specimens of the third and fourth groups were additionally given 30% die deformation to achieve a nominal 200 ksi strength level. The specimens of Group 3 were tested in the un-wetted condition (Fig. 38) whereas the specimens in Group 4 were surface wetted with the Pb-Sn alloy (Fig. 39). By comparing the RA data from Groups 1 and 2, i.e., non-wetted and wetted respectively, at 162 ksi, the degradation in RA associated with LME is seen (maximum embrittlement occurring between 550 and 800°F).

The degradation of RA resulting from 30% cold work for the steel bars not subject to LME can be obtained by comparing the RA values from Group 3 (in which the final strength of 200 ksi was achieved by heat treatment plus 30% die deformation) with those RA values obtained from the base line material which was only heat treated to a final strength of 200 ksi (Fig. 33). For the test temperature range of RT to 800°F it was found that 30% cold work decreased the RA values by 5 to 15% points. There was a greater exhaustion of ductility with increasing amounts of cold work to achieve a final 200 ksi strength level (Fig. 46).

The effects of cold work on LME can be shown by two comparisons. The first comparison was made between the two groups of wetted specimens wher one group at 162 ksi had not been cold worked (Group 2) and the other group at 200 ksi had been additionally cold worked to achieve this higher strength (Group 4) (Fig. 40). It was found that LME was less severe and the transition temperature shifted to a lower temperature for the higher strength cold worked specimens. These changes, which demonstrate the reduction of LME severity, were even more pronounced for the 50% cold work series (Fig. 45). Figs. 40 and 45 show that at 650°F for 30 and 50% cold worked material (at 200 ksi), the RA for the specimens in the deformed condition were respectively 15 and 40% points higher than the RA of the specimen in the non-cold worked condition. This was true in spite of the fact that the cold worked specimen had a higher strength than the non-cold worked specimen and that the 50% cold worked specimen had a lower intrinsic ductility than the 30% cold worked specimen in the non-wetted condition (Fig. 46). The second comparison was made between two groups of cold worked specimens where one group was non-wetted (Group 3) and the other group was wetted (Group 4). In Fig. 40 it can be seen that the curve for the wetted specimens cold worked 30% showed significant embrittlement and deviated markedly (by as much as 28% points) from the RA values for non-wetted specimens in the temperature range of 400° to 800°F. At 50% cold work (Fig. 45) both curves, non-wetted and wetted, essentially coincided except at 600°F where the curve for wetted specimens was lower by 12% points. Fig. 47 contains the RA ratio data comparing the wetted to the non-wetted ductility values for both the 30 and 50% cold worked specimens. Again, it was illustrated that 50% cold work greatly reduces the LME.

As had been found in the previous studies for the internally leaded steel specimens, the severity of embrittlement for the externally wetted steel specimens decreased as the amount of cold work increased and was drastically reduced for 50%

die deformation. We concluded from these data that the effect of cold work on lead embrittlement was not controlled by the location of the lead, but rather by the effect of deformation as it influenced the fracture path in the steel matrix.

Photomacrography and electron fractography were used to examine the effects of cold die drawing on the fracture path and fracture mode of LME. The photomacrographs of Fig. 48 are the fracture surfaces of two non-leaded 4145 steel specimens heat treated to 154 ksi, one of which had been further cold worked 50% by die drawing; both were surface wetted with Pb-4.0 w/o Sn alloy and tested at 600°F. The fracture surface of the as-heat-treated specimen exhibited considerable LME (fracture type D)[24] while the fracture surface of the 50% cold worked specimen exhibited a ductile cup-cone fracture (type E). The effects of cold work on fracture path are illustrated in the photographs in Fig. 49 which are longitudinal cross-sections of the fractured tensile specimens. It was observed, in Fig. 49a, that secondary microcracks propagated from the primary fracture surface of the undeformed specimen at angles of approximately 30 - 60° to the specimen axis. The nature of the branching can be seen more easily at higher magnification. Fig. 49b is a photomicrograph of the terminus area of the microcrack indicated by arrow A in Fig. 49a. It was also noted that the dark appearing lead-tin alloy was present in these cracks. An entirely different fracture mode appearance can be noted for the 50% cold worked specimen. Small secondary microcracks were observed as indicated by arrow B in Fig. 49c. Fig. 49d is a photomicrograph of area B at 100X magnification. It was noted in this case that there was one large microcrack plus many smaller microcracks which ran parallel to the specimen axis (the drawing direction). Thus, cold work changed the secondary microcrack orientation from angles of 30 - 60° to the specimen axis for the undeformed specimen to an angle of 0° to the specimen axis for the deformed specimen.

The location of the secondary microcracks indicated that in the undeformed specimen the primary LME crack initiated at the surface and propagated to failure in a path perpendicular to the specimen axis. On the other hand, in the 50% cold worked specimen, the crack initiated in the central region and was blunted. It is suggested that cold work changed the fracture path by preventing the LME crack from propagating along the prior austenitic grain boundaries and forced it to propagate along the α-Fe_3C boundaries which were oriented parallel to the drawing direction. Although the austenitic grain boundaries could not be completely revealed, the polished and etched photomicrographs shown in Figs. 50 and 51 tend to support this line of reasoning. Photomicrographs of the undeformed fractured specimen are shown in Fig. 50. These are high magnification photomicrographs of the areas indicated by arrows C and F in Fig. 49. It was observed that the microcracks could have propagated along the prior austenitic grain boundaries (arrow C). It was also observed that some of the microcracks were discontinuous in the terminus region (arrow F). Photomicrographs of the 50% cold worked specimen are shown at 500X and 1000X in Figs. 51a and 51b respectively. Arrows D and E in Fig. 49d indicate the location of these areas. It was noted at these higher magnifications that microcracks propagate along the α-Fe_3C boundaries.

The effects of cold work by die drawing on fracture mode for internally-leaded steel were also studied using macrofractography and electron fractography. Photomacrographs of tensile fractures for various specimens of internally-leaded 4145 steel heat treated and cold worked by die drawing various percentages to achieve 200 ksi nominal strength and tested at 650°F are shown in Fig. 52. The heat treatment-processing schedule is given in Table 2 and a summary of the tensile properties at 650°F is given below. (The complete ETT properties were given in the First and Second Annual Technical Progress Reports.)

Table 2

ROOM TEMPERATURE TENSILE PROPERTIES OF INTERNALLY-LEADED 4145 STEEL AS ACHIEVED BY HEAT TREATMENT AND THE HEAT TREATMENT DEFORMATION PROCESSING

Thermal Processing	Room Temperature Tensile Properties Achieved by Thermal Processing Only		Deformation by Die Drawing at Room Temperature	Room Temperature Tensile Properties Achieved by Thermal Processing and Die Drawing	
1525°F Aus. Oil Quench plus 900°F Temp.	Y.S.	186.3 ksi	0%	Y.S.	186.3 ksi
	T.S.	194.8 ksi		T.S.	194.8 ksi
	T.F.S	283.5 ksi		T.F.S.	283.5 ksi
	R. A.	50.0 %		R. A.	50.0%
1525°F Aus. Oil Quench plus 970°F Temp.	Y.S.	173.9 ksi	10%	Y.S.	201.3 ksi
	T.S.	184.9 ksi		T.S.	209.1 ksi
	T.F.S.	274.7 ksi		T.F.S.	283.2 ksi
	R. A.	50.7 %		R. A.	45.3 %
1525°F Aus. Oil Quench plus 1010°F Temp.	Y.S.	168.5 ksi	20%	Y.S.	198.5 ksi
	T.S.	179.9 ksi		T.S.	206.3 ksi
	T.F.S.	270.2 ksi		T.F.S.	281.4 ksi
	R. A.	50.8%		R. A.	48.2%
1525°F Aus. Oil Quench plus 1060°F Temp.	Y.S.	156.0 ksi	30%	Y.S.	174.7 ksi
	T.S.	163.6 ksi		T.S.	195.6 ksi
	T.F.S.	251.5 ksi		T.F.S.	274.6 ksi
	R. A.	55.5%		R. A.	47.5%
1525°F Aus. Oil Quench plus 1150°F Temp.	Y.S.	140.5 ksi	50%	Y.S.	194.0 ksi
	T.S.	154.0 ksi		T.S.	195.2 ksi
	T.F.S.	259.0 ksi		T.F.S.	256.0 ksi
	R. A.	57.4%		R. A.	43.4%

Y.S. = Yield Strength 0.2% Offset
T.S. = Tensile Strength
T.F.S. = True Fracture Stress (uncorrected)
R. A. = Reduction in Area at Fracture

% CW	% RA	% Elong	σ_{ULT} (ksi)	σ_{TFS} (ksi)	Fracture Type[24]
0	0.8	2.2	152.0	153.2	D
10	0.0	1.6	161.9	161.9	D
20	7.8	3.2	167.8	169.6	D
30	31.8	5.5	162.6	205.8	E
50	46.8	8.8	159.0	212.5	E

The fracture for the 0, 10, and 20% cold worked specimens was characterized by one large "fish eye" (type D) and by a cup-cone geometry (type E) for the 30 and 50% cold worked specimens.

The LME crack initiates in the "fish eye" of the type D fracture and then propagates to failure. A schematic drawing of a typical "fish eye" is given in Fig. 53. Zipp, Warke, and Breyer[24] used electron fractography to separate the "fish eye" into 3 regions: origin, intermediate region, and outer region. They showed that the origin area was completely intergranular. The surrounding intermediate region was a mixture of both intergranular and transgranular fracture while the outer region was completely transgranular. Present efforts are concentrated on determining the effects of die drawing on the nature of the fracture in the origin area. The origin area was easily identified because it contained a high concentration of reddish-brown or golden-brown spots. Visual examination revealed that these spots covered approximately one-half of the "fish eye" for the 0% cold worked specimen, one-third for the 10% cold worked specimen, and one-tenth for the 20% cold worked specimen. There were only a few, small reddish-brown spots in the central fibrous zone for the 30% work specimen, and there were none present on the fracture surface of the 50% cold worked specimen. More careful examination revealed that there were other subtle changes in the fracture surfaces with deformation. As a function of increasing cold work it was found that first, the size of the "fish eye" decreased and it appeared to move towards the tensile axis of the specimen. Second, the number of colored spots in the origin area was correspondingly smaller, and located

farther away from the edge of the "fish eye", i.e., towards the center of the fish eye. Third, the fibrous area was larger for the type E fracture common to the higher (30% and 50%) cold work specimens.

Figs. 54 through 58 are fracture surface replicas from the origin areas of the "fish eyes" and central fibrous areas of the internally leaded 4145 tensile specimens shown in Fig. 52. Fig. 54 shows the intergranular facets present in the origin area of the "fish eye" of the as heat treated specimen. These intergranular facets had the typical "rock candy" appearance. The appearance of the intergranular facets were altered for specimens which had been subjected to cold work. It was observed in Figs. 55 and 56, for the 10 and 20% cold worked specimens respectively, that the intergranular facets were rougher and more irregular than those present in the 0% cold worked specimen. In fact, at 20% cold work, the facets were so jagged that they appeared to have undergone some type of tearing process during fracturing. This would indicate an increase in ductility. There also appeared to be considerable distortion of the grain boundaries with increased cold work. These effects were more pronounced for the intergranular facets present in the origin area of the 30% cold worked specimen. A comparison of these facets, shown in Fig. 57a, with those of the non-cold worked specimen, shown in Fig. 54, clearly illustrated that cold work by die drawing significantly altered the nature of the intergranular facets. There were also quasi-cleavage facets, Fig. 57b, present in the origin area of the 30% cold worked specimen. The irregular intergranular facets and the quasi-cleavage facets indicated that the severity of the LME fracturing process had been reduced. It had been noted in Fig. 52d that the dominant fracture mode for the 30% cold worked specimen was transgranular, and this was verified in Fig. 57c. The intergranular and quasi-cleavage facets were surrounded by the transgranular matrix. The reddish-brown spots observed in the central fibrous zone of the 30% cold worked specimen corresponded to these embrittlement areas. The fracture mode for the 50%

cold worked specimen was transgranular. Fig. 58 shows a typical transgranular area.

Thus, cold work by die drawing changed the LME fracture mode from intergranular for the specimens cold worked 0, 10 and 20%, to a mixture of transgranular, intergranular, and quasi-cleavage for 30% cold work, and to transgranular for 50% cold work.

Plans: Changes in carbide morphologies and structural damage will be examined as a function of cold work. Metallographic techniques will include ordinary light metallography, transmission electron microscopy, and scanning electron microscopy. The effects of strain rate on the elevated temperature tensile properties of both the internally-leaded 4145 steel cold worked by die drawing 50% (tempered martensite condition) and the internally-leaded 1041 steel cold worked by die drawing 44% (normalized condition) will also be examined. The investigation of the effects of cold work of LME on alloy steels will be expanded to include liquid metals other than the Pb-4.0 w/o Sn alloy. Possible embrittling agents include Sn, In, and Zn.

9. Fracture Toughness of Engineering Metals in LME

Chief Investigator: J. W. Dally

This task was terminated in the Second Annual Technical Progress Report submitted in June 1971.

10. Effect of Combined Stresses on LME

Chief Investigator: L. J. Broutman
Associate Investigator: J.W. Dally
Graduate Student: T. F. Fugiel

This task was terminated in the Second Annual Technical Progress Report submitted in June 1971.

11. Statistical Mechanics of Fracture and Embrittlement

Chief Investigator: R. D. Larsen
Postdoctoral Associate: C. G. Miller

This task was terminated in the Second Annual Technical Progress Report submitted in June 1971.

12. Dynamic Aspects of Liquid Metal Embrittlement

Chief Investigator: P. Gordon
Associate Investigator: D. L. Albright
Graduate Student: J. R. Zych

Purpose: To study the effect of stress on the delayed failure behavior of a normally ductile material embrittled by a liquid metal agent in order to gain further insight into the dynamic aspects of LME crack propagation.

Progress: As noted in the previous reports the dynamic aspects of liquid metal embrittlement were examined with high speed photographic recordings of LME-induced failure. The experiments utilized sheet specimens of Al 2024-T3 subjected to a static uniaxial stress prior to the sudden application of the mercury embrittling agent. The failure phenomena could be divided into four distinct phases including initiation, primary LME crack propagation, LME branch propagation followed by a transition from brittle-to-ductile failure, the latter occurring as a high velocity shear fracture.

The initiation period is that time required to produce a visible crack, probably at a grain boundary. This phase has been found to be dependent upon an applied stress-time interrelationship:

$$\log_{10} t_i = A + B\ (\sigma/\sigma_y);$$

where t_i is the initiation time in seconds, σ is the applied static stress, σ_y the yield

stress, A and B are empirical constants. This delay time may be due to several thermally-activated processes, either alone or in combination. The more likely candidates are: 1) Diffusion of Hg atoms through grain boundaries within the aluminum, 2) Hg diffusion along moving dislocations during low temperature creep, and 3) several surface adsorption and surface diffusion mechanisms for which, however, few appropriate experimental data exist.

After initiation, crack propagation occurs in the direction essentially normal to the direction of the maximum principal stress. The crack growth is discontinuous, with frequent arrest and re-initiation. The average crack tip velocity during this primary LME propagation phase ranges from 7 to 21 in/sec., depending on the applied stress level.

Branching occurs after modest crack growth and is so profuse that it is often described as feathering. Crack velocity during the branching phase is decreased appreciably and is usually less than 10 in/sec., but again, is a function of the applied stress level.

While instantaneous velocities of LME propagation may be as high as several hundred in/sec., the average velocities are an order of magnitude lower, or several tens of in/sec.

In comparison, the crack velocities in non-embrittled, highly stressed aluminum approach 10^5 in/sec. In view of this large difference it seems probable that the LME crack velocity is limited by the transport of the embrittling agent to the crack tip, i.e., the supply velocity. This supply velocity represents an upper bound for the LME crack velocity and has been measured here to be of the order of a few hundred in/sec. A further indication that the LME crack propagation rate is limited by the rate of supply of mercury to the crack front region is that a propagating LME crack, when deprived of its mercury supply, will become arrested until the crack is resupplied with mercury whereupon crack propagation will resume.

The reason for the average LME crack velocity being an order of magnitude lower than the maximum instantaneous crack velocities is the start-stop behavior of the propagation process. A fast-moving crack, well-supplied with liquid metal, suddenly stops; either because it became arrested by an obstacle in its path such as a second-phase particle, an inclusion, or a nearly perpendicular grain boundary; or because the crack had begun to curve out of the stress field so that the stress at the crack tip dropped below the critical level for continued crack propagation. The crack propagation process must now await a re-initiation process. A new crack front must be established beyond the obstacle, oriented approximately perpendicular to the maximum principal stress. Whatever mechanism or combination of mechanisms contributing to the initial crack initiation process must now operate again to re-initiate the fast-moving crack. This sequence of steps is then repeated throughout the LME-crack propagation stage.

The final fracture stage is a period of high velocity shear rupture which is initiated when the LME-crack length reaches a critical value, for the particular stress level applied to the specimen, at which a brittle-to-ductile fracture transition occurs, with the shear rupture operating at crack tip stress levels sufficiently high to be independent of the embrittling agent.

Future Work: Further tests are planned, using high purity aluminum instead of 2024-T3 aluminum alloy to test the generality of the results and conclusions derived from the previous tests.

13. Liquid Embrittlement of Crystalline Polymers

Chief Investigator: L. J. Broutman
Graduate Student: T. Kobayashi

Purpose: To study the embrittlement of crystalline polymers by liquids in order to relate this phenomenon to liquid metal embrittlement

Progress: Polycarbonate polymers can exist in either a wholly amorphous or semi-crystalline form. The rate of crystallization is very slow and in conventional forming methods the structure of polycarbonate is amorphous. However, crystallinity can be created by thermal annealing at a temperature of 190°C. At this temperature the rate of crystallization is a maximum but it still requires several hundred hours in order to fully crystallize the polymer. Thus, thermal degradation may also occur at this temperature unless the annealing is done in an inert atmosphere. Another technique for inducing crystallization is by solvent vapor swelling. In other words, amorphous polycarbonate sheet is exposed to acetone vapor which diffuses into the polymer causing swelling and thus allowing crystallization to occur. During the present report period, we have explored both methods of crystallization, using sheets of polycarbonate up to 1/4 inch in thickness. Previous studies of other investigators have been limited to the crystallization of thin films which is a much simpler problem than crystallizing thick sheets. Techniques have been developed for crystallizing thick sheets and also for drying the sheets afterwards to remove the acetone vapor. The properties of these sheets are being determined as a function of the degree of crystallinity and amount of remaining acetone. The fracture or crack propagation energies are being measured and studies of the effect of liquids or vapors on the crack propagation energy are being planned.

14. The Vapor Embrittlement of Metals

Chief Investigator: N. N. Breyer
Graduate Student: J. Simoudis

Purpose: The discovery that the so-called "liquid" metal embrittlement of solid metals can take place with the embrittler in the solid state has essentially destroyed the widely held view that embrittler must be liquid to produce "LME" effects. As a result, it was proposed by S. Mostovoy and N. N. Breyer[13] that the embrittling species can approach a growing crack tip from the source by a vapor transport mechanism. In our last semi-annual report, the details of many of the experiments performed to discriminate between liquid and vapor transport mechanisms were described. In this report only a summary of the important findings will be presented.

Progress:

Introduction: Mostovoy and Breyer[13] in their investigation of the elevated temperature mechanical properties of both leaded and non-leaded 4145 steel found that the presence of internally added lead affected the properties of the leaded steel product. Tensile tests performed in the range of 300 to 900°F revealed that the true fracture strength, reduction of area and impact strength for the leaded material were severely degraded. Since the embrittlement temperature range included the interval from 300 up to 621° (the M.P. of lead), they proposed a vapor transport mechanism to account for the availability of lead atoms from a solid source.

Later Warke and Breyer[25] showed that similar embrittlement occurred in non-leaded steel specimens to which either pure lead or lead alloys were soldered. Again it was found that the embrittlement was present at temperatures well below the melting temperatures of the externally applied alloys. This finding was consistent with the LME vapor transport model.

Johnson and Breyer[26], using surface wetting experiments, established that very small percentages of antimony when added to the externally applied alloy resulted in an increase of embrittlement over that exhibited by lead alone.

In the present study, stressed E-4130 steel specimens were exposed to the vapors from a lead-2% antimony bath at specimen temperatures above the lead melting temperature but considerably below that of pure antimony. The choice of this specimen temperature, it was felt, would permit detailed examination of the fracture surface to determine if the lead and/or antimony atoms were present as a continuous film, consistent with liquid transport or solid diffusional transport, or as distinct clusters consistent with the vapor transport mechanism.

Materials and Test Methods:

General: Static fatigue and dynamic bend tests were performed on specimens of E-4130 alloy steel heat treated to strength levels of 180,000 to 210,000 psi. This alloy steel was chosen because it is available in sheet form. Specimen configuration is shown in Fig. 59. Specimens were tested in four point bending (see Fig. 60) under various surface conditions, (fluxed, scratched, surface wetted with embrittling material, etc.), in air and in vacuum, over a range of loads, and in the presence or or absence of the lead-antimony embrittling species. All tests were performed at elevated temperatures ranging from 30°F above the melting point of pure lead (621°F) to 316°F below the melting point of pure antimony (1166°F).

A lead evaporation furnace and a fixture for loading high strength steel strip specimens by bending were incorporated in a vauum chamber. Electrical resistance heating was employed both for evaporation of the lead-antimony alloy and heating of the gauge section of the specimens.

Experimental Results:

At the beginning of this test program a number of tests, not reported on herein, were performed below the yield point of the specimens. These specimens

were loaded, exposed to lead vapors in vacuum, and heated to their respective test temperatures. No special provisions were taken to insure wetting of the specimens by the lead vapors. None of the specimens failed or cracked after days of testing at their test temperature. Tests were also performed below the yield point on previously fluxed specimens on which lead was deposited in vacuum. None of these specimens failed after heating to temperatures in the range of 600 to 700°F and holding for up to four days. On the basis of the above preliminary tests, it was decided that stresses exceeding the yield point of the material would be used. Many tests, reported in the last semi-annual report, will not be presented again in this report. Rather, the most significant findings will here be summarized.

It was found when heat treated specimens of a nominal tensile strength of 200 ksi were loaded above the yield strength of the material and subjected to lead-2% antimony vapors that cracks could be induced on the tensile stressed side of the specimens. A scanning electron micrograph of typical cracks are shown in Fig. 61. Examination of the yawned-open cracks of area A noted on Fig. 61 revealed globules typical of deposit from a vapor (see Fig. 62). No continuous film which would be expected for liquid or solid transport was detected.

Some of the specimens fractured completely by a brittle mode when subjected to the vapors. Fig. 63 is an SEM photograph of a typical fracture surface. A brittle thumbnail crack (400 microns, in depth) can be seen extending from the tension surface approximately one third of the way through the section thickness (approximately 1250 microns). With the aid of scanning electron microscopy the fracture surface of this specimen was examined in detail.

Fig. 64 was taken approximately 40 microns below the specimen surface. It should be noted that the specimen thickness was 0.125 cm or 1250 microns. Globules of the low melting phase are present at this location. An important observation is the

absence of a continuous liquid film, although the globules of Fig. 64 are not perfectly spherical.

Fig. 65 exhibits the fracture surface 200 microns below the tension surface of the specimen. It is observed that the condensed vapors have assumed a well defined crystallographic shape. These crystals are believed to be antimony, based on the following reasoning. The specimen was tested at 747°F. At this temperature, the condensed lead vapor atoms were above their melting point (621°F) and would thus be expected to exhibit the globular morphology. Antimony, on the other hand, melts at 1166°F and would thus be solid at 747°F. The vapor pressures of lead and antimony at the evaporation temperature of 1216°F are 2.5 and 250 microns [27], respectively. Assuming Raoult's law, the vapor pressures of lead and antimony in the alloy would be approximately 2.42 and 0.9 microns respectively; these values, it is believed, are high enough to provide both atomic species to the growing crack tip. Further, the crystal structure of antimony is rhombohedral, a special case of the hexagonal system. The crystal structure of lead, on the other hand, is face-centered cubic. The symmetry of the crystals observed in Fig. 65 does not seem to be cubic and could easily be reconciled with hexagonal symmetry. In addition it can be noted that the crystals are solid at the test temperature. Both of these factors, the non-cubic crystal symmetry and the solid crystal morphology are consistent with the probability that the crystals of Fig. 65 are antimony.

Fig. 66 was taken 400 microns from the tension surface of the specimen, at area C shown in Fig. 63. A well-developed whisker texture is noted. Fig. 67, taken at a location just to the right of Fig. 66, shows an enlarged view of one whisker. Here again a hexagonal symmetry seems to exist. It is believed that the whisker texture developed while the crack was open since no such whiskers are observed in Fig. 68 which was taken at 600 microns below the tension surface and inside the fibrous final fracture zone (area D of Fig. 63).

Conclusions: The findings of this investigation have indicated that crack initiation and propagation is governed by the transport of the embrittling species to the crack tip. The absence of a continuous film of the embrittling species strongly supports the vapor transport mechanism of embrittlement proposed by Mostovoy and Breyer[13]. In addition, the indications of the well-formed crystals of non-cubic symmetry near the crack tip strongly support the contention that antimony is transported to the crack tip from the vapor.

Based on this investigation the following conclusions are offered:

1. Static fatigue of heat treated E-4130 steel occurs by stressing above the yield point when the tension surface is exposed to vapors of the lead-antimony alloy.
2. Crack initiation and propagation requires the establishment of a true interface ("wetting") between the solid metal and the embrittling vapor species.
3. Formation of a liquid film is not a requirement for crack propagation and such a film was not observed.
4. The evidence supports the vapor mechanism for the transport of the embrittling species to the crack tip.
5. Embrittling of E-4130 steel specimens at the test temperatures employed was the result mainly of antimony vapors condensing at the crack tip with a preferred orientation as evidenced by the crystallographic morphology of the grown embryos.

Plans: At the present time activities on this phase of the program have ceased since the student involved has completed his academic efforts. A report for eventual submission to a technical journal will be written. When another student is engaged on this phase of the program, work will again be resumed.

15. Grain Boundary Segregation and LME

Chief Investigator: W. R. Warke
Associate Investigator: P. Gordon
Graduate Student: U. Nanda

Purpose: To study the effect of segregation of trace impurities to grain boundaries on the embrittlement in LME in simple binary alloy systems.

Introduction: The research reported in Section 3 of this report has established firmly that impurities segregated to the grain boundaries in steel affect the fracture strength and ductility in an LME environment. The effect has been observed[28] in AISI 3340 steel when Sn and Sb were segregated to the grain boundaries and the steel was embrittled by liquid lead on the surface. With this in mind it was thought to extend the above studies of impurity segregation and its role in the LME fracture process to simple binary ferrous and non-ferrous systems.

A literature survey was carried out to determine the systems where impurities segregate to grain boundaries. J. H. Westbrook[29] has listed a number of such systems. In selecting a particular system for the study, the following factors were felt to be of prime importance:

a. The alloy should be readily available.
b. The heat treating procedures required to cause segregation of trace impurities to the grain boundaries should be relatively short and simple.
c. The base metal of the alloy should be such that it is known to be susceptible to liquid metal embrittlement in easily controlled and handled environments.

Considering these factors, only a few simple systems are available from which to select a system for study:

Base Metal	Trace Impurities
Cu	Bi, Sb or Sn
Brass	Bi, Sb or Sn
Al	Fe or Sn
Ni	S
Fe	P or O

Copper, brass and aluminum are embrittled by liquid mercury. It has been recently reported[30] that Na, K, and Cs wet nickel, and it is expected that these metals would embrittle nickel. However, difficulties in handling these metals, probably would preclude their use. Preliminary studies have also shown that mercury wetted and embrittled a commercially pure nickel (Nickel 200). Further literature study and experimental work will be done on these systems to select potential LME environments.

Several workers[31-38] have conducted studies on Cu-Sb, Cu-Sn, Cu-Bi, Brass-Sb and Brass-Bi and have shown that after appropriate annealing treatments, brittle intergranular fractures were obtained at low temperatures. The results were interpreted in terms of the impurities having been segregated to the grain boundaries during the annealing treatment. Recently Stein and Joshi[39] have shown unequivocably, by Auger electron spectroscopy, that bismuth segregates to the grain boundaries in the Cu-Bi system and causes intergranular fracture. Brittle fracture was observed with as little as 0.002 wt.% Bi in copper. It was also shown that at fracture 30 wt.% Bi was present at the grain boundaries. In view of this documentation of grain boundary segregation, their availability and ease of embrittlement, these copper base alloys were selected for the initial stages of the research.

Westbrook and Floreen[40] also have shown that S (1-150 ppm) in Ni causes hot shortness. It is again interpreted that S segregated to the grain boundaries and weakens them. This system is being considered for study, as well, and some preliminary tests have been run as indicated above.

Depending on the outcome of the work in progress, others of the candidate systems may be selected for study.

Experimental Procedure: Five vacuum melted high purity copper alloy ingots weighing 6 lbs. each were obtained from Chase Brass and Copper Company. Special additions to the high purity copper were 0.0025 wt.% Bi, 0.005 wt.% Bi, 0.01 wt.% Bi, 1.0 wt.% Sb and 3.0 wt.% Sn. Raw materials for melting of high purity Ni-S alloys have also been received from International Nickel Company, Suffern, New York. However, difficulty has been encountered in finding facilities for melting and fabricating the nickel alloys.

Since 0.01 wt.% Bi has been shown to produce the maximum amount of embrittlement of copper[32, 39], it was decided to study the LME by mercury of this alloy first and then the 0.005 wt.% Bi and 0.0025 wt.% Bi alloys, respectively. The cast size of the ingots was 6" x 3" x 1/2". The 0.01 wt.% Bi ingot was first cold rolled by 36% to a thickness of 0.314" on a 2-high Loma Rolling Mill. At this thickness, surface cracks began to appear so the bar was process annealed at 1500°F for 45 minutes in a dry Nitrogen atmosphere and water-quenched. The bars were wrapped in a thin copper sheet in order to minimize the loss of bismuth from the Cu-Bi alloy on annealing.[32] Next the ingot was pickled in dilute nitric acid to remove any thin oxide layer which might have formed. The ingot was further reduced by 90% to a sheet of 0.031 in. thickness. Small sheet coupons of size 3" x 0.5" were cut from this sheet and were further process annealed at 1500°F for 45 minutes and water quenched. A final reduction of 25% was given to each coupon to achieve a final thickness of 0.025 inch. The coupons were given a final process annealing treatment at 1500°F for 15 minutes under dry N_2 and water quenched. This treatment was expected to give a coarse grain size which would show the maximum embrittlement. The specimens at this stage will be termed as unsegregated-unembrittled. To achieve the segregation of bismuth to the grain boundaries

(segregated-embrittled state), half of the above unsegregated-unembrittled specimens were given a segregating heat treatment consisting of heating the samples at 550°C (1022°F) for 45 minutes in dry N_2 and then water quenching.

After the heat treatment the sheet samples were machined on a high speed router. The standard sheet specimen had a gage section 0.275 in. wide and 0.75 in. long. The edges of the tensile specimens were subsequently polished with high grade number emery papers.

Tensile tests were carried out at various temperatures (-80°F to 600°F) on an Instron TT-C testing machine for the following conditions:

a. Unsegregated, not wetted

b. Segregated, not wetted

c. Unsegregated, wetted

d. Segregated, wetted.

Temperatures from -80°F to +350°F were attained in an Instron environmental chamber and temperatures above +350°F were achieved in a quartz tube radiation furnace equipped with an automatic temperature controller. Special wedge type grips made out of Inconel were used for high temperature testing. Two gage marks 0.6 in. apart were scribed on all the specimens in order to measure the percent elongation. All the tests were carried out at a crosshead speed of 1.0 inch/min. Stress-extension curves were plotted directly on a stress-time chart on the Instron machine. The speed of the chart could be varied from 0.2 inch/min to 50.0 inch/min. Percent elongations were also calculated from the time scale of the chart. Yield strength, ultimate tensile strength, fracture strength (based on the original area of the specimen) and percent elongation were measured and calculated from the data.

Wetting of the copper alloys was achieved by placing a saturated solution of mercuric chloride on the prepolished specimen surface.[41,42] The mercuric chloride is immediately reduced to metallic mercury by the copper and a thin layer of mercury

is deposited on the copper surface. To ensure an ample supply of mercury for the embrittlement, additional pure metallic mercury (99.999%) was placed in the wetted area.

Experimental Results: Test for Cu-0.0% Bi were carried out at various temperatures for the four different conditions mentioned above and the results are plotted in Figs. 69 through 74. Fig. 69 shows the strength and elongation vs. temperature for the unsegregated-unwetted alloy. The strength as well as the ductility decreased as the temperature increased. The strength and ductility of the segregated-unwetted samples (Fig. 70) were somewhat less than for the first condition. For example at 50°F an unsegregated-unwetted specimen showed 52.5% elongation as compared to 50.0% for segregated-unwetted samples. This difference (2.5 - 3%) remained uniform at all temperatures. Similarly, an unsegregated-unwetted sample had a fracture strength of 28.0 ksi as compared to 26.5 ksi for the segregated-unwetted one. The strength differences decreased as the temperature decreased.

Fig. 71 shows the relationships between strength and ductility as a function of temperature for unsegregated-wetted samples. Both the fracture stress and elongation decreased on wetting. Comparing the elongations with those of unsegregated unwetted specimens, the difference was a maximum around 300°F. Above 300°F there was no further decrease in ductility but rather a recovery so that a brittle-to-ductile LME transition was observed.

Fig. 72 shows the corresponding relationship for segregated-wetted samples. Here again, on wetting, the strength and ductility decreased but the decrease here was more than that for unsegregated-wetted samples. For example at 150°F (Fig. 73) ductility decreased from 46.5% to 19.0% on wetting in the unsegregated condition, i.e., a decrease of 60% from the unwet condition. On the other hand, in the segregated state, the elongation decreased from 45.5 % to 12.0% i.e., a decrease of 74% from the unwet condition. Similar behavior was observed with fracture stress.

For example at 150°F fracture stresses were 31.0, 30.0, 28.5 and 26.5 ksi for unsegregated-unwetted, segregated-unwetted, unsegregated-wetted and segregated-wetted, respectively (Fig. 74). These differences were again maximum around 300°F and seem to decrease at very low and very high temperatures. High temperatures of more than 450°F gave erroneous results because the liquid mercury evaporated (B.P. = 675°F) and for this reason tests were not carried out above 450°F.

At temperatures where the mercury is solid (M.P. -40°F), embrittlement can still be observed. For example at -80°F a segregated-unwetted sample had an elongation at 46.8% while a segregated-wetted one had an elongation of 41.0%. Numerous secondary cracks were observed at temperatures below the melting point of mercury as compared to two or three primary cracks at higher temperatures. This verifies the belief that below freezing point LME is controlled by the process of crack propagation and above freezing point LME is controlled by crack nucleation.

Future Work: Tensile tests at various temperatures will be carried out for Cu-0.005% Bi, Cu-0.0025 wt.% Bi, Cu-1% Sb and Cu-3.0% Sn. This will aid in evaluating the effect on LME of the amount of bismuth present on the grain boundaries and the severity of the impurity. All the alloys will be rolled and annealed so as to produce about the same grain size as that of the Cu-0.01% Bi alloy. Also by varying percentage deformation and annealing times and temperatures the grain size of the Cu-0.005 wt.% Bi alloy will be varied, thus changing the amount of impurity/grain boundary area. The effect on LME of this parameter will be evaluated. Similar studies will be carried out on other selected binary alloys.

REFERENCES

1. M. A. Brimi and J. R. Luck, Electrofinishing, American Elsevier Publishing Co., Inc., N. Y. 1965.

2. N. M. Geyer, G. W. Lawless, and B. Cohen, "A New Look at the Hydrogen Embrittlement of Cadmium Coated High Strength Steel," Hydrogen Embrittlement in Metal Finishing (edited by H. J. Read), Reinhold, N. Y. 1961, p. 109.

3. K. Farrell and A. G. Quarrell, "Hydrogen Embirttlement of an Ultra-High Tensile Steel," JISI, Vol. 202, 1964, p. 1002.

4. Y. Iwata, Y. Asayama, and A. Sakamoto, "Delayed Failure of Cadmium Plated Steels at Elevated Temperatures," Journal of the Japan Institute of Metals, Vol. 31, 1967, p. 77.

5. D. N. Fager and W. F. Spurr, "Solid Cadmium Embrittlement: Titanium Alloys," Corrosion, Vol. 24, Oct. 1969, p. 409.

6. D. N. Fager and W. F. Spurr, "Solid Cadmium Embrittlement: Steel Alloys," Corrosion, Vol. 27, Feb. 1971, p. 72.

7. J. R. Low, Jr., D. F. Stein, A. M. Turkals and R. P. Laforce, "Alloy and Impurity Effects on Temper Brittleness of Steel," Trans. AIME, Vol.242, 1968, p. 14.

8. C. J. McMahon, Jr., "Temper Brittleness - An Interpretive Review," Temper Embrittlement in Steel, ASTM STP 407, 1968, p. 127.

9. R. Viswanathan, "Temper Embrittlement in a Ni-Cr Steel Containing Phosphorous as Impurity," Met. Trans., Vol. 2, 1971, p. 809.

10. J. B. Cohen, A. Hurlich, and M. Jacobson, "A Metallographic Etchant to Reveal Temper Brittleness in Steel," Trans. ASM, Vol. 39, 1947, p. 109.

11. A. Joshi and D. F. Stein, "Temper-Brittleness of Low Alloy Steels," ASTM STP 499, 1972.

12. S. Dinda and W. R. Warke, "The Effect of Structural Metal Purity on LME," Second Annual Progress Report, Environmental Sensitivity of Structural Metals: Liquid Metal Embrittlement, Contract No. DAAA-25-69-C0608, Illinois Institute of Technology, 1971.

13. S. Mostovoy and N. N. Breyer, "The Effect of Lead on the Mechanical Properties of 4145 Steel," Trans. ASM, Vol. 61, June 1968, p. 219.

14. W. Rostoker, J. M. McCaughey, and H. Markus, Embrittlement by Liquid Metals, Reinhold Publishing Corporation, New York, 1960.

15. M. B. Ives and P. C. Hancock, U. S. Govt. Rept. AD 657 376, 1967 as quoted by reference 19.

16. A. Kelly, W. R. Tyson, and A. H. Cottrell, Phil. Mag., Vol. 15, 1967, p.567.

17. N. S. Stoloff and T. L. Johnston, Acta Met., Vol. 11, 1963, p. 251.

18. A. R. C. Westwood and M. H. Kamdar, Phil. Mag., Vol. 8, 1963, p. 787.

19. S. J. Cytron, J. V. Rinnovatore, and J. D. Corrie, unpublished report, Frankford Arsenal, April 1971.

20. F. A. Shunk, "Constitution of Binary Alloys, Second Supplement," p. 289, McGraw-Hill Book Co., New York, 1969.

21. C. G. Miller and R. D. Larsen, Journal of Computational Physics, Vol. 7, 1971, p. 465.

22. S. Mostovoy, et al., Journal of Materials, Vol. 2, 1967, p. 661.

23. K. H. Buchner, M. S. Thesis, May 1971, Illinois Institute of Technology, Chicago.

24. R. D. Zipp, W. R. Warke, and N. N. Breyer, "A Comparison of Elevated Temperature Tensile Fractures in Non-Leaded and Leaded 4145 Steel," Electron Microfractography, ASTM STP 453, American Society for Testing and Materials, pp. 111-133, 1969.

25. W. R. Warke and N. N. Breyer, "The Effect of Lead on Microcrack Initiation and Propagation in Alloys Steels," Final Report - Phase II, Contract No. DA-20-113-AMC-10820(T), Illinois Institute of Technology, 1969.

26. K. L. Johnson and N. N. Breyer, "The Effect of Purity on the Embrittling Liquid Metal," Second Annual Progress Report, Contract No. DAAA-25-69-C0608, Illinois Institute of Technology, 1971.

27. S. Dushman, Scientific Foundations of Vacuum Technique, Laferty, J. M. (editor), John Wiley and Sons, Inc., New York, N. Y. Oct. 1966.

28. Work in progress at Illinois Institute of Technology.

29. J. H. Westbrook, "Segregation at Grain Boundaries," Met. Rev., Vol. 9, No. 36, 1964, p. 415

30. M. Barlow and P. J. Plating, "Wetting of Metal Surfaces by Liquid Alkali Metals," Z. Metallkde, Vol. 60, 1969, p. 719.

31. E. A. Lee [illegible]. Gregory and R. Eborall, "A Hot Impact Tensile Test and its Relation to Hot Working Properties," J. Inst. Metals, Vol. 83, 1954-55, p. 347.

32. E. Voce and A. C. Hallows, "The Mechanism of the Embirttlement of De-oxidized Copper by Bismuth," J. Inst. Metals, Vol. 73, 1947, p. 323.

33. T. H. Schofield and F. W. Cuckow, "The Microstructure of Deoxidized Copper Containing Small Quantities of Bismuth," J. Inst. Metals, Vol. 73, 1947, p. 377.

34. E. C. W. Perryman, "Microscopical Examination of Tin Bronzes in γ-range," Trans. AIME, Vol. 197, 1953, p. 906.

35. D. W. D. Showell, "Hot Working of Tin Bronzes," J. Inst. Metals, Vol. 76, 1949-1950, p. 527.

36. D. McLean, "The Embrittlement of Cu-Sb Alloys at Low Temperatures," J. Inst. Metals, 1952, p. 121.

37. L. M. T. Hopkins, "Intergranular Brittleness of Single Phase Cu-Sb Alloys," J. Inst. Metals, Vol. 84, 1955-56, p. 102.

38. A. R. Bailey, R. McDonald and L. E. Samuels, "The Effect of High and Low Temperature on the Notched Bar Characteristics of a Cast High Tensile Brass," J. Inst. Metals, Vol. 89, Sept. 1956, p. 25.

39. A. Joshi and D. F. Stein, "An Auger Spectroscopic Analysis of Bismuth Segregated to Grain Boundaries in Copper," J. Inst. Metals, Vol. 99, 1971, p. 178.

40. J. H. Westbrook and S. Floreen, "Grain Boundary Segregation and Grain Size Dependence of Strength of Ni-S Alloys, Acta Met, Sept. 1969, Vol. 17(a), p. 1175.

41. H. Nichols and W. Rostoker, "Delayed Failure of a Be-Cu Alloy Wetted with Mercury," Trans. ASM, Vol. 58, 1965, p. 155.

42. J. V. Rinnovatore, J. D. Corrie and H. Markus, "The Effect of Grain Boundary Penetration on the Delayed Failure of Cu-2% Be," Trans. ASM, Vol. 59, 1966, p.665.

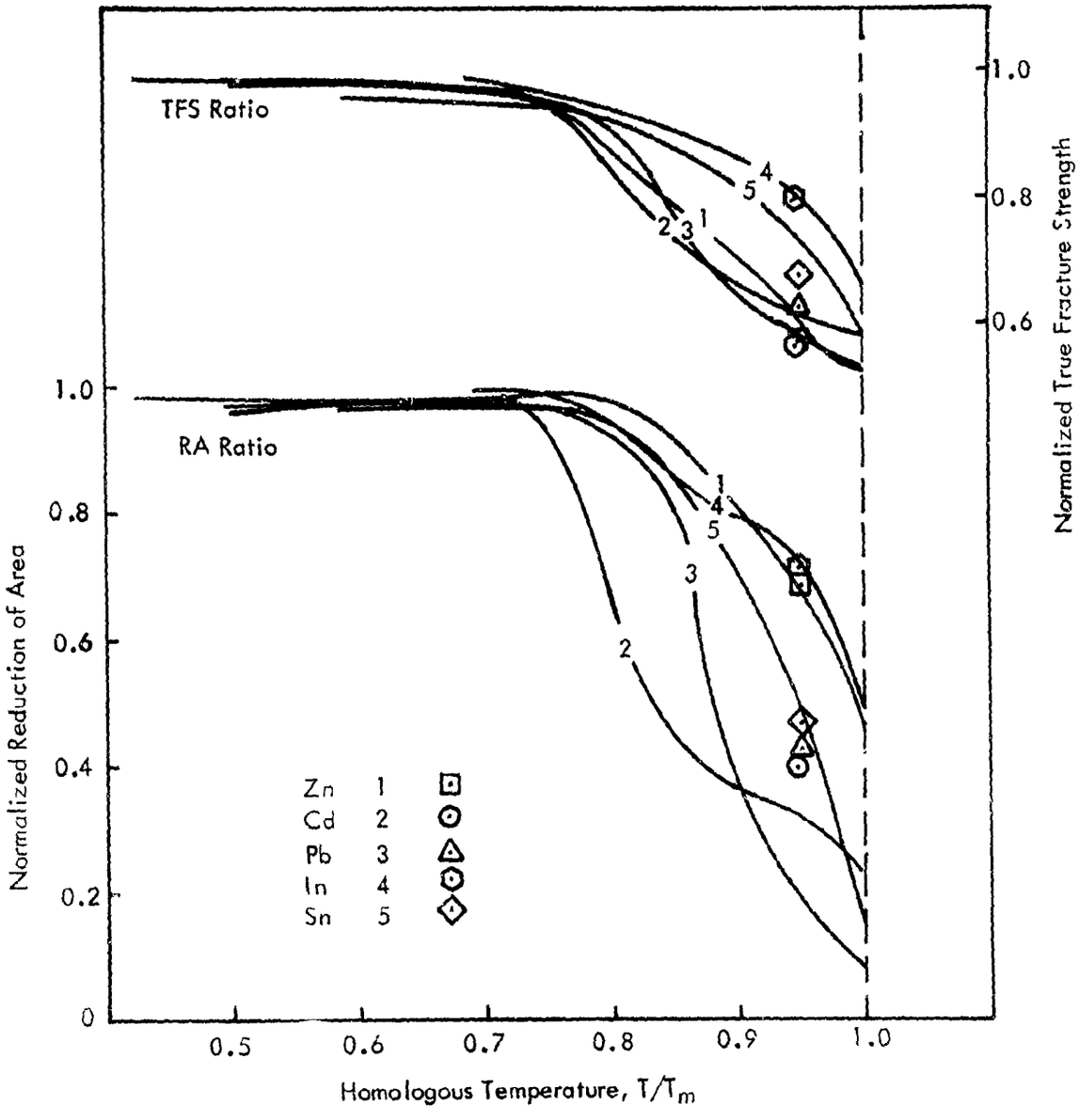

Fig. 1. Comparison of Normalized True Fracture Strength and Reduction of Area as a Function of Homologous Temperature for 4140 Steel Surface Wetted as Indicated. The data points represent those specimens which were wetted circumferentially.

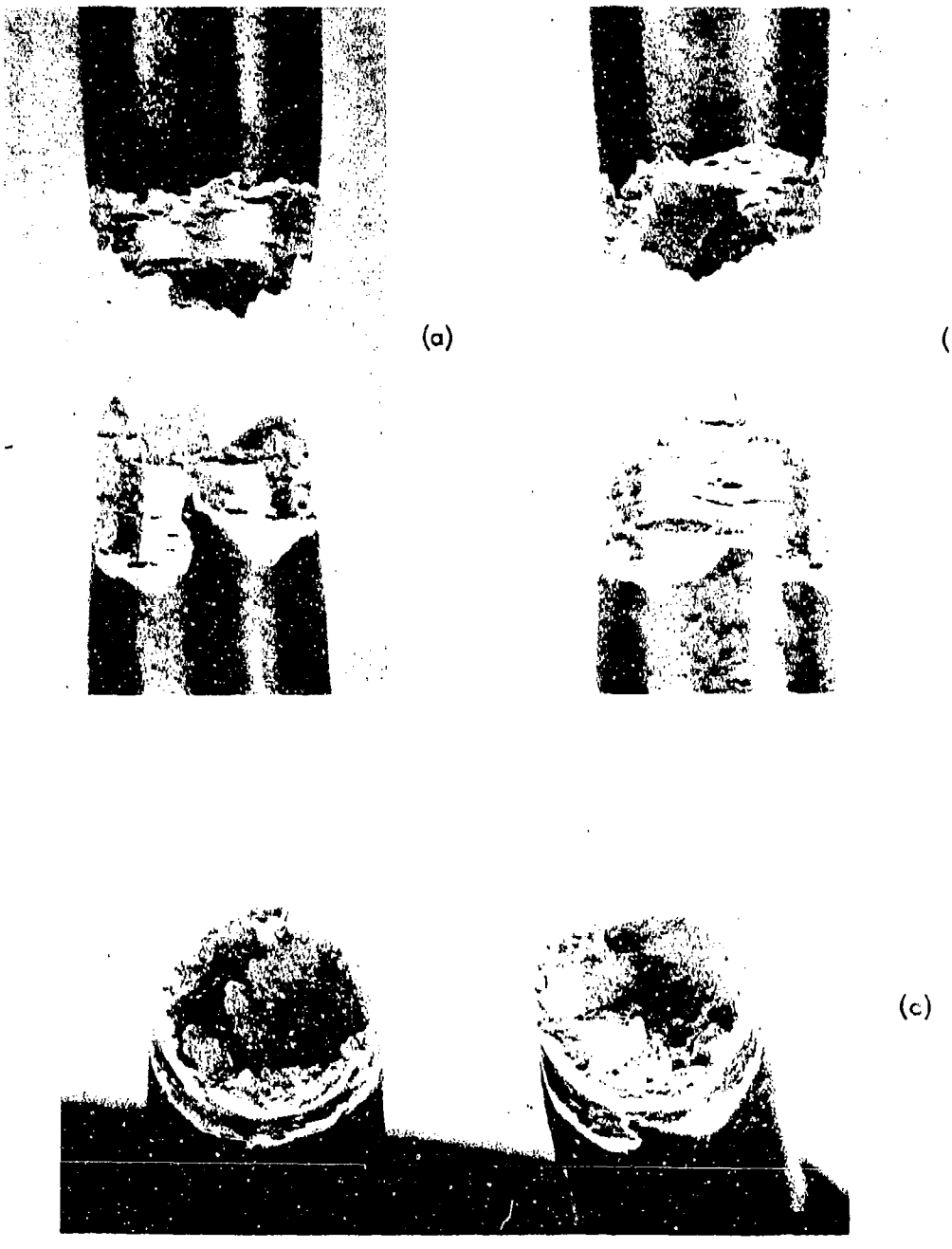

Fig. 2. Cadmium Embrittlement of Steel

Specimen Condition: B-13, Surface Wetted with Cadmium Circumferentially and Tested at 550-563/m.p. 610°F

(a), (b) and (c) Fracture Surfaces of the Specimen, 6X

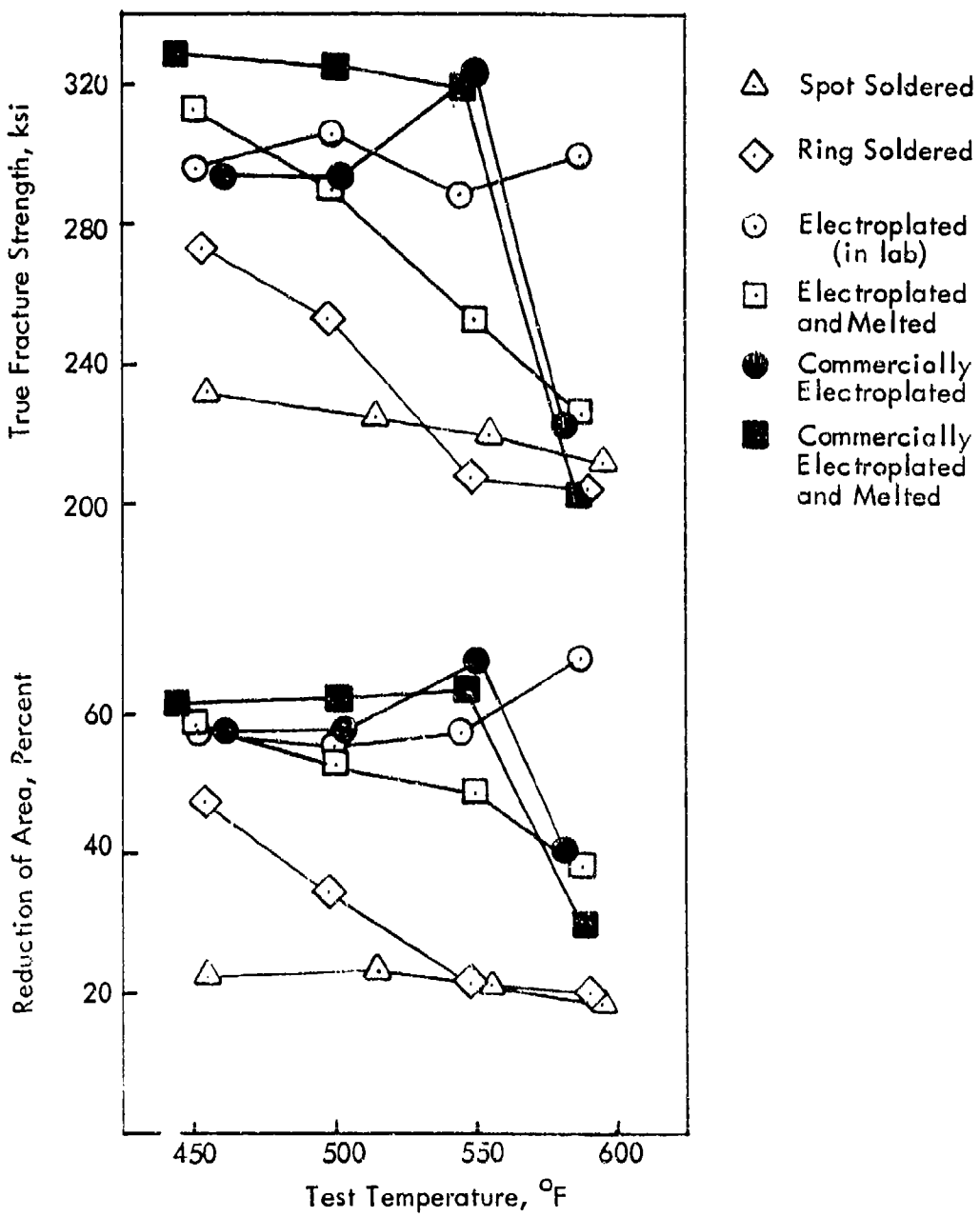

Fig. 3. Elevated Temperature Tensile Properties of 4140 Steel at 200 ksi RT Nominal Strength Level, and Surface Coated with Pure Cadmium by Various Methods as Indicated.

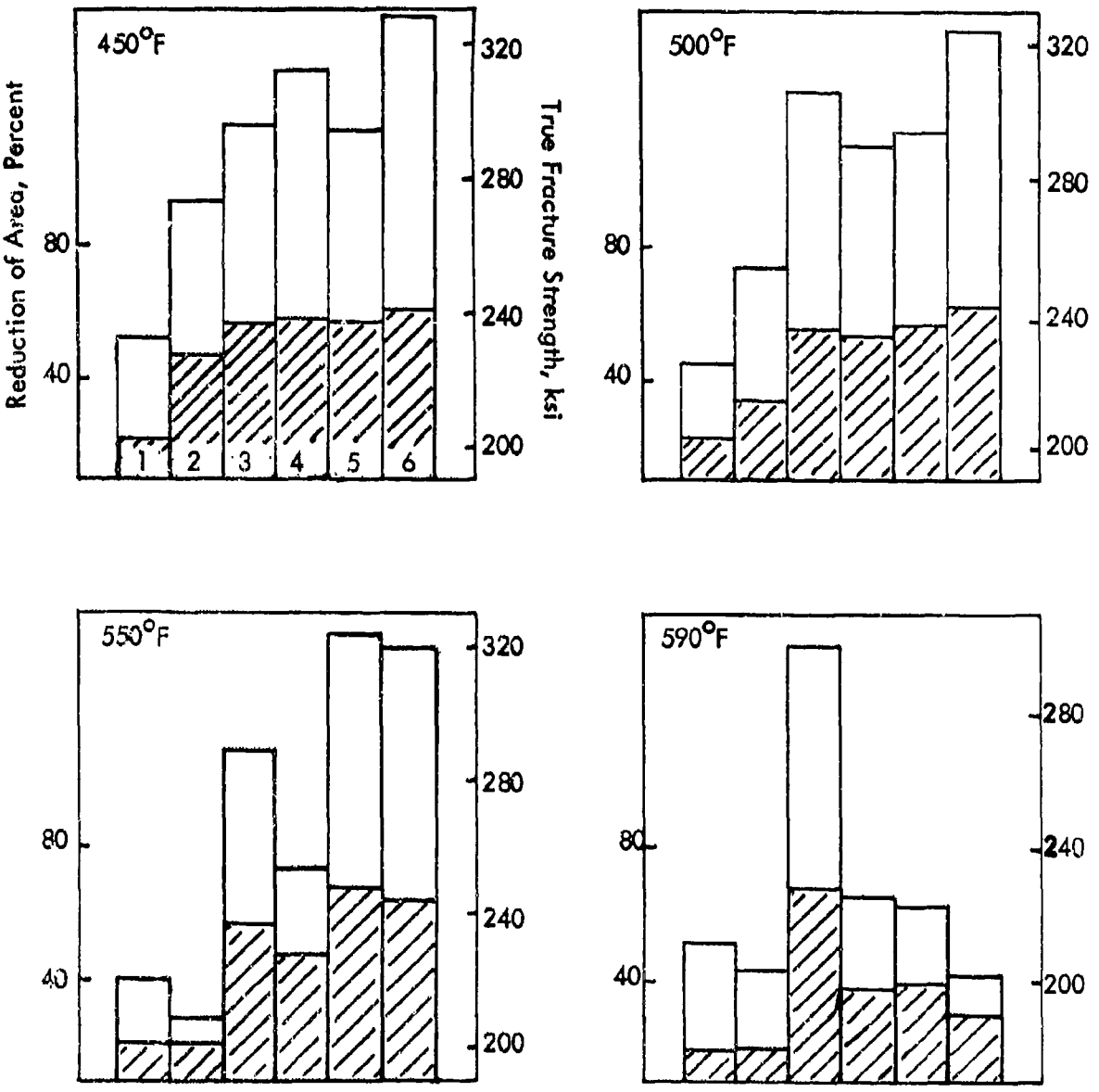

Fig. 4. Tensile Properties of 4140 Steel at 200 ksi RT Nominal Strength Level, Surface Coated with Pure Cadmium by Various Methods as Indicated, and Tested at Four Temperatures (Cross-hatched areas are values for reduction of area).

1. Spot Soldered
2. Ring Soldered
3. Electroplated in Lab.
4. Electroplated and then Melted
5. Commercially Electroplated
6. Commercially Electroplated and then Melted

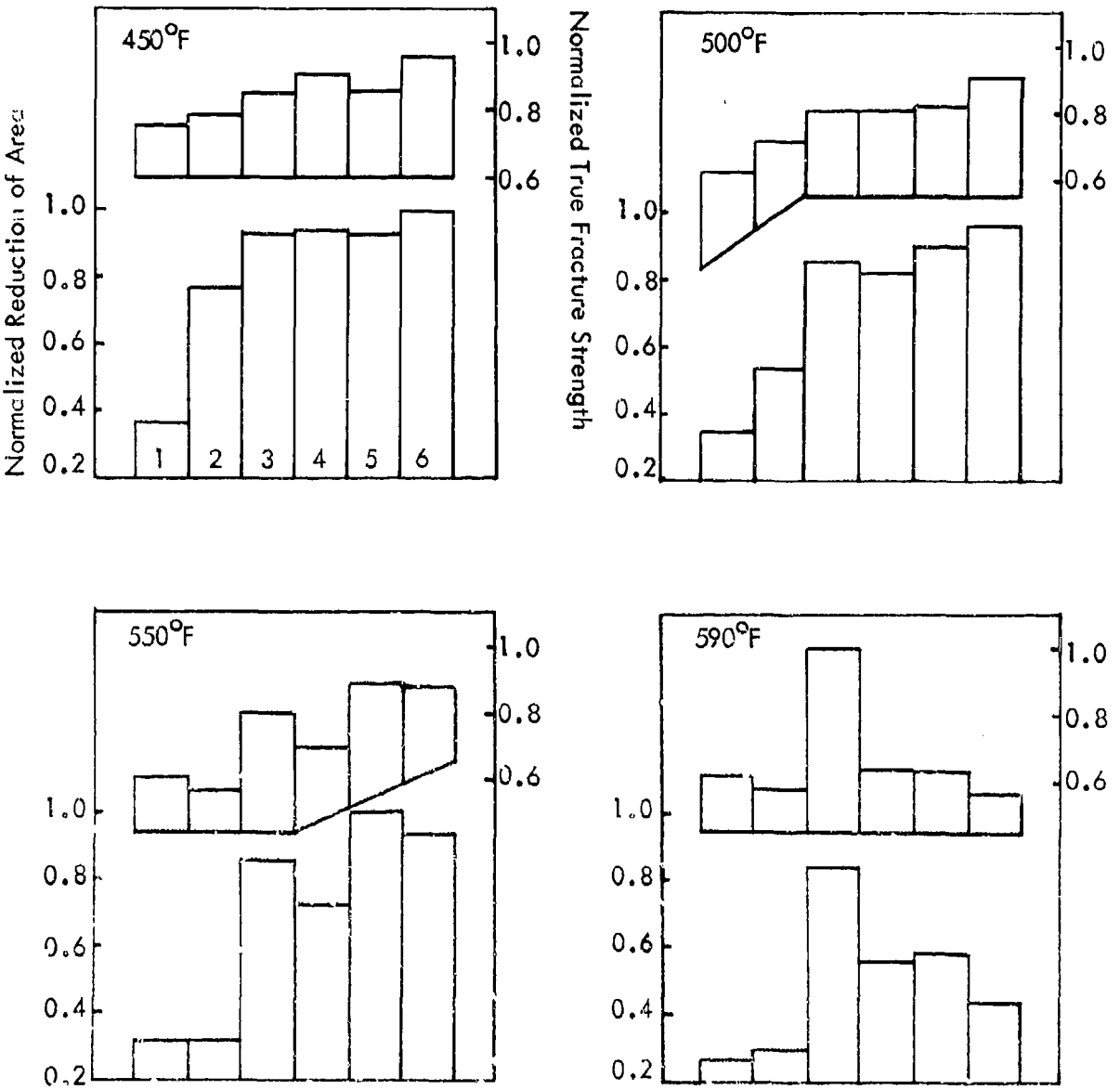

Fig. 5. Comparison of Cadmium Embrittlement of Steel at Four Temperatures. Specimen Surfaces Were Coated with Pure Cadmium by Various Methods as Indicated.

(Numbers within columns are the same as those in Fig. 4)

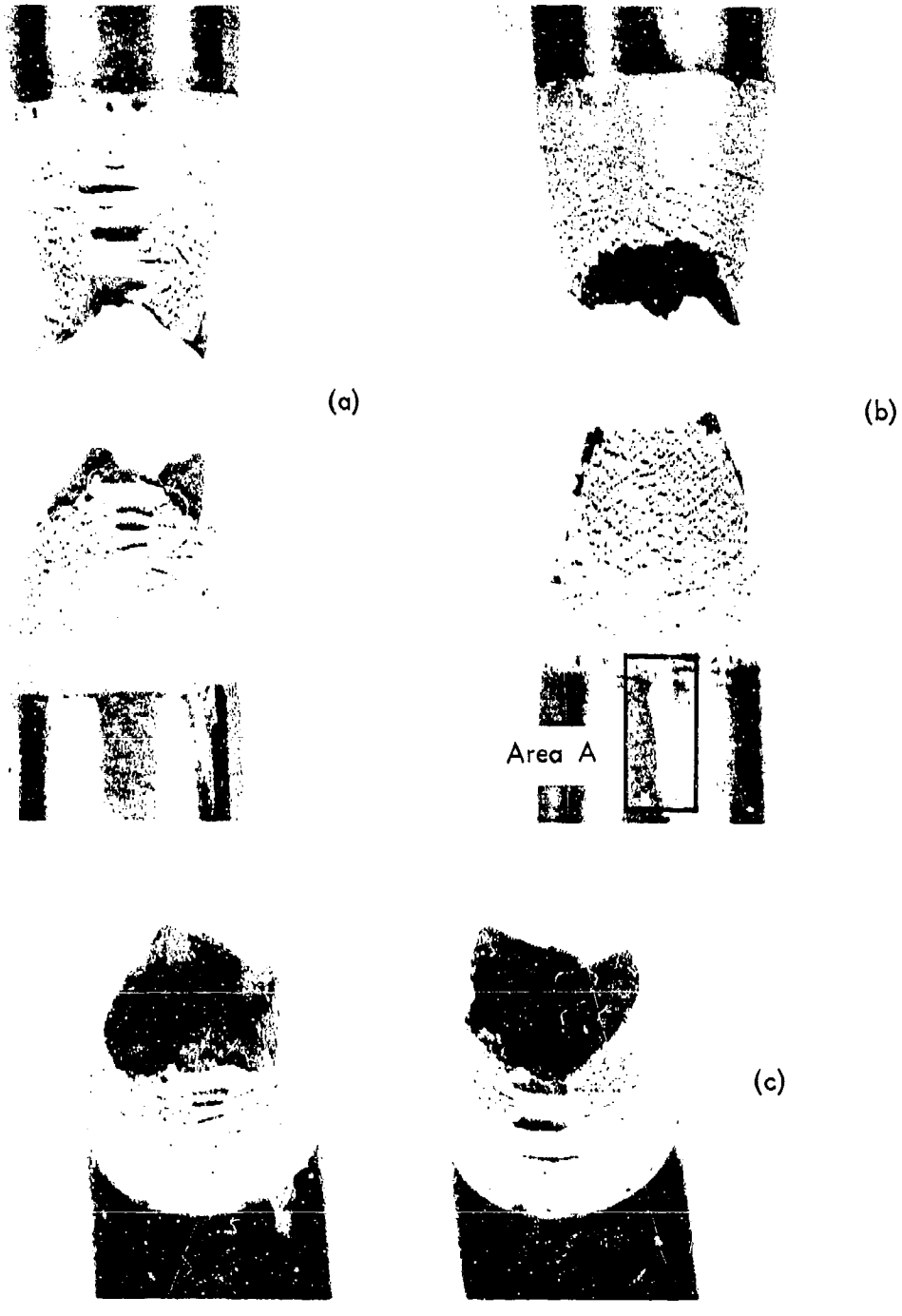

Fig. 6. Cadmium Embrittlement of 4140 Steel

Specimen Condition: B-16, Electroplated with Cadmium and Tested at 585-606/m.p. 610°F

(a), (b) and (c) Fracture Surfaces of the Specimen, 6X

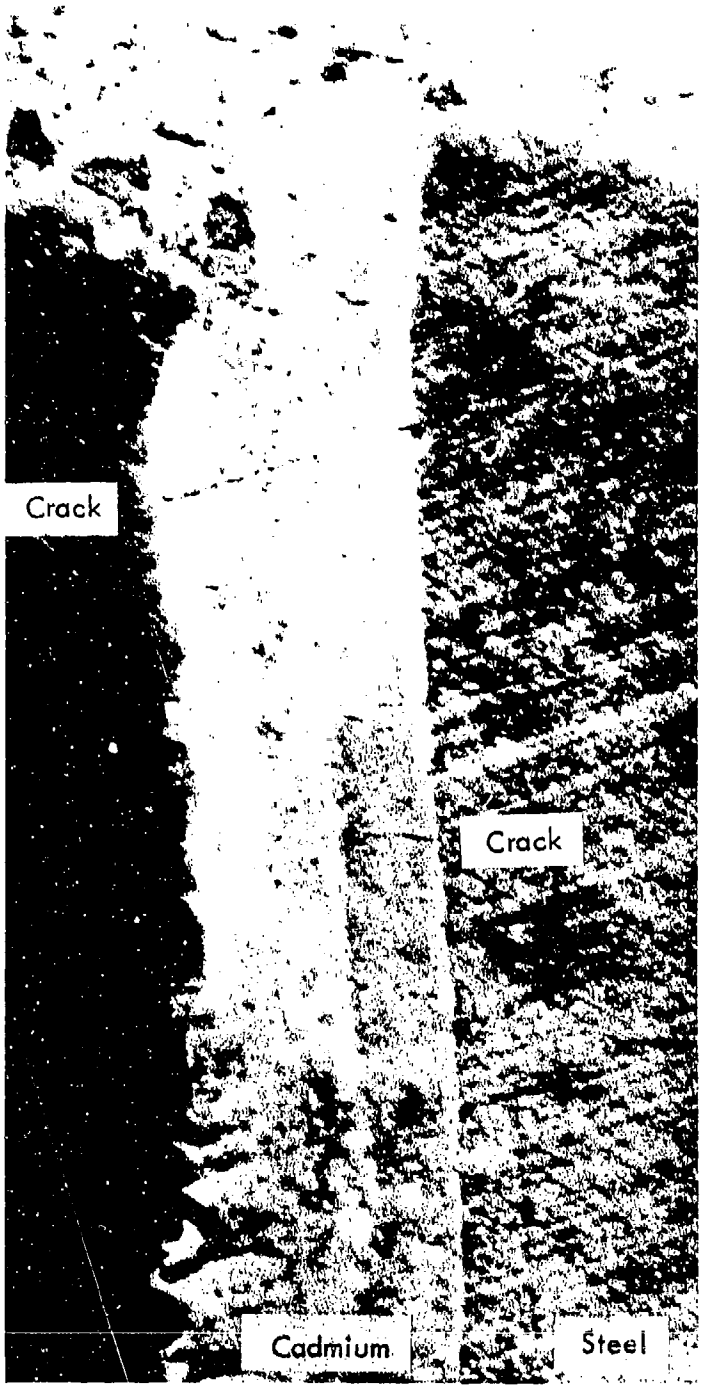

(d)

Fig. 6. (Continued)

(d) Photograph of Area A Indicated in (b), 60X.

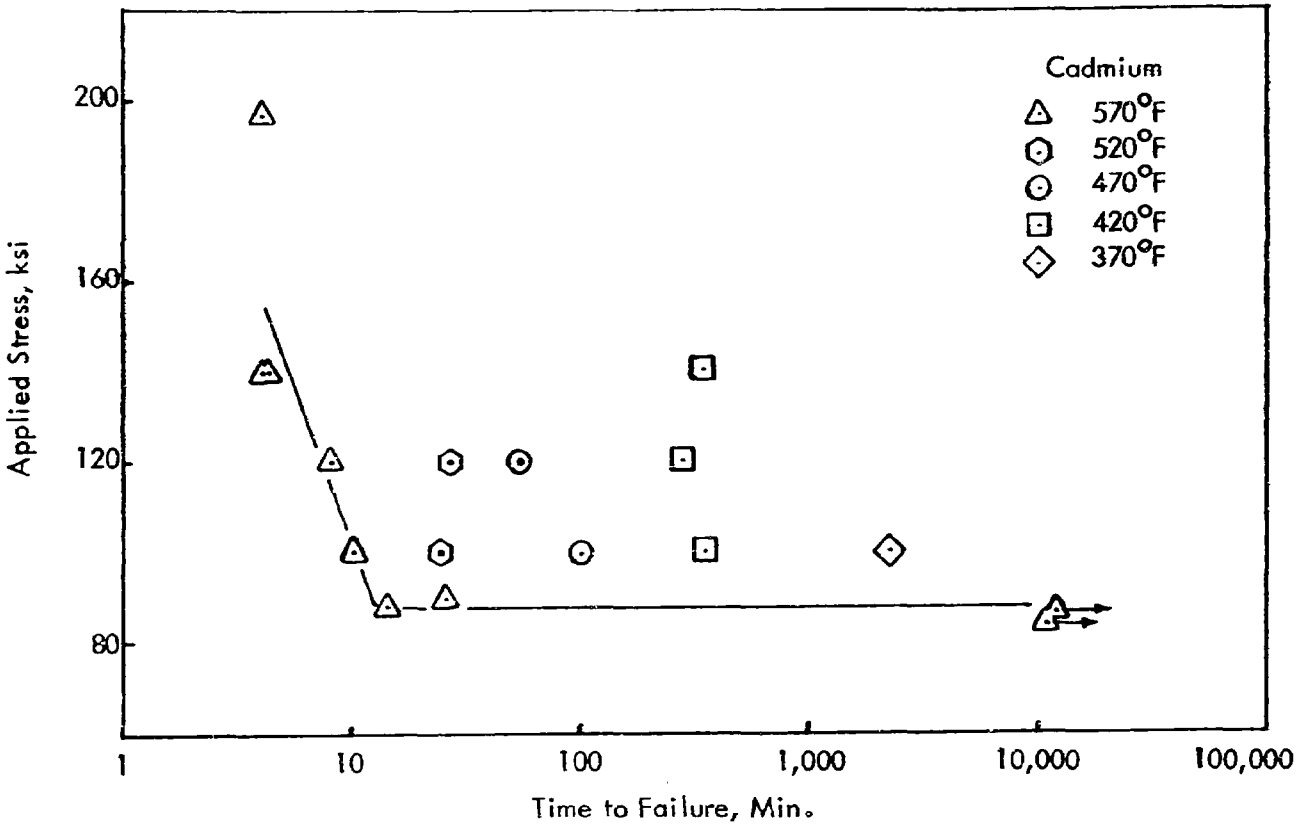

Fig. 7. Delayed Failure of 4140 Steel by Cadmium Tested at Elevated Temperatures as Indicated.

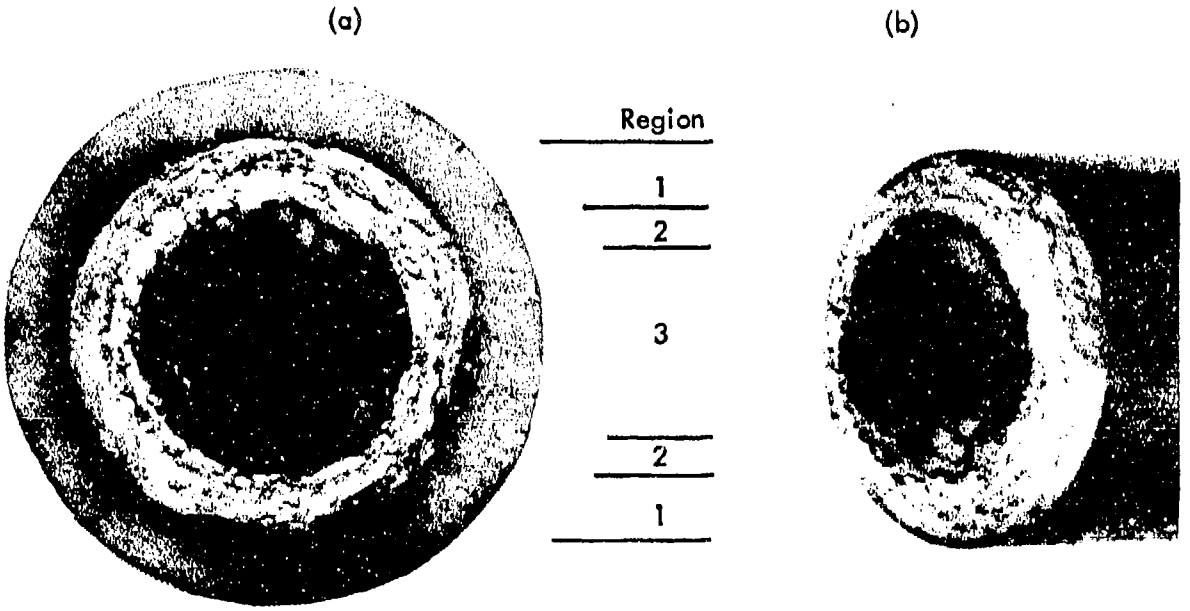

Region 1 - notch and soldered cadmium
2 - slow crack region
3 - fast fracture region

Fig. 8. Delayed Fracture of 4140 Steel by Cadmium
(a), (b) Fracture Surface of the Specimen, 6X.

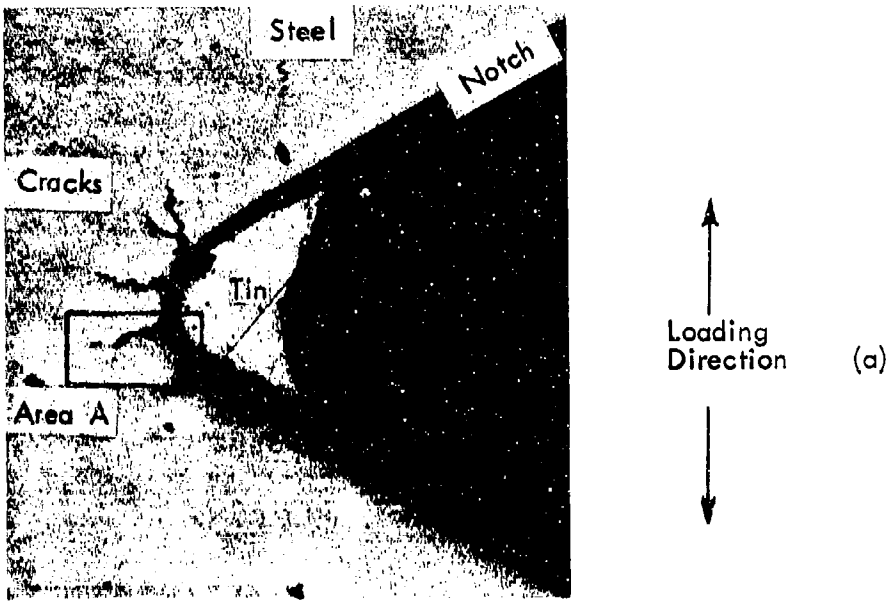

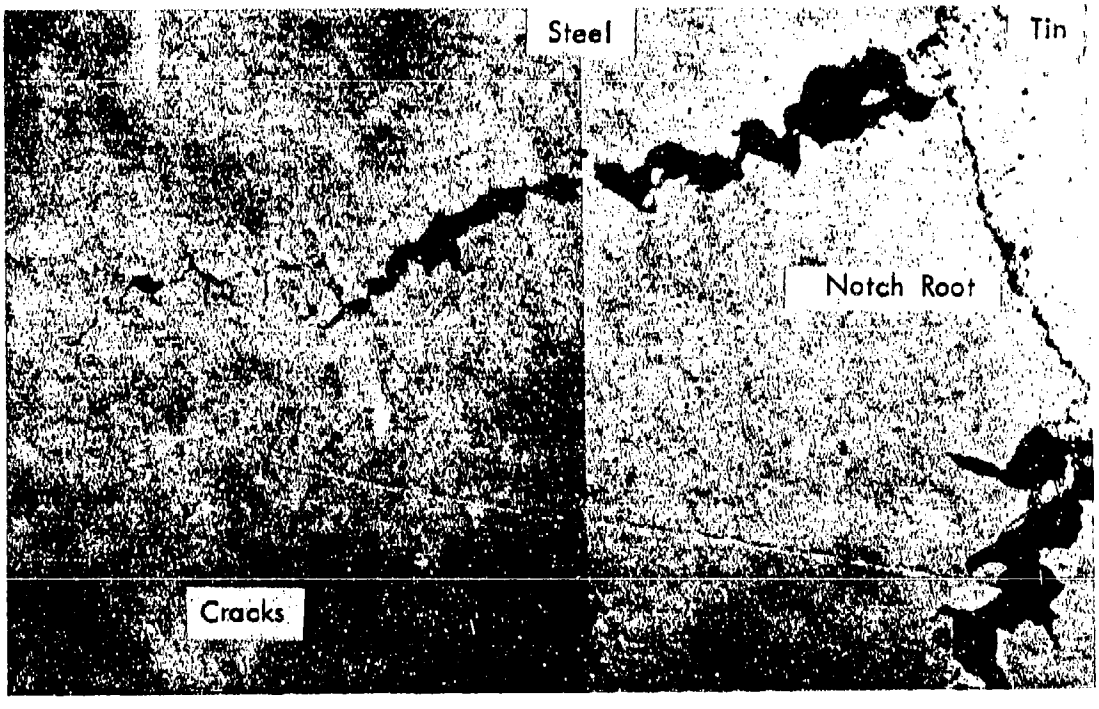

(b)

Fig. 9. Photomicrographs of Longitudinal Section of a Tin Coated Notch Specimen. The Static Loading was Terminated Before the Specimen was Broken.

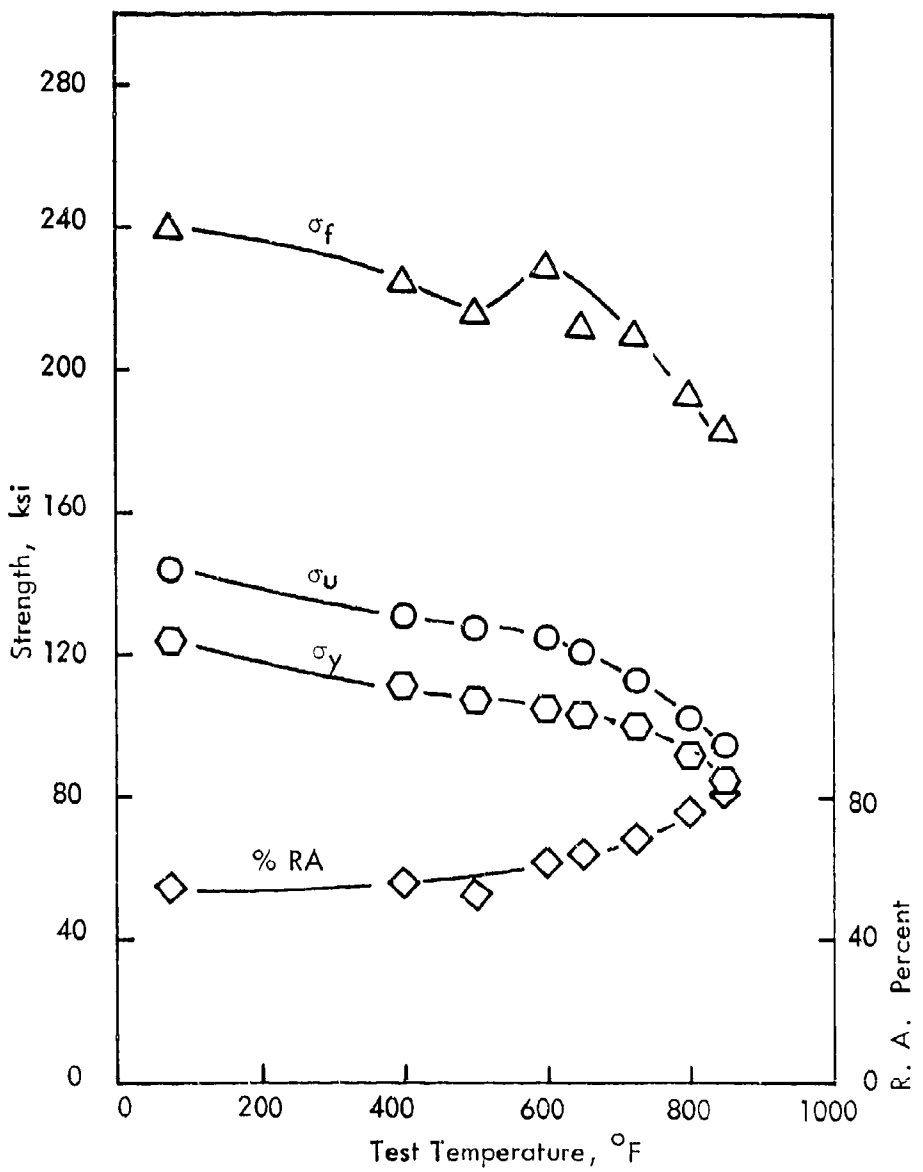

Fig. 10. Elevated Temperature Tensile Properties of Tin Doped Steel in the Unsegregated Condition.

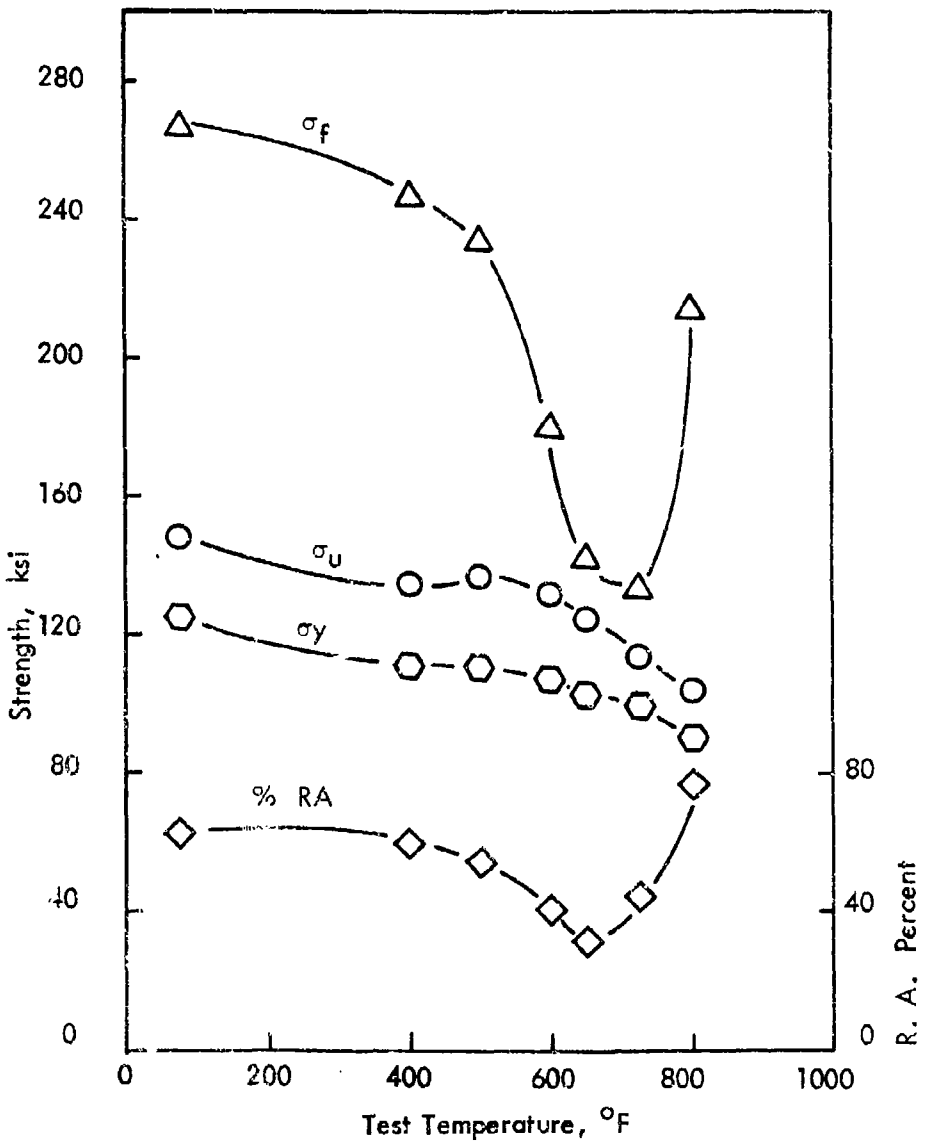

Fig. 11. Elevated Temperature Tensile Properties of Tin Doped Steel in the Unsegregated Condition with Pure Lead Soldered on the Surface.

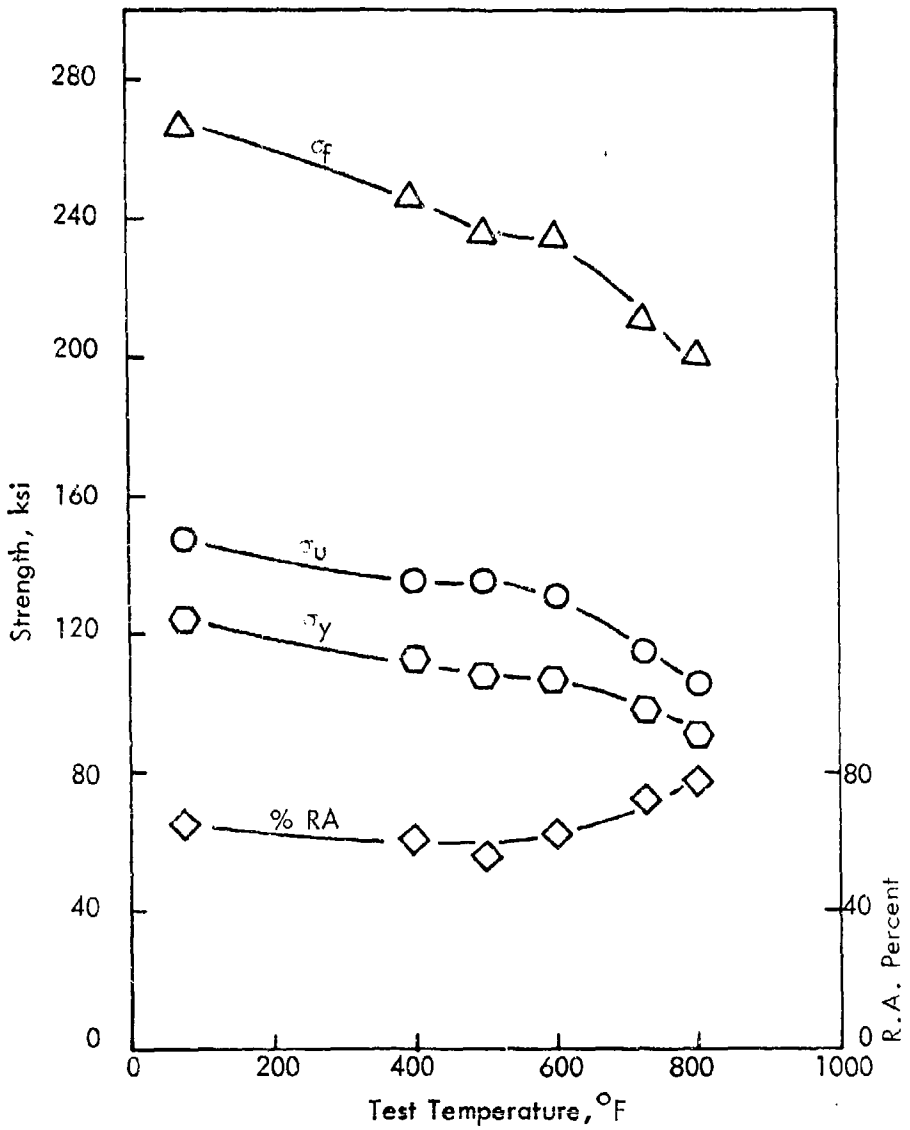

Fig. 12. Elevated Temperature Tensile Properties of Tin Doped Steel in the Segregated Condition.

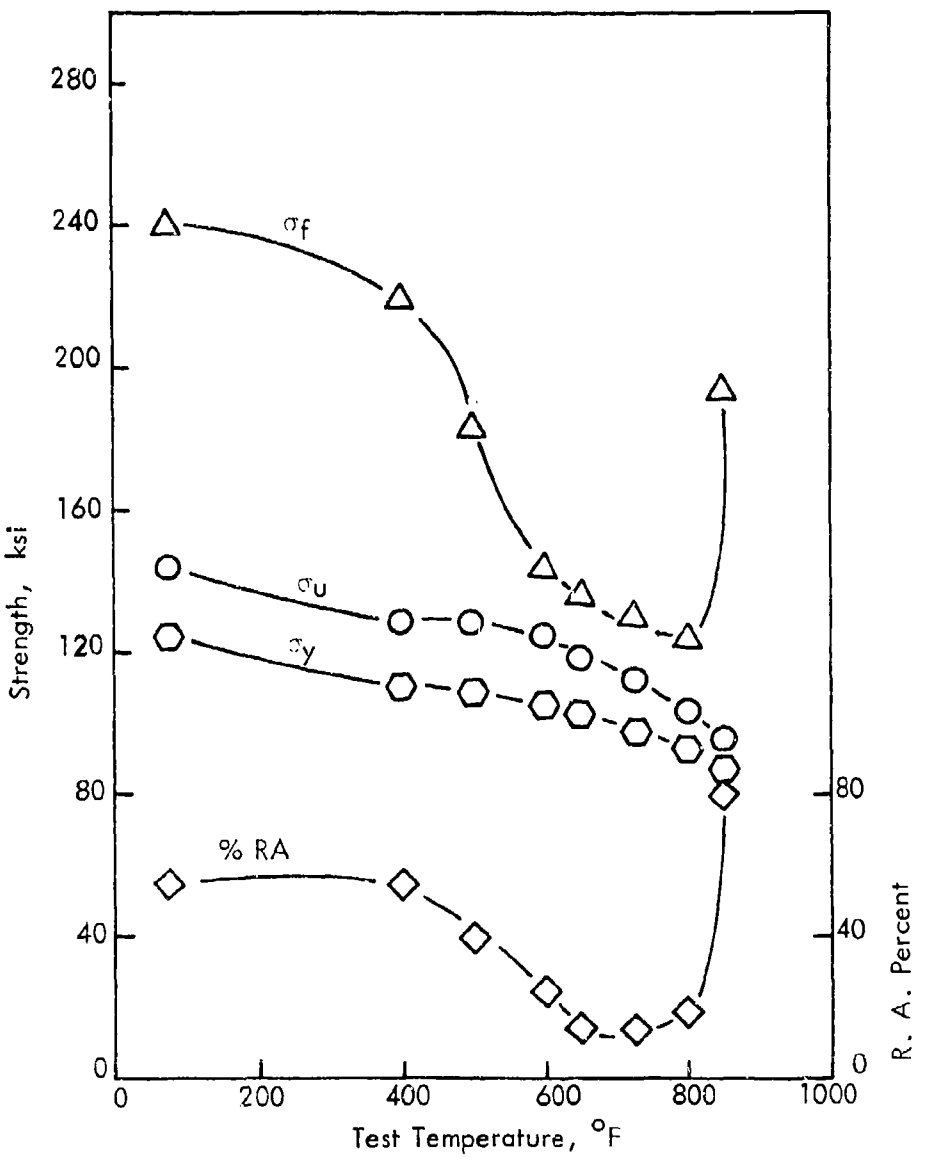

Fig.13. Elevated Temperature Tensile Properties of Tin Doped Steel in the Segregated Condition with Pure Lead Soldered on the Surface.

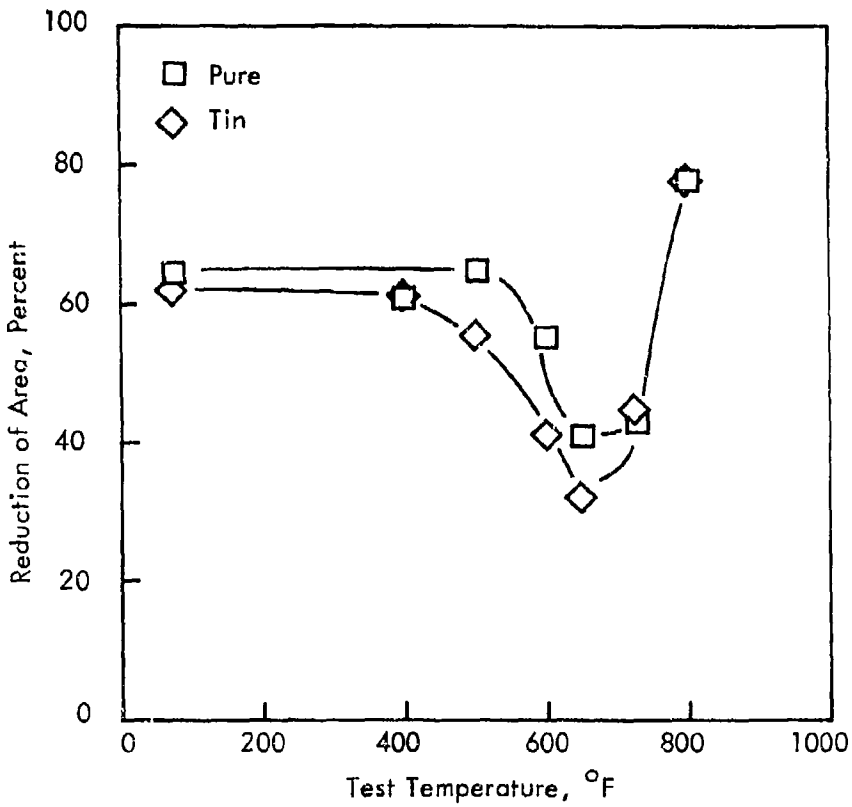

Fig.14. Pure Steel vs. Tin Doped Steel in the Unsegregated Condition with Lead Soldered on Surface.

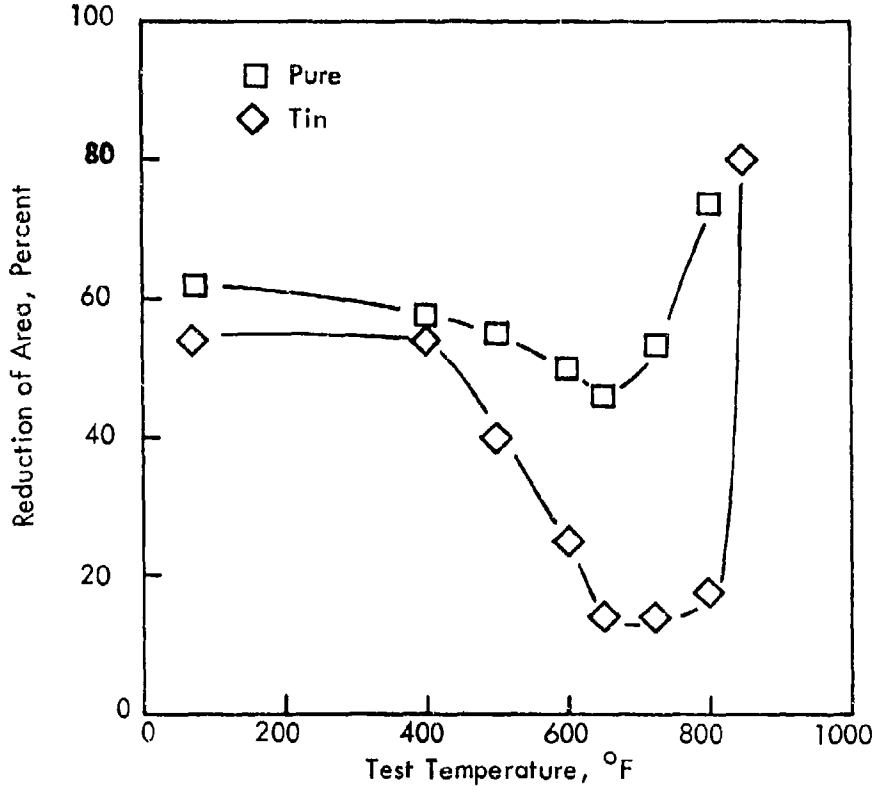

Fig.15. Pure Steel vs. Tin Doped Steel in Segregated Condition with Lead Soldered on Surface.

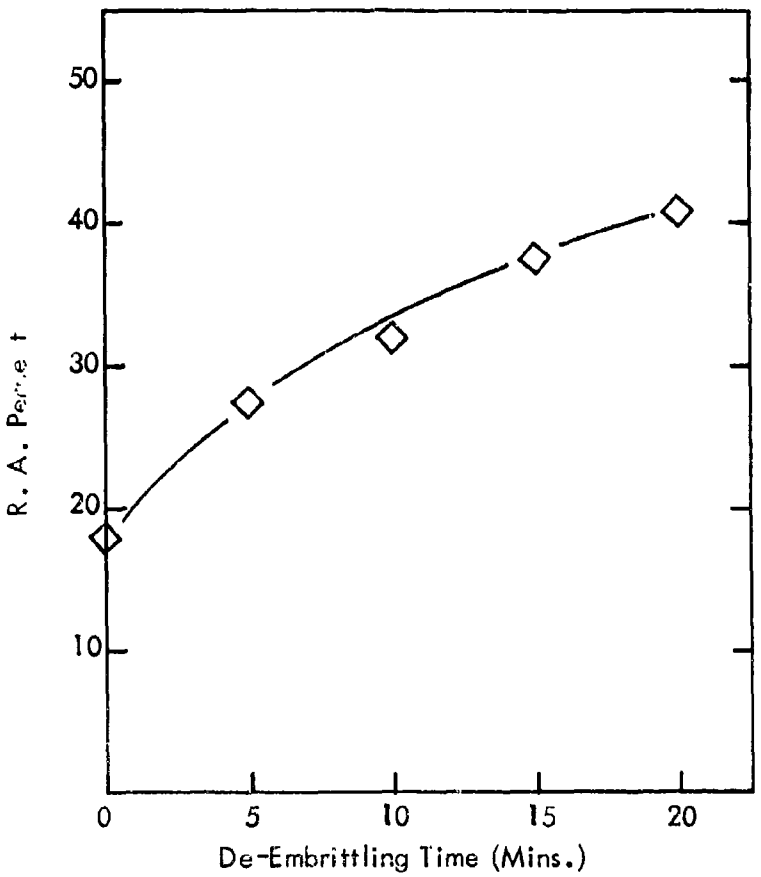

Fig.16. Percentage Reduction of Area vs De-embrittling Time for Tin-Doped Steel with Pure Lead Soldered on the Surface. Tested at 650°F.

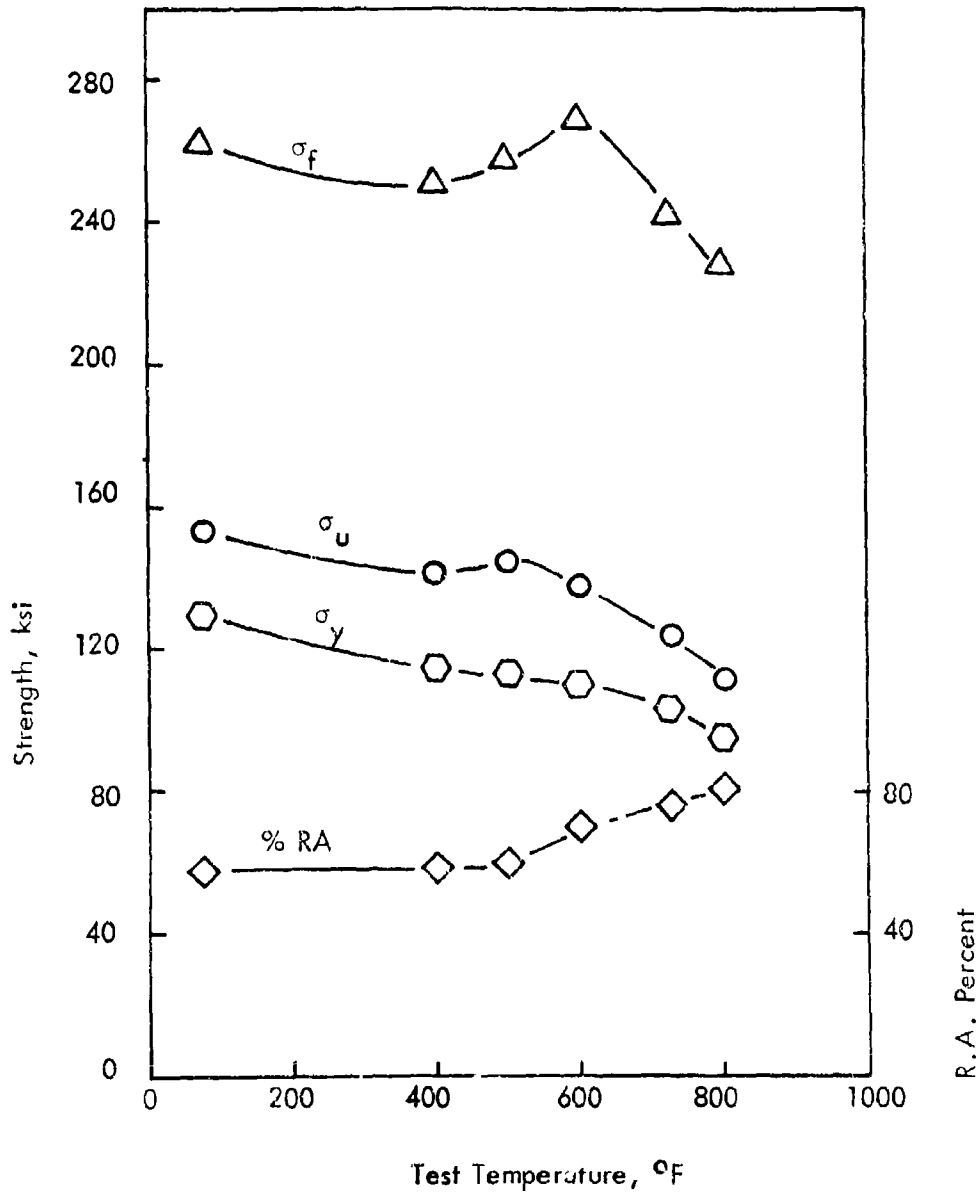

Fig.17. Elevated Temperature Tensile Properties of Phosphorous Doped Steel in the Unsegregated Condition.

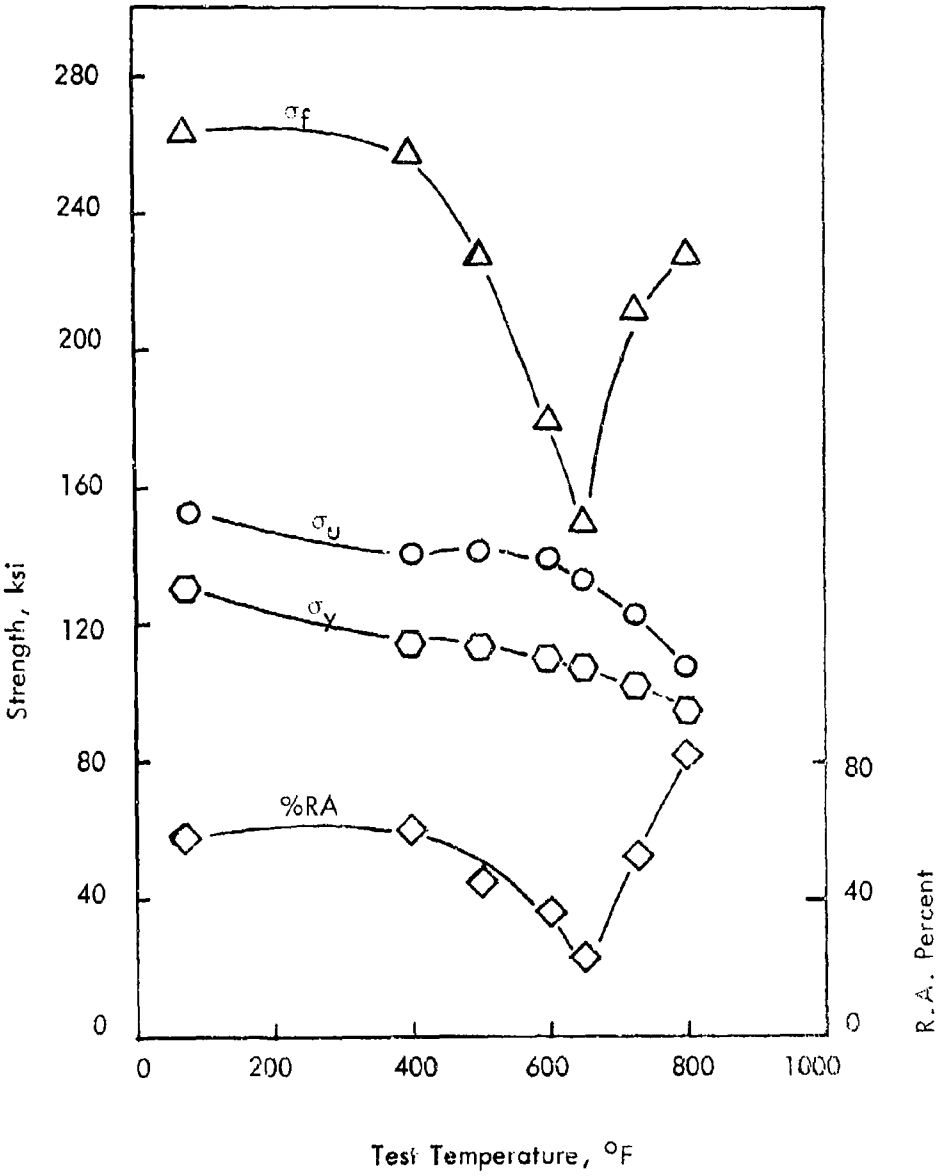

Fig. 18. Elevated Temperature Tensile Properties of Phosphorous Doped Steel in the Unsegregated Condition with Pure Lead Soldered on the Surface.

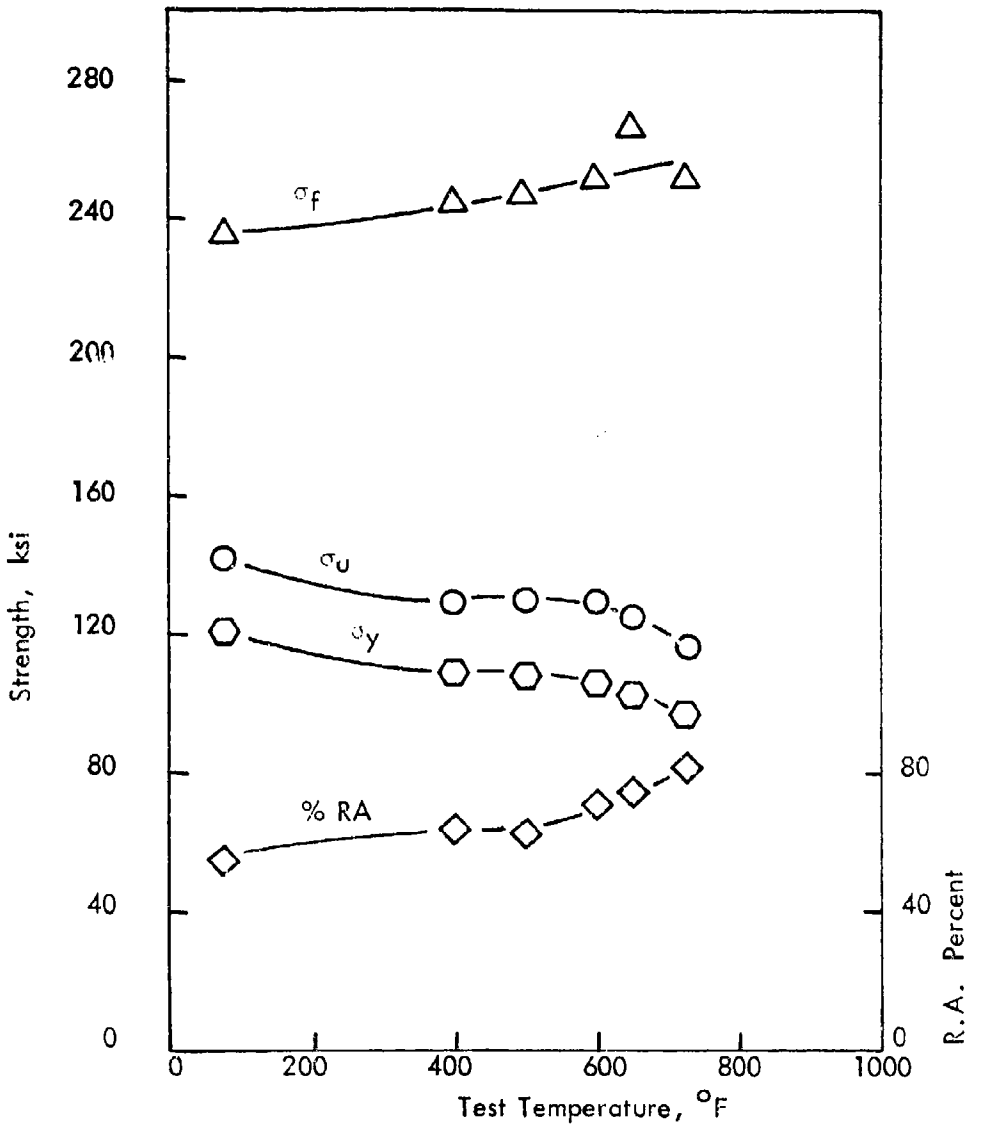

Fig. 19. Elevated Temperature Tensile Properties of Phosphorous Doped Steel in the Segregated Condition.

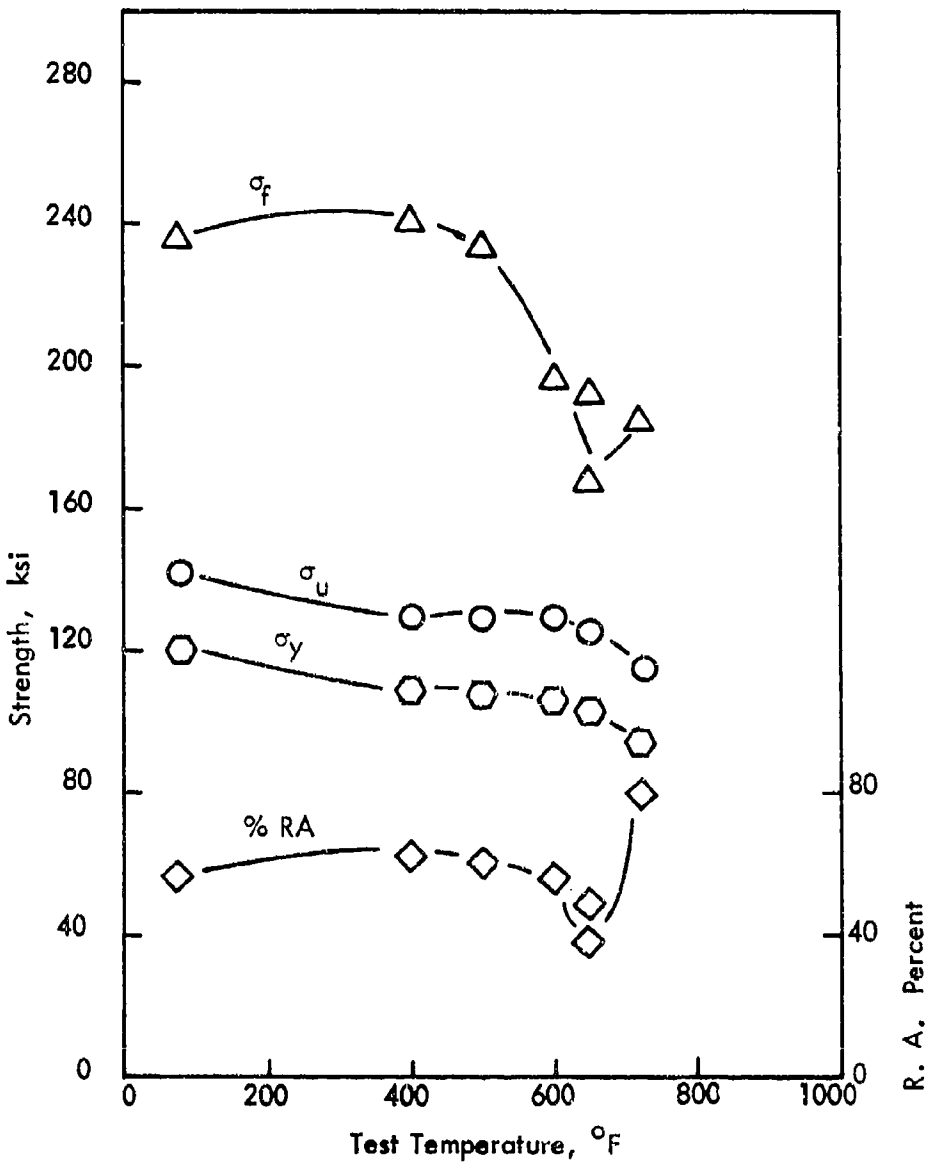

Fig. 20. Elevated Temperature Tensile Properties of Phosphorus Doped Steel in the Segregated Condition with Pure Lead Soldered on the Surface.

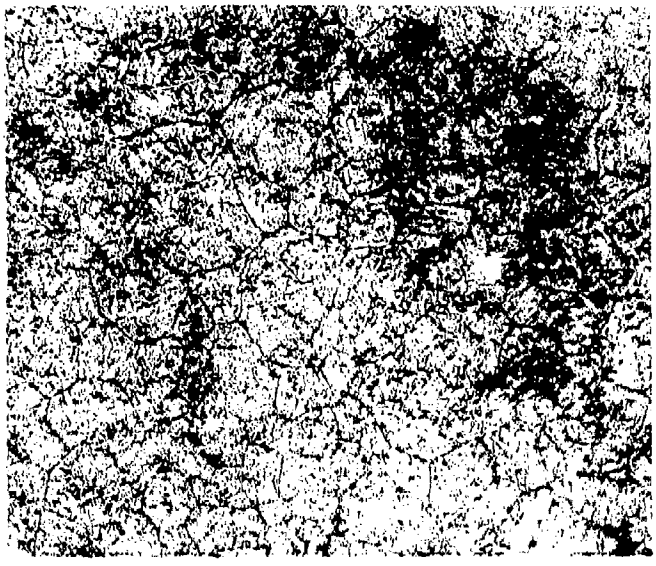

(a) Unsegregated

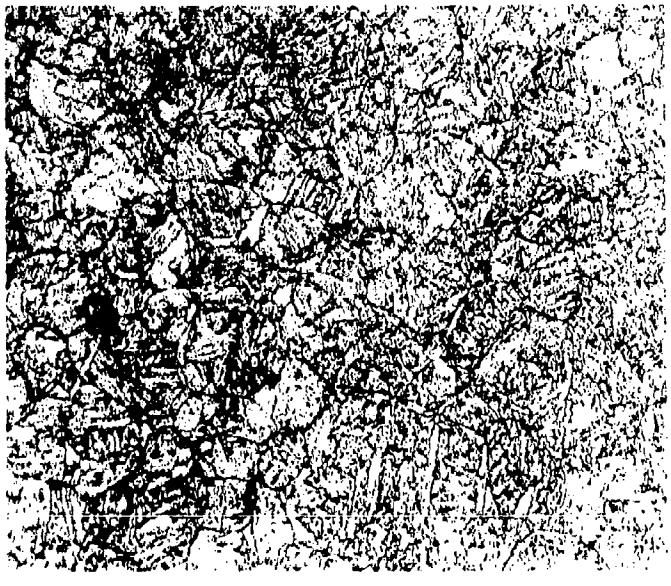

(b) Segregated

Fig. 21. Micrograph of Phosphorous Doped Steel in Two Different Conditions.
Etched with Temper Brittle Reagent. 500X
(a) Unsegregated (b) Segregated

Fig. 22. Micrograph of Phosphorous Doped Steel After Austenitization.
Etched with Temper Brittle Reagent. 500X

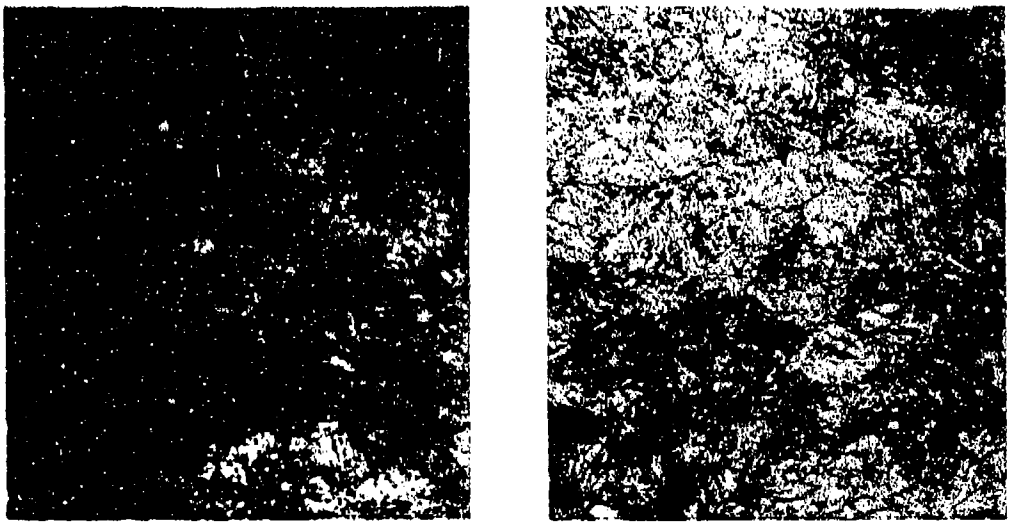

(a) (b)

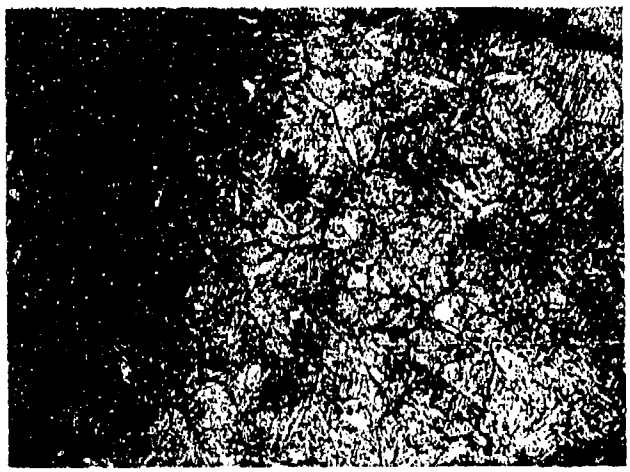

(c)

Fig. 23. Microcraphs of Phosphorous Doped Steel Tempered at Three Different Temperatures.
Etched with Temper Brittle Reagent. 500X
(a) Tempered at 1200°F for 20 minutes
(b) Tempered at 1250°F for 5 minutes
(c) Tempered at 1300°F for 5 minutes

Fig. 24. Micrographs of Phosphorous Doped Steel.
De-Embrittled at 1157°F for 1 Hour.
Etched with Temper Brittle Reagent. 500X

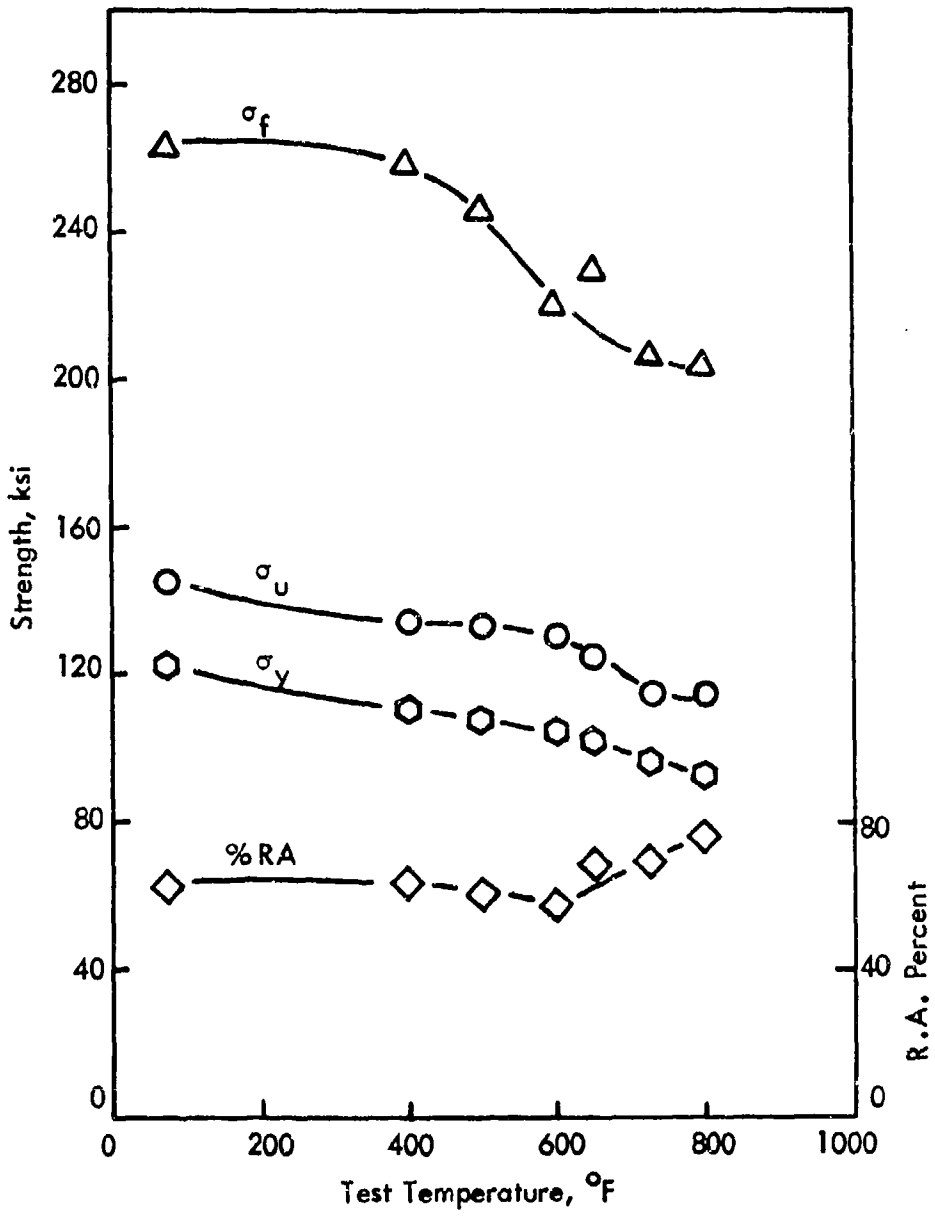

Fig. 25. Elevated Temperature Tensile Properties of Arsenic Doped Steel in the Unsegregated Condition.

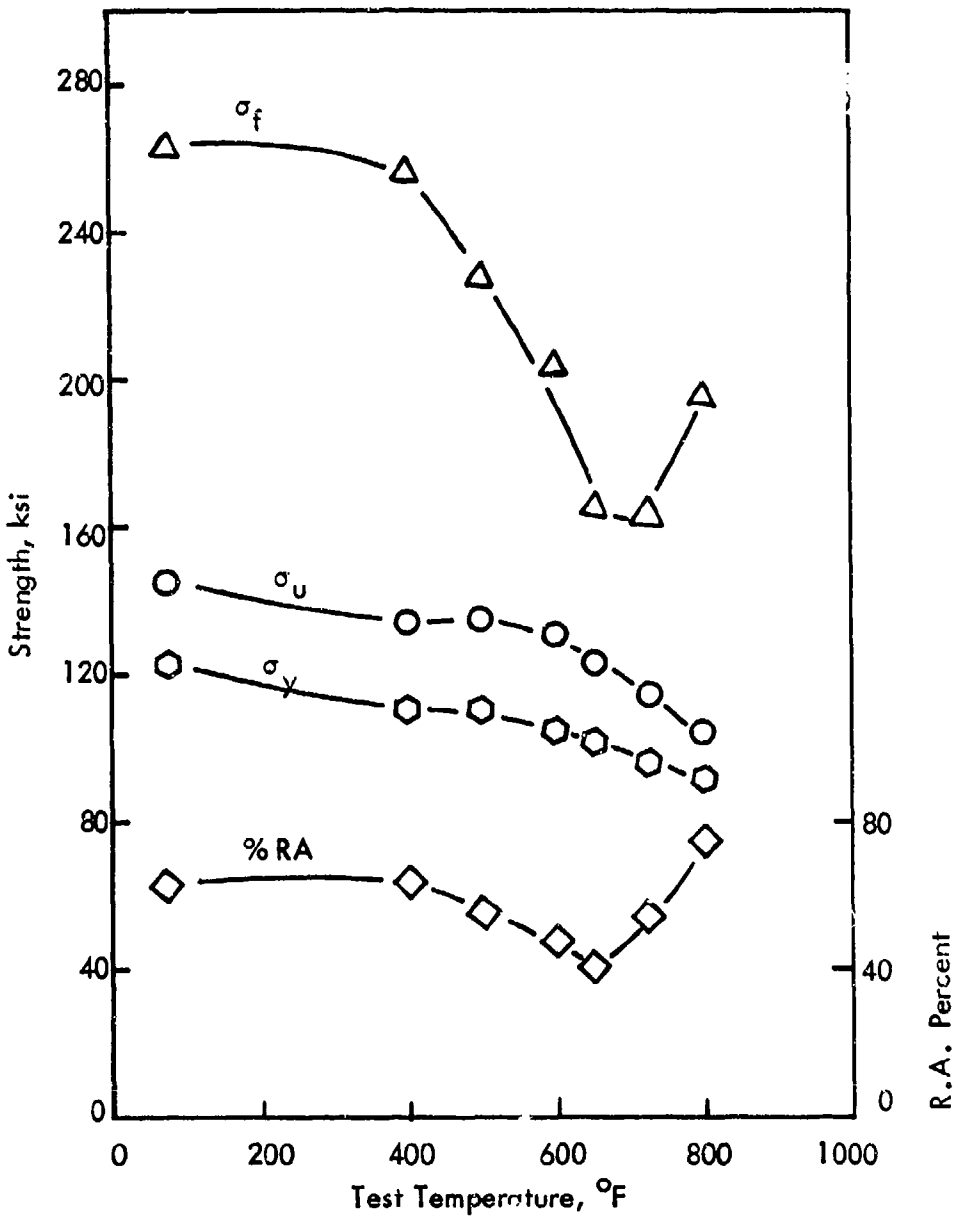

Fig. 26. Elevated Tempered Tensile Properties of Arsenic Doped Steel in the Unsegregated Condition with Pure Lead Soldered on the Surface.

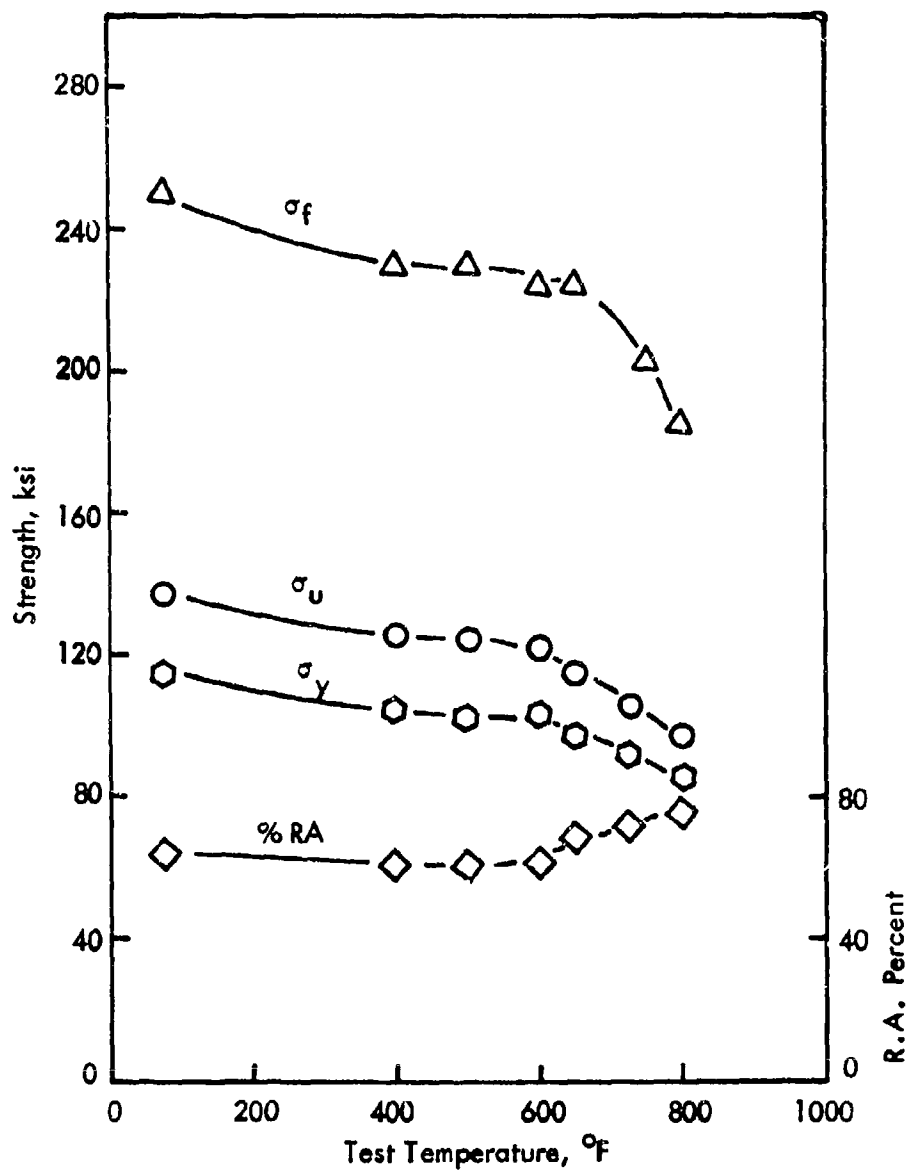

Fig. 27. Elevated Temperature Tensile Properties of Arsenic Doped Steel in the Segregated Condition.

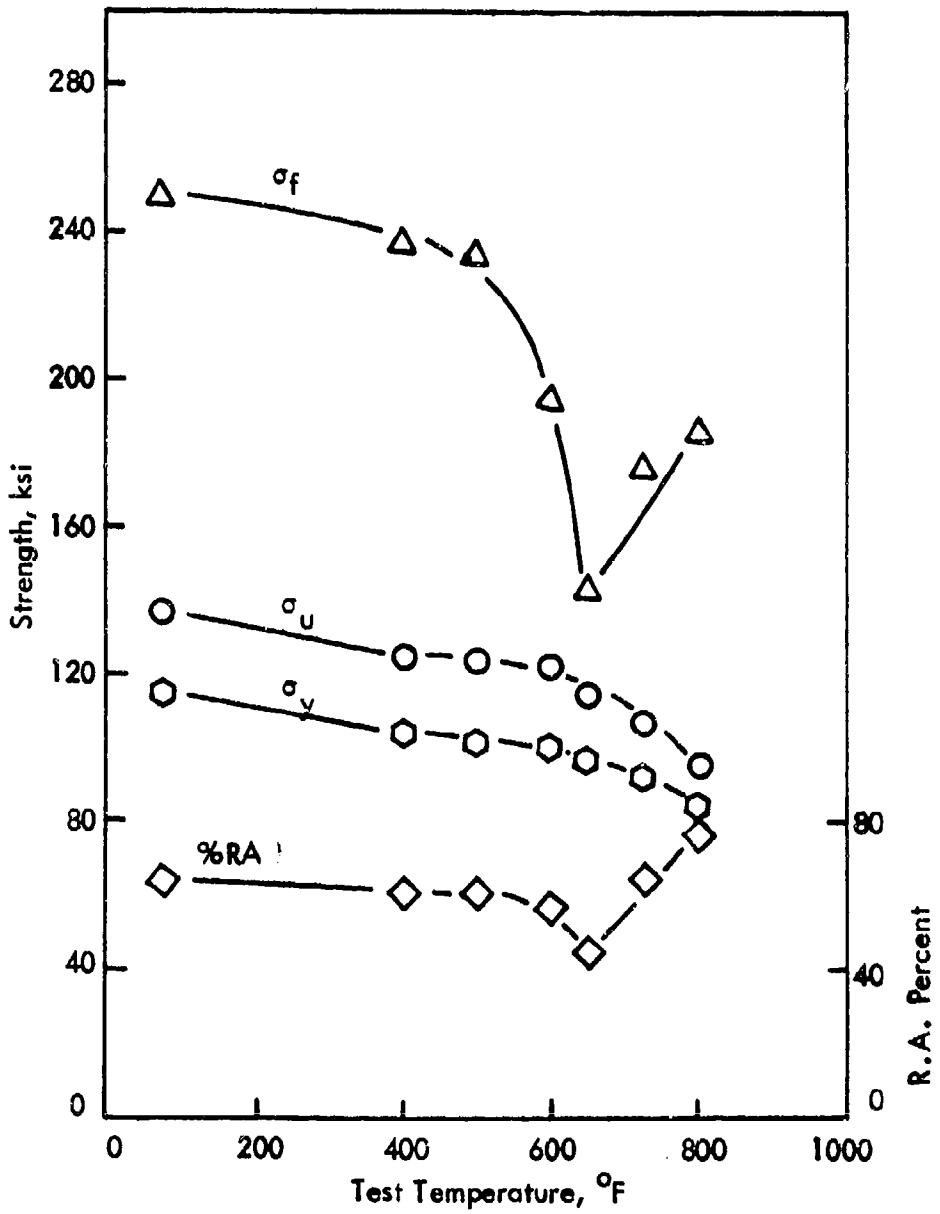

Fig. 28. Elevated Temperature Tensile Properties of Arsenic Doped Steel in the Segregated Condition with Pure Lead Soldered on the Surface.

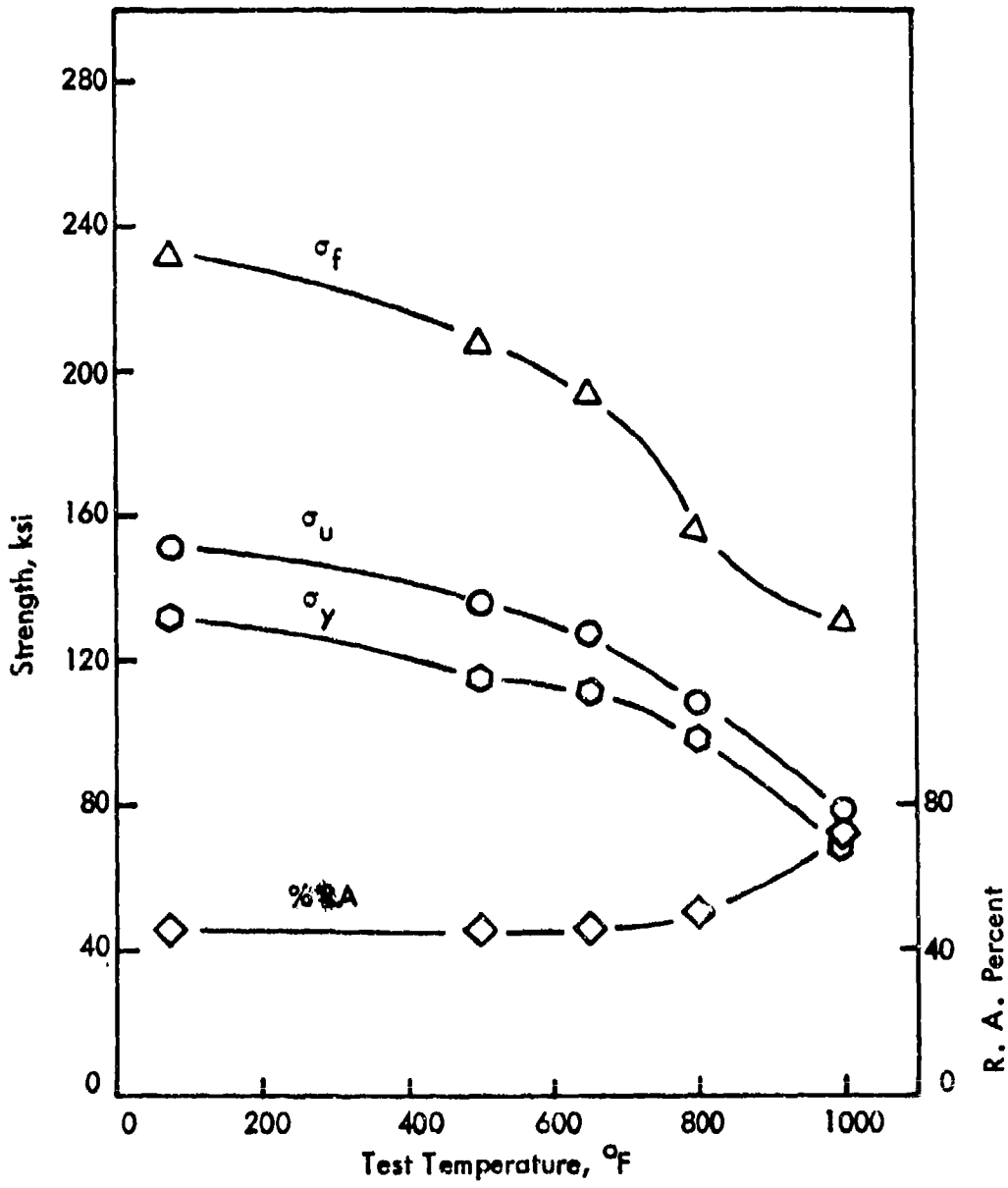

Fig. 29. Elevated Temperature Tensile Properties of Antimony Doped Steel Furnace-cooled from 1100°F to Room Temperature for Segregated Condition.

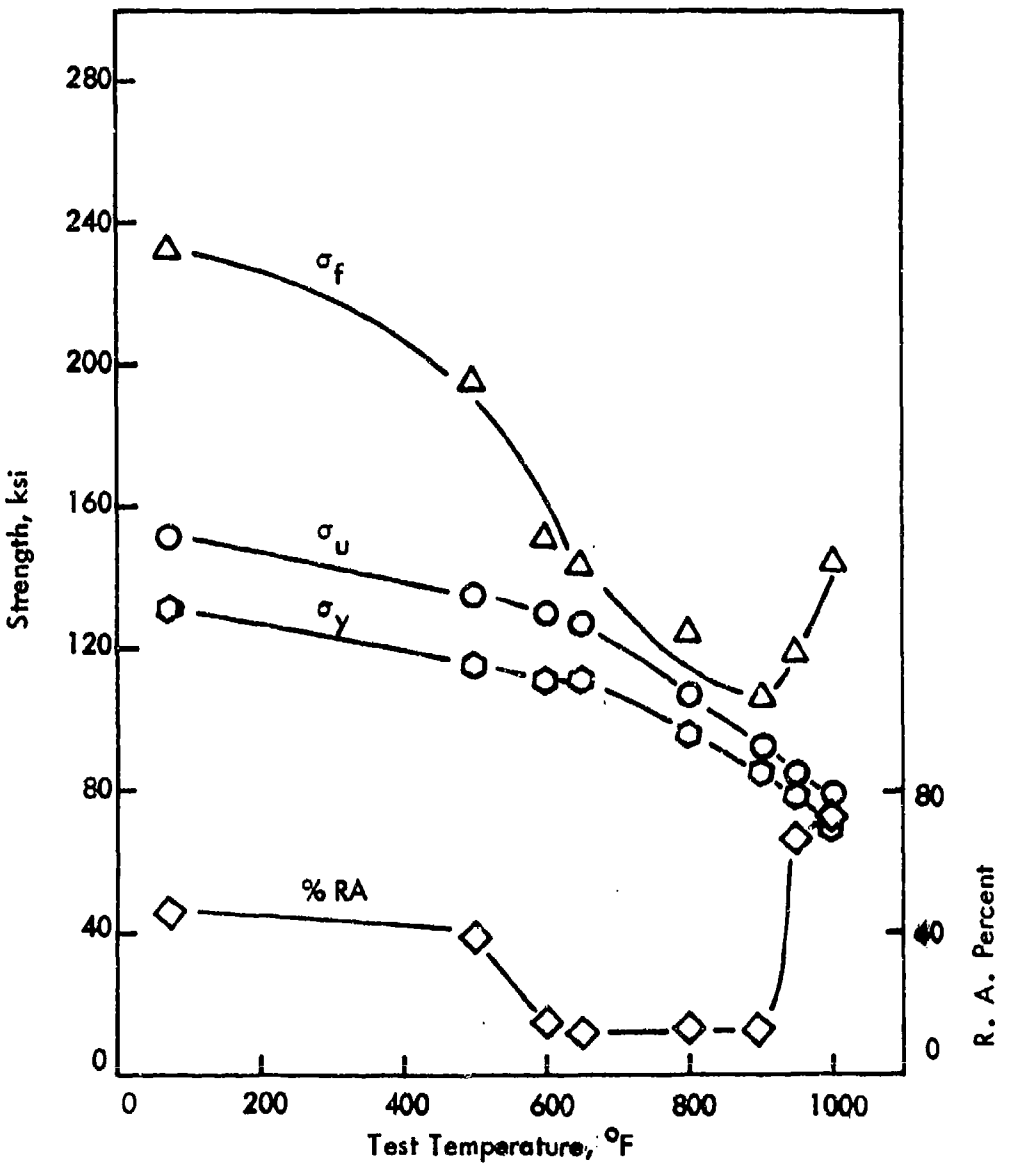

Fig. 30. Elevated Temperature Tensile Properties of Antimony Doped Steel Furnace-cooled from 1100°F to Room Temperature for Segregated Condition. Tested with Pure Lead Soldered on the Surface.

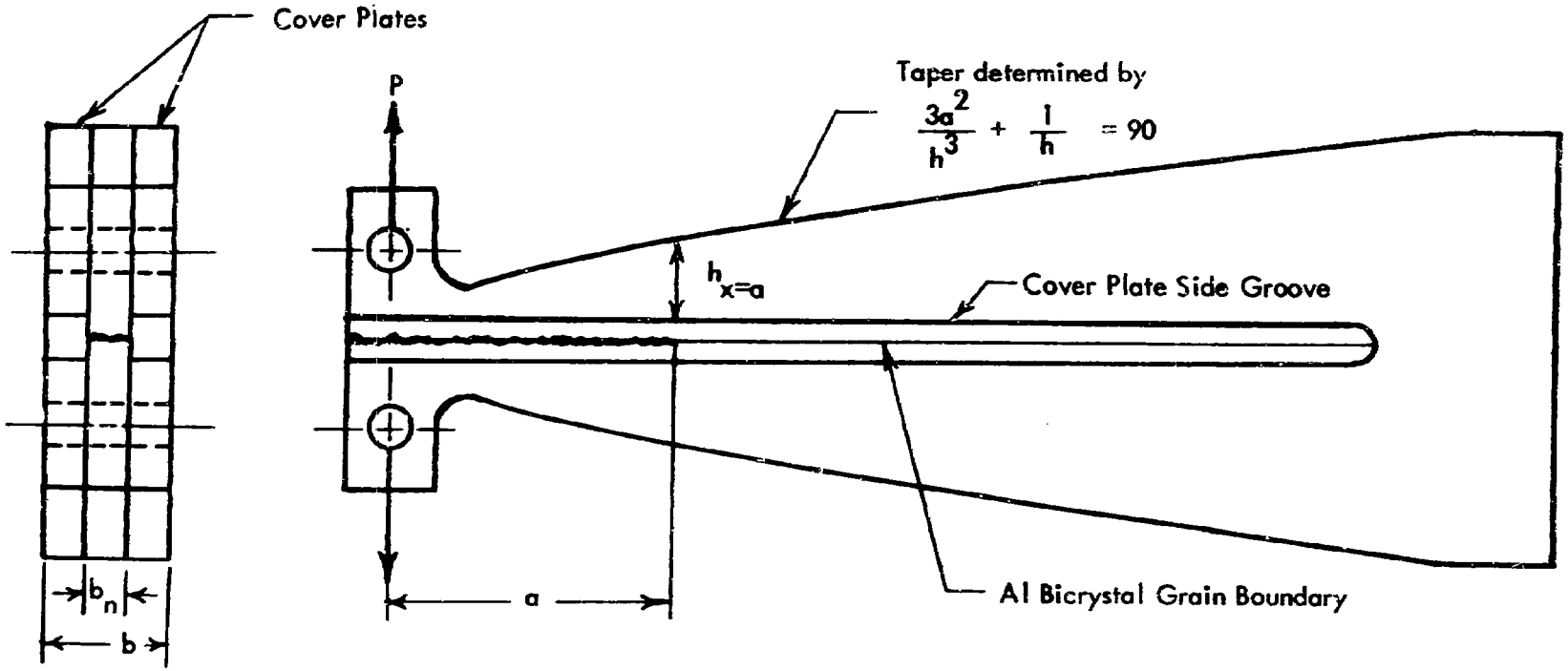

Fig. 31. Tapered, Double Cantilever Beam, Aluminum Bicrystal Fracture Specimen with Attached Cover Plates.

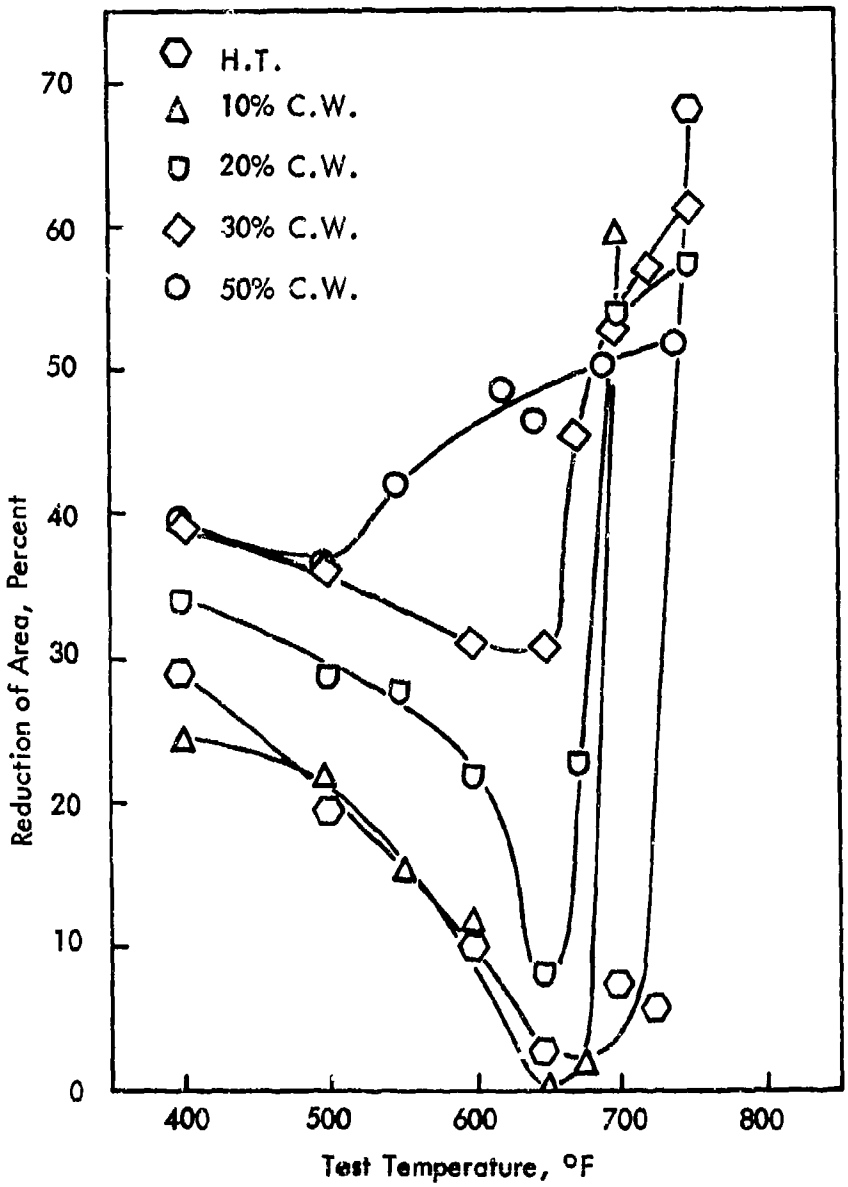

Fig. 32. Comparison of Ductility Properties of Internally Leaded 4145 Steel Processed to 200 ksi Nominal UTS by Heat Treatment Alone and Heat Treatment Plus 10, 20, 30, and 50% Reductions by Die Drawing.

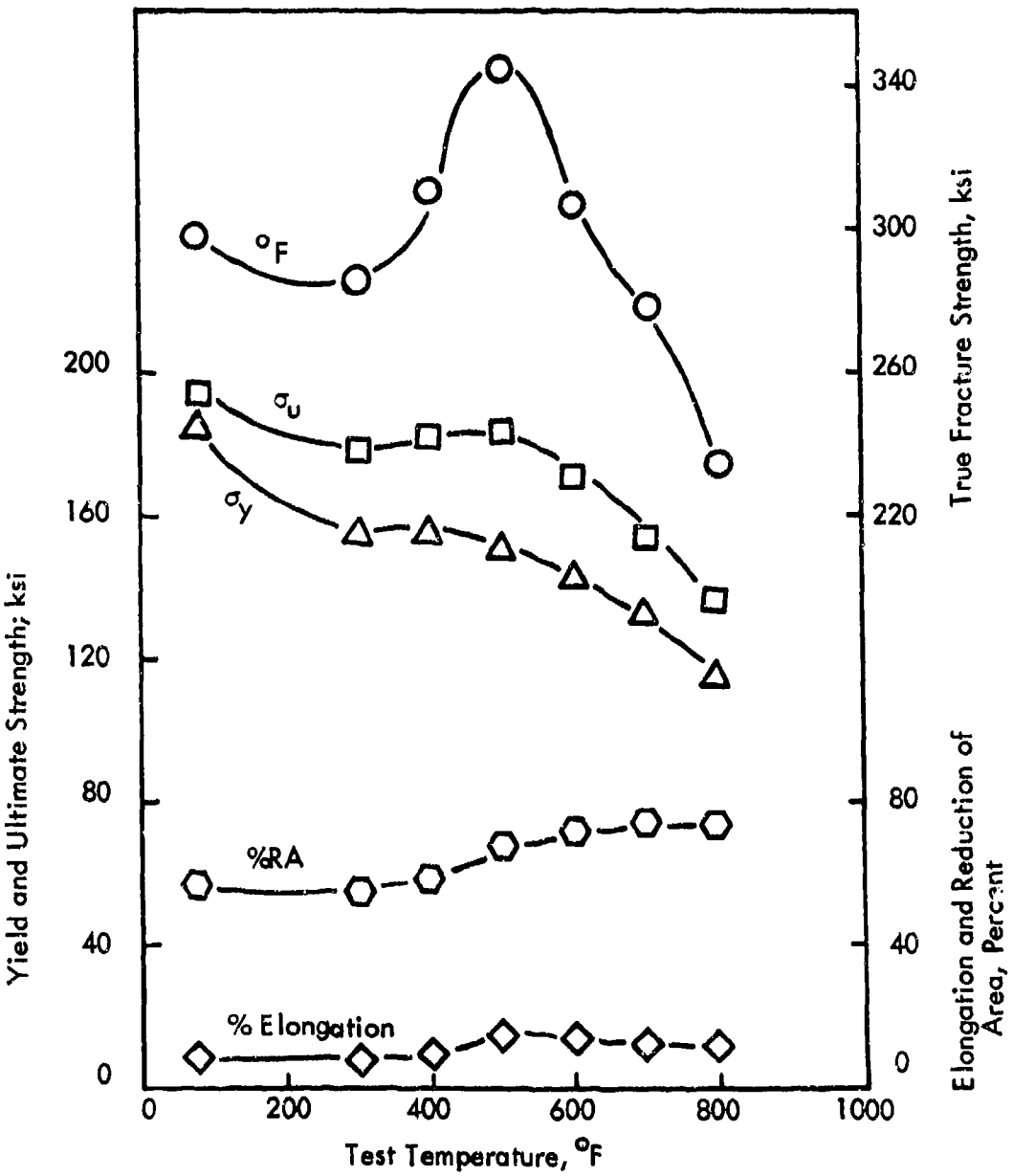

Fig. 33. Elevated Temperature Tensile Properties of Non-Leaded 4145 Steel Heat Treated to 200 ksi Nominal UTS.

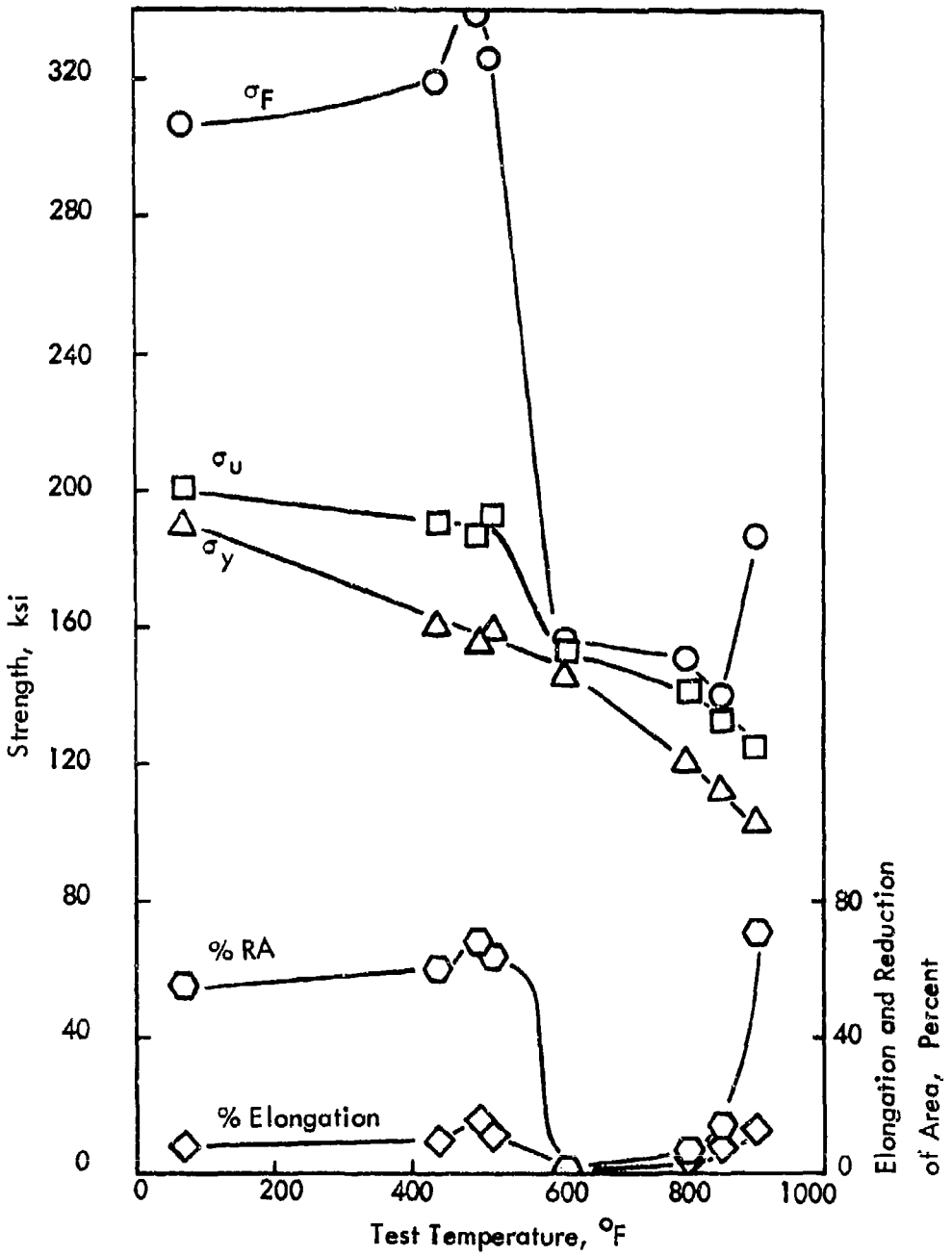

Fig. 34. Elevated Temperature Tensile Properties of Non-Leaded 4145 Steel, Surface Wetted with Pb 4.0 w/o Sn Alloy, and Heat Treated to 200 ksi Nominal Strength.

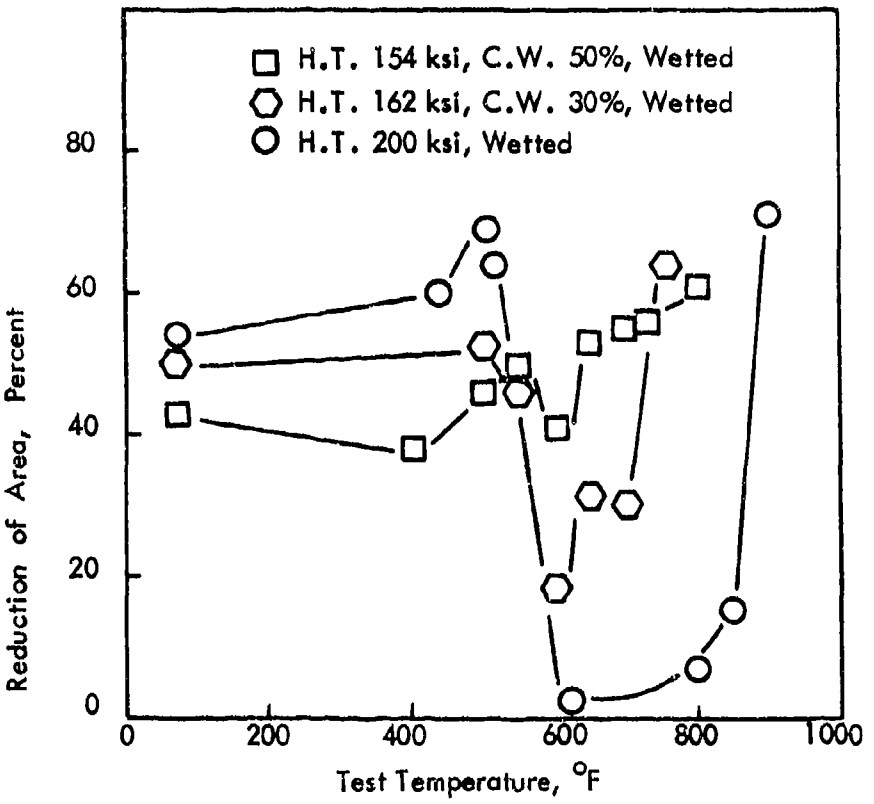

Fig. 35. Comparison of Ductility Properties of Non-Leaded 4145 Steel Processed to 200 ksi Nominal Strength by Heat Treatment Alone and Heat Treatment Plus 30 and 50% Reductions by Die Drawing; Surface Wetted with Pb-4.0 w/o Sn Alloy.

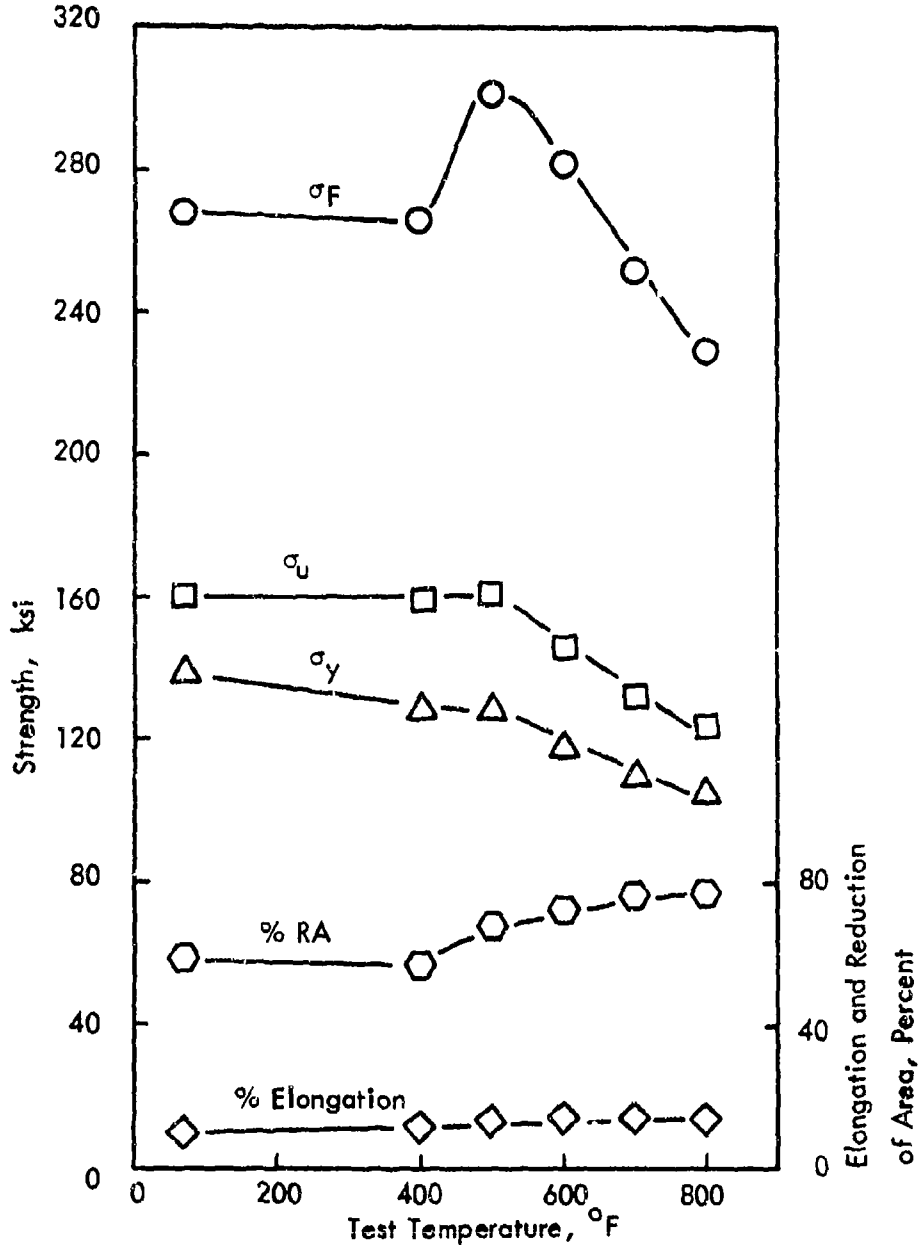

Fig. 36. Elevated Temperature Tensile Properties of Non-Leaded 4145 Steel Heat Treated to 162 ksi Nominal Strength.

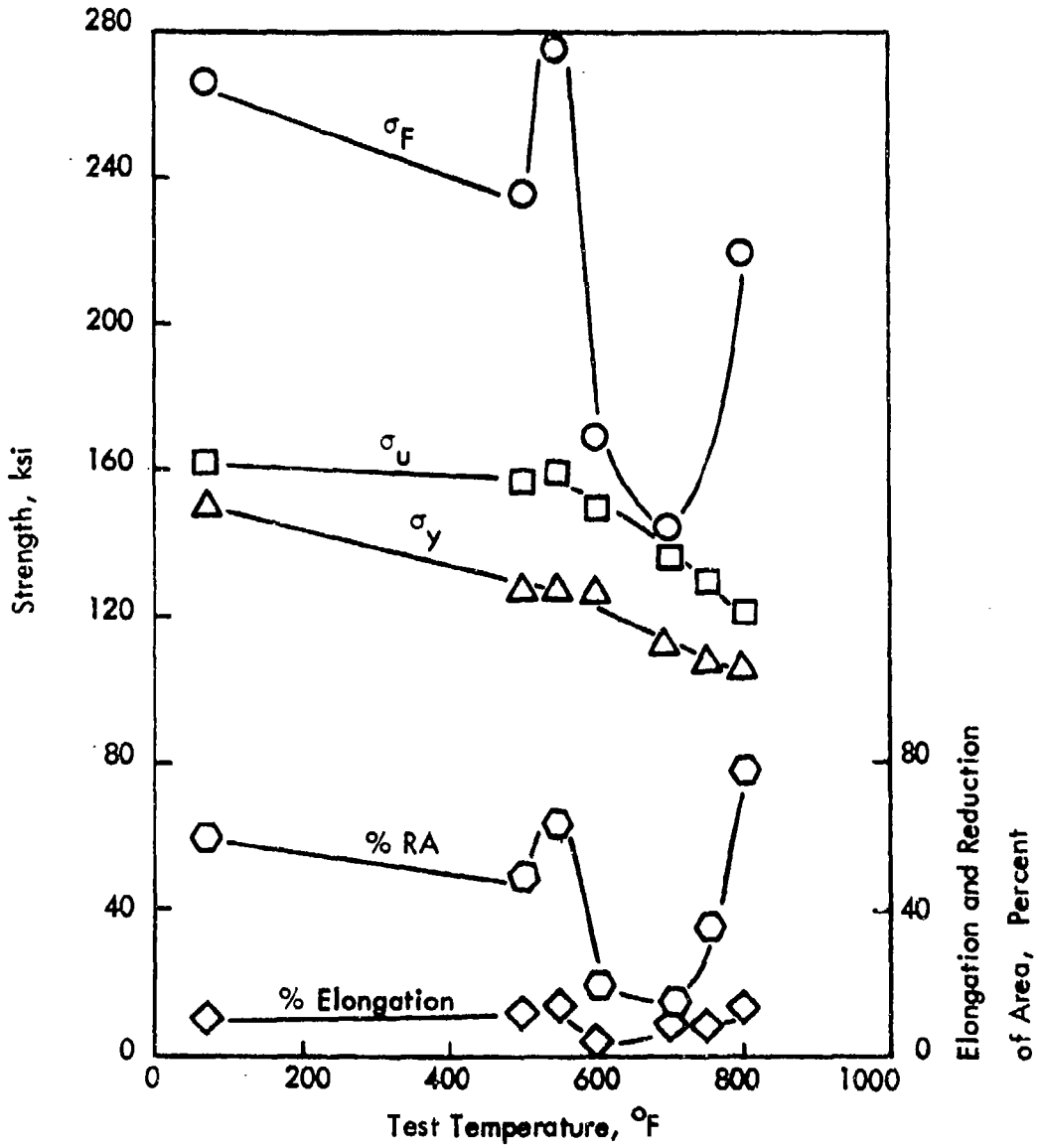

Fig. 37. Elevated Temperature Tensile Properties of Non-Leaded 4145 Steel Heat Treated to 162 ksi Nominal Strength and Surface Wetted with Pb-4.0 w/o Sn Alloy.

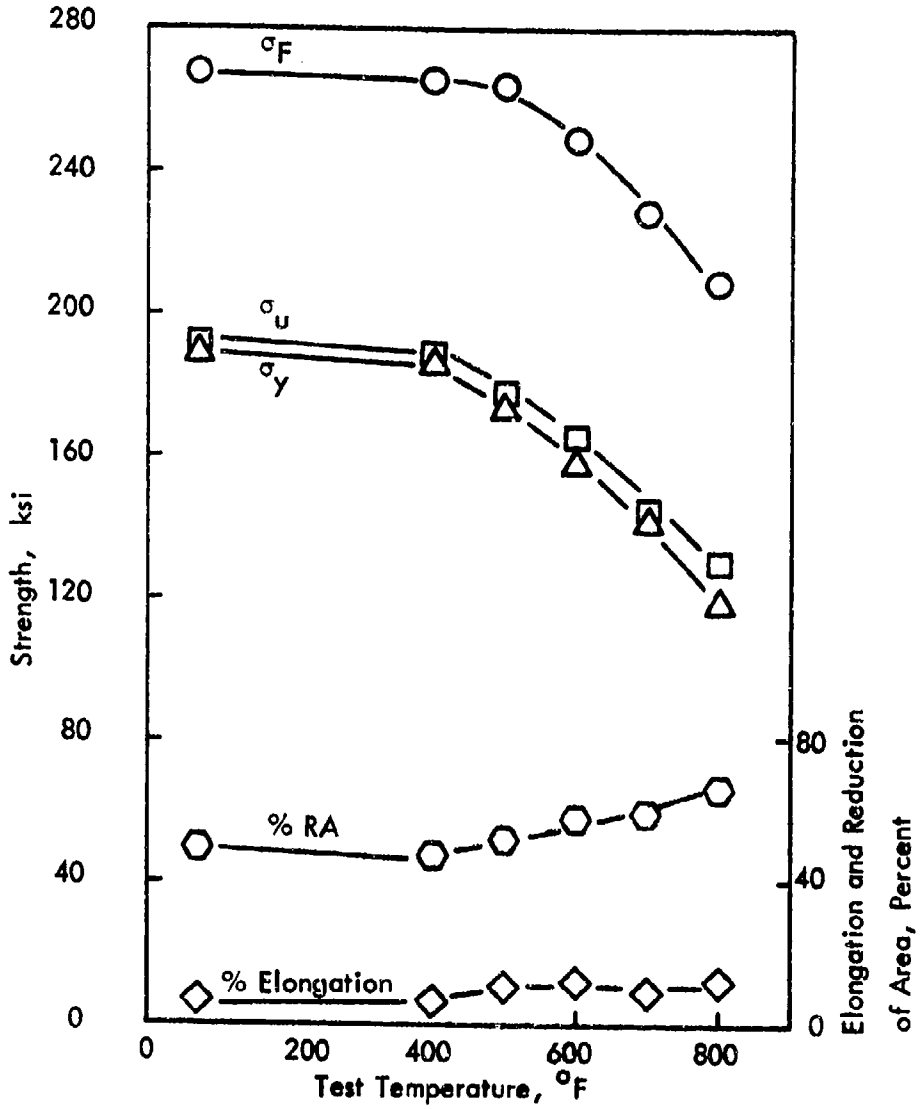

Fig. 38. Elevated Temperature Tensile Properties of Non-Leaded 4145 Steel Heat Treated to 162 ksi and Cold Worked 30% to Achieve 200 ksi Nominal Strength.

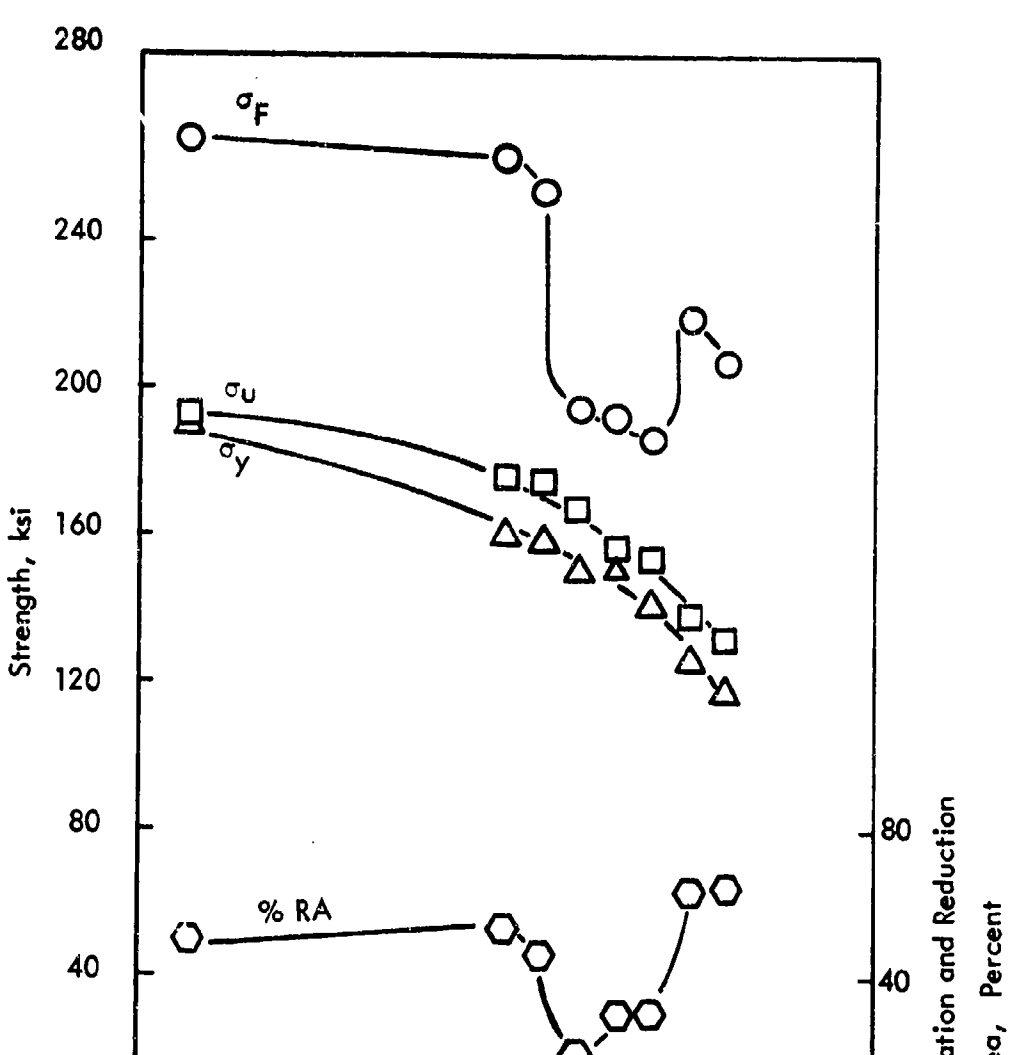

Fig. 39. Elevated Temperature Tensile Properties of Non-Leaded 4145 Steel Heat Treated to 162 ksi, Cold Worked 30% to Achieve 200 ksi Nominal Strength, and Surface Wetted with Pb-4.0 w/o Sn Alloy.

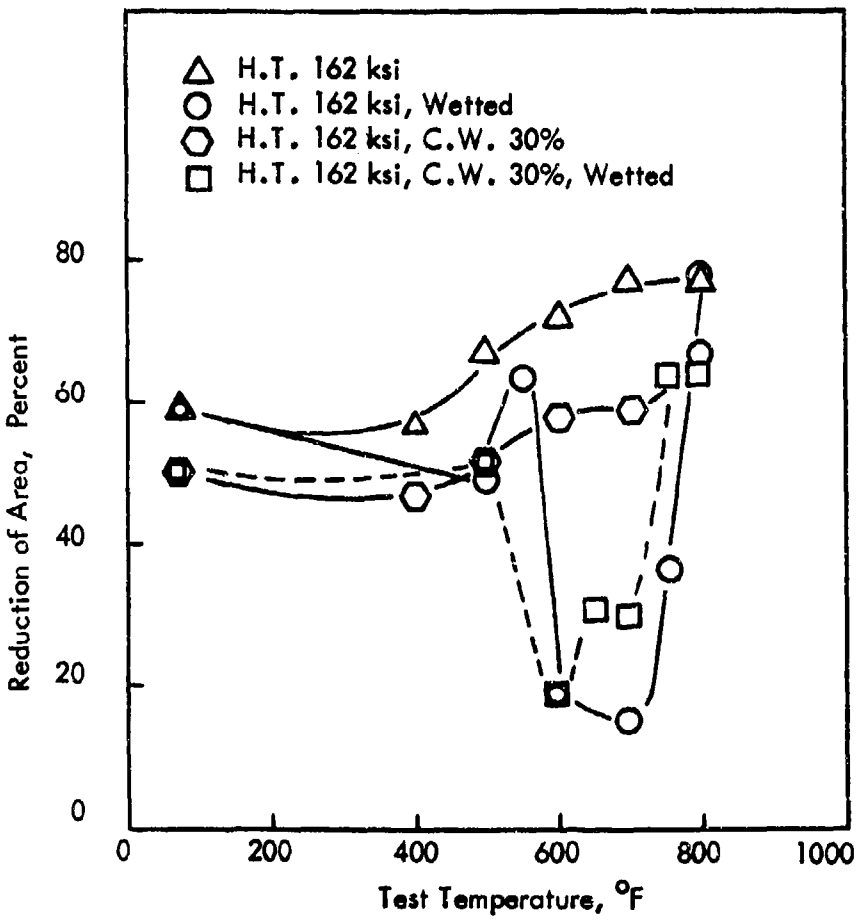

Fig. 40. Comparison of Ductility Properties of Non-Leaded 4145 Steel Heat Treated to 162 ksi; Surface Wetted with Pb-4.0 w/o Sn Alloy.

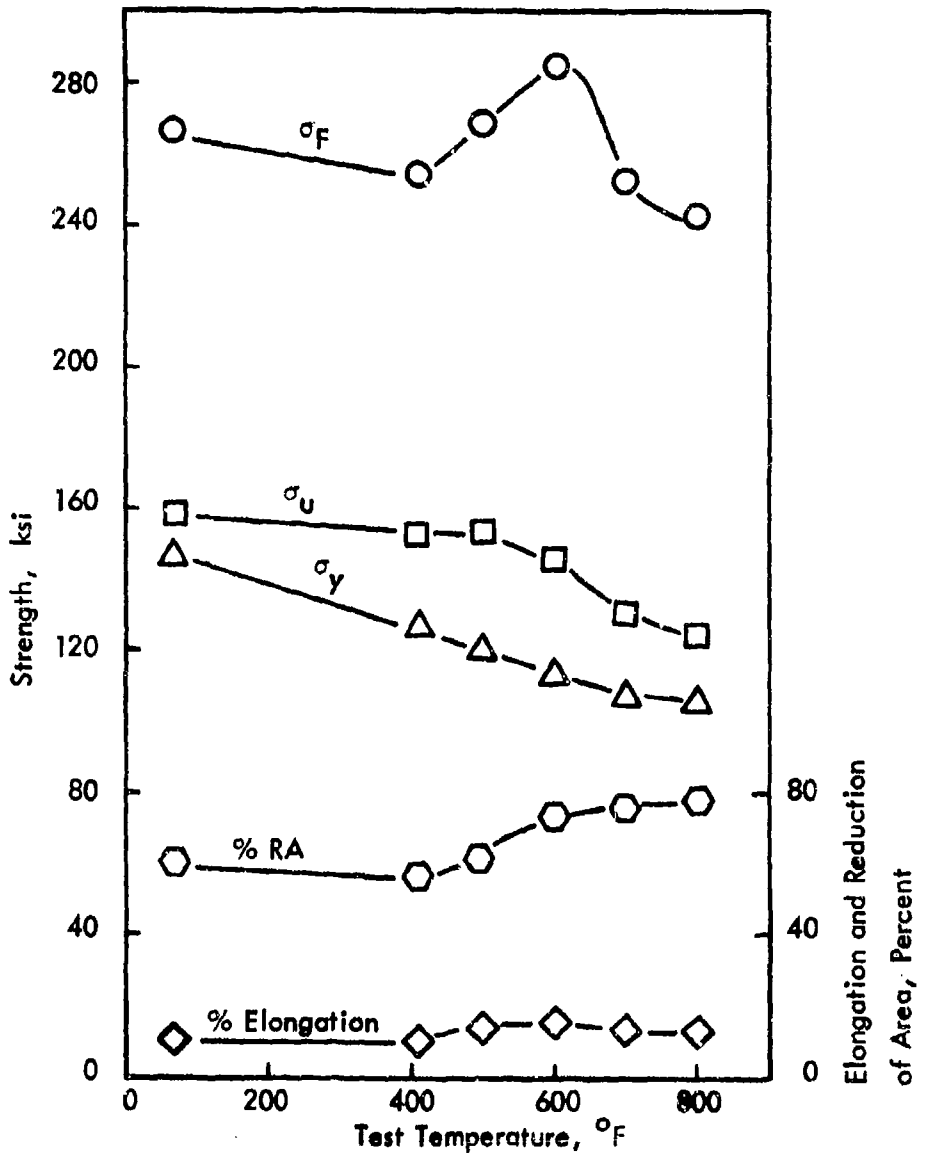

Fig. 41. Elevated Temperature Tensile Properties of Non-Leaded 4145 Steel Heat Treated to 154 ksi Nominal Strength.

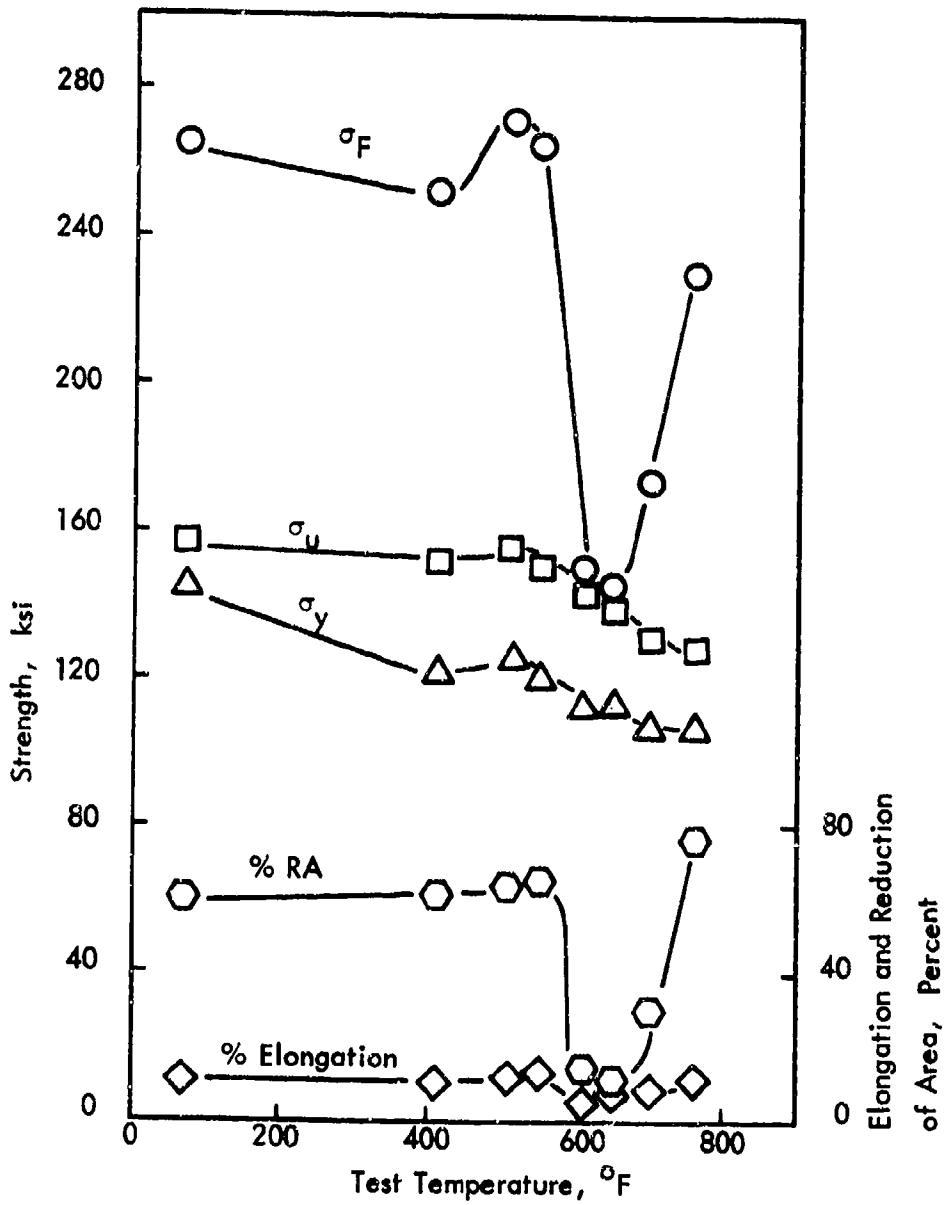

Fig. 42. Elevated Temperature Tensile Properties of Non-Leaded 4145 Steel Heat Treated to 154 ksi Nominal Strength and Surface Wetted with Pb-4.0 w/o Sn Alloy.

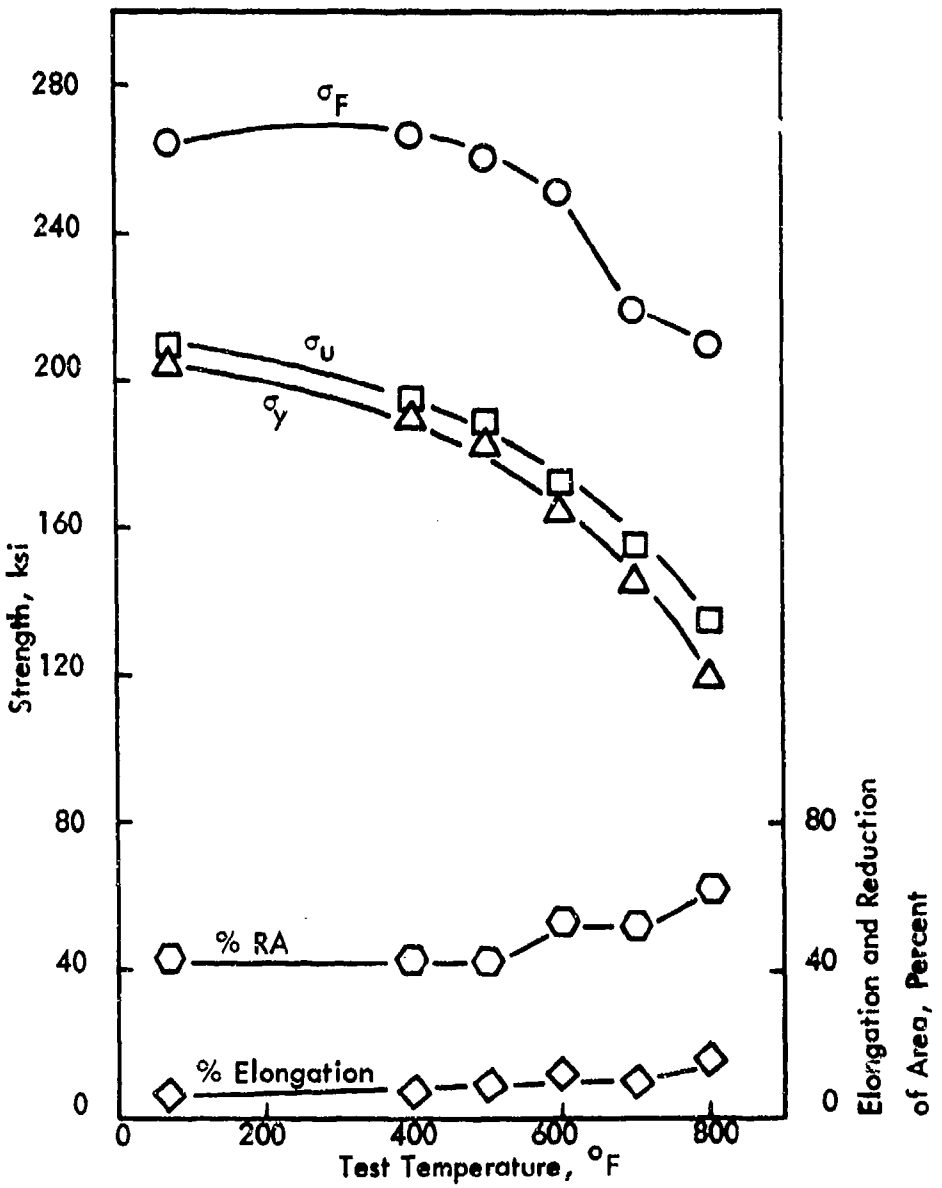

Fig. 43. Elevated Temperature Tensile Properties of Non-Leaded 4145 Steel Heat Treated to 154 ksi Strength and Cold Worked 50% to Achieve 200 ksi Nominal Strength.

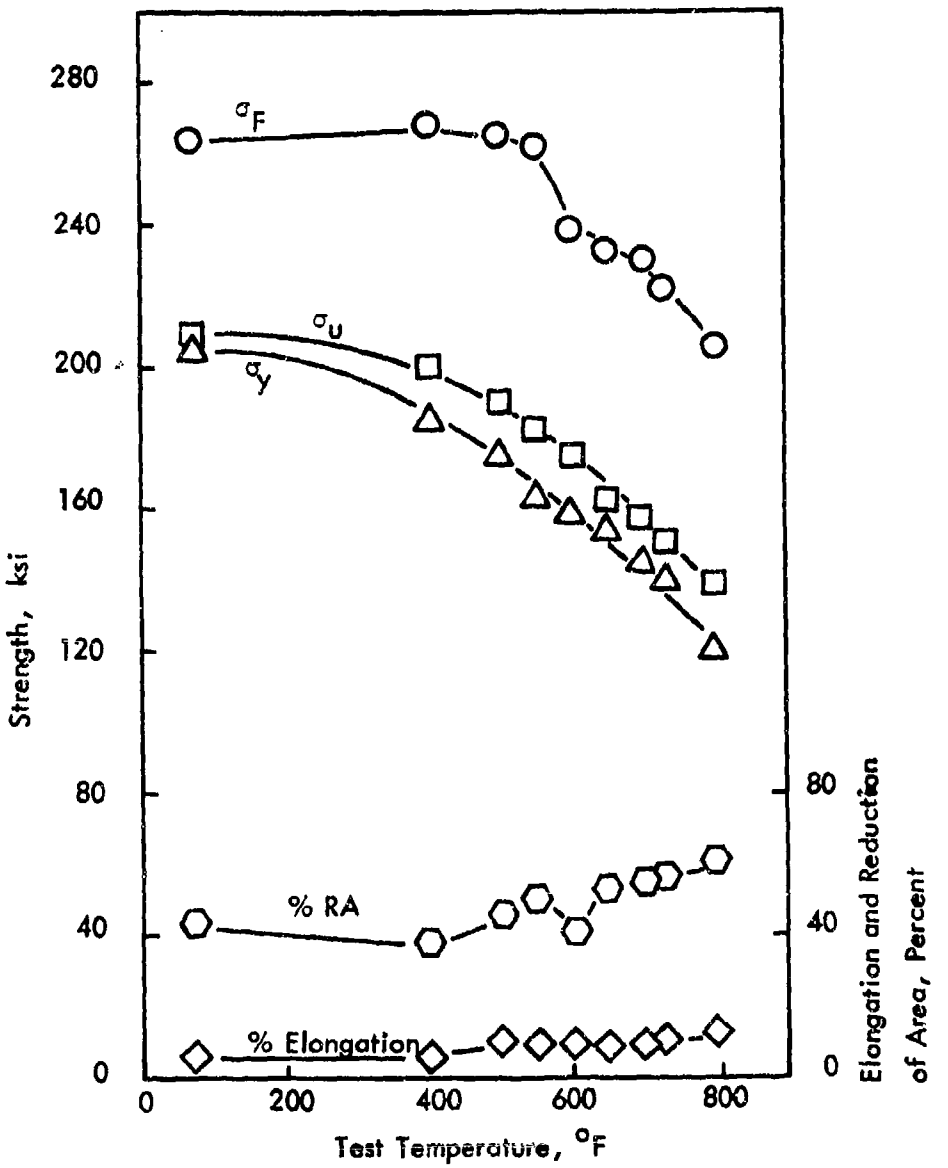

Fig. 44. Elevated Temperature Tensile Properties of Non-Leaded 4145 Steel Heat Treated to 154 ksi, Cold Worked 50% to Achieve 200 ksi Nominal Strength, and Surface Wetted with Pb-4.0 w/o Sn Alloy.

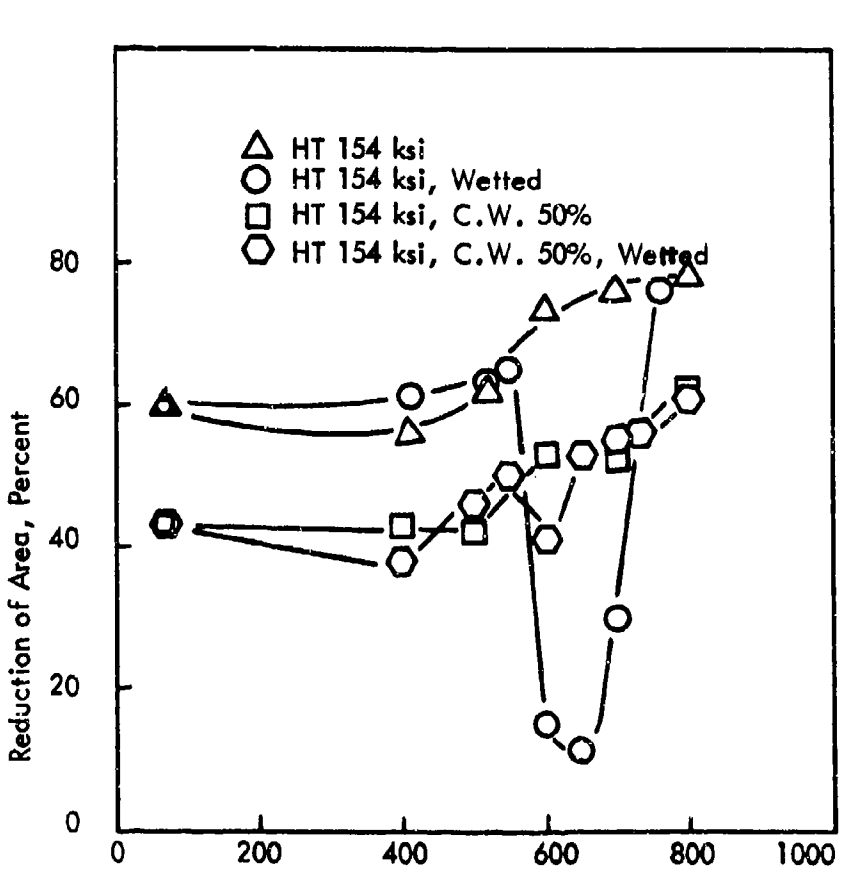

Fig. 45. Comparison of Ductility Properties of Non-Leaded 4145 Steel Heated Treated to 154 ksi Nominal Strength; Surface Wetted with Pb-4.0 w/o Sn Alloy.

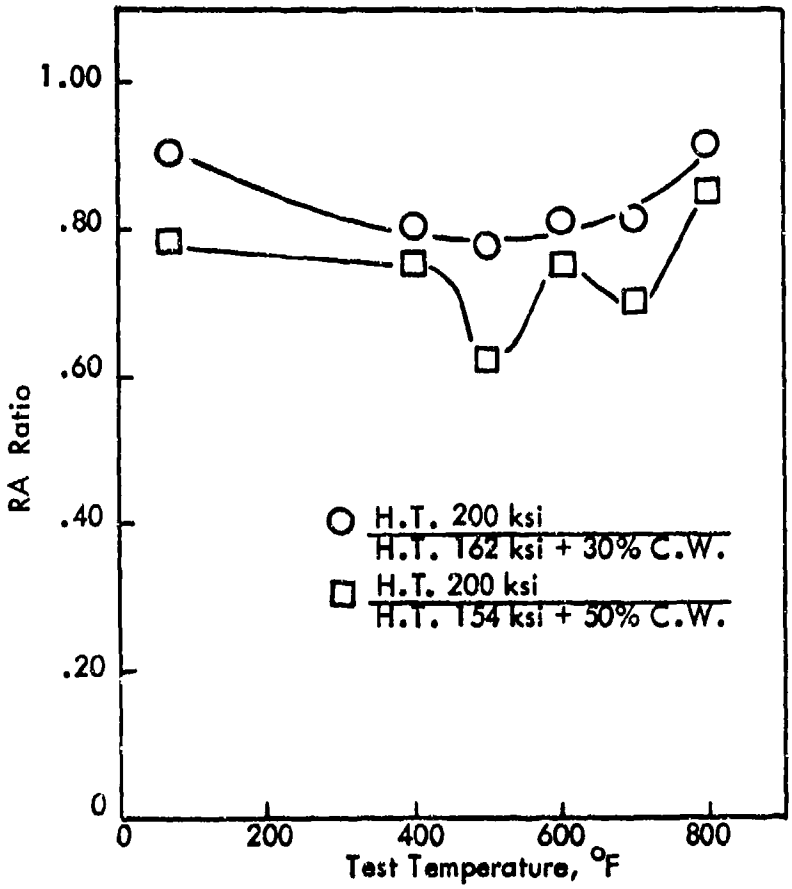

Fig. 46. RA Ratio for Non-Leaded 4145 Steel Heat Treated and Cold Worked Various Amounts to Achieve 200 ksi Nominal Strength.

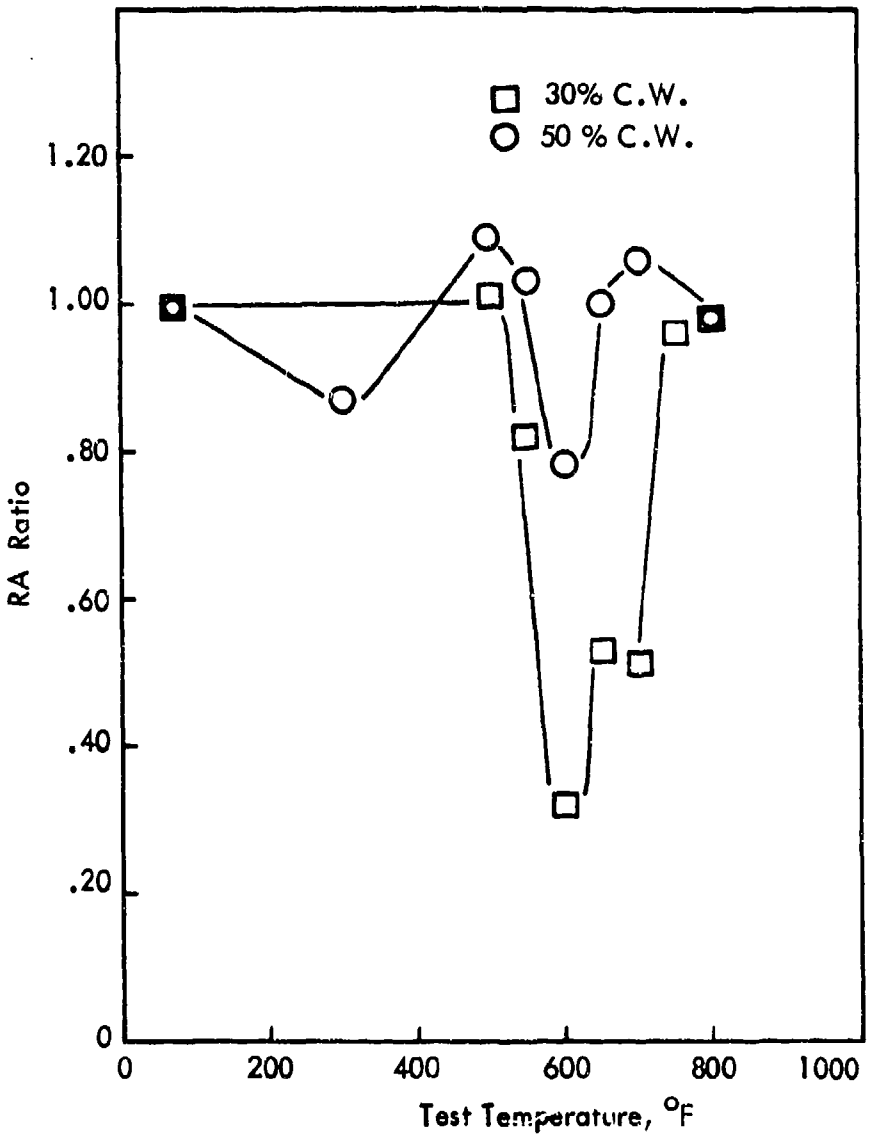

Fig. 47. RA Ratio of Surface Wetted (Pb-4.0 w/o Sn Alloy) to Non-Wetted for Non-Leaded 4145 Steel Heat Treated and Cold Worked Various Amounts to Achieve 200 ksi Nominal Strength.

(a) (b)

Fig. 48. Fracture Surfaces of Non-Leaded 4145 Steel Heat Treated to 154 ksi Nominal Strength, Surface Wetted with Pb-4.0 w/o Sn Alloy, and Tested at 600°F. (a) Heat Treated Condition, and (b) Heat Treated plus 50% Die Drawn Condition; 10X.

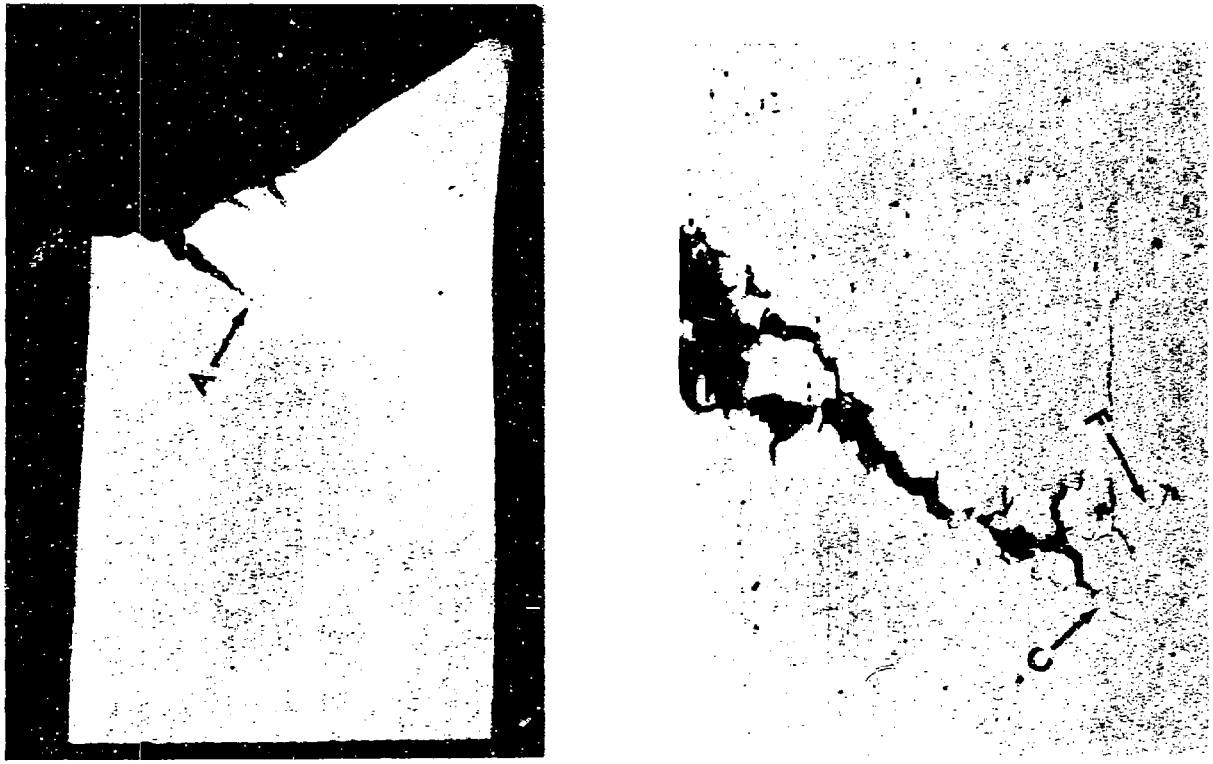

(a) (b)

Fig. 49. Longitudinal Cross-Section of the Non-Leaded 4145 Steel Fractures Shown in Fig. 48. (a) As Heat Treated Condition; 10X. (b) Crack Terminus Indicated by Arrow A in (a); 200X. Arrows C and F Indicate the Nature of the Branching. (c) As Heat Treated Plus 50% Die Drawn Condition; 10X. (d) Microcrack Indicated by Arrow B in (c); 100X.

(c)

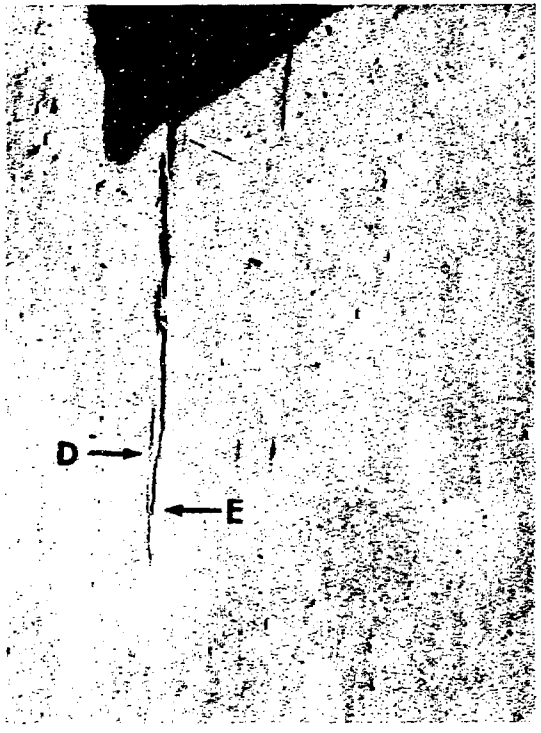

(d)

Fig. 49. (Continued)

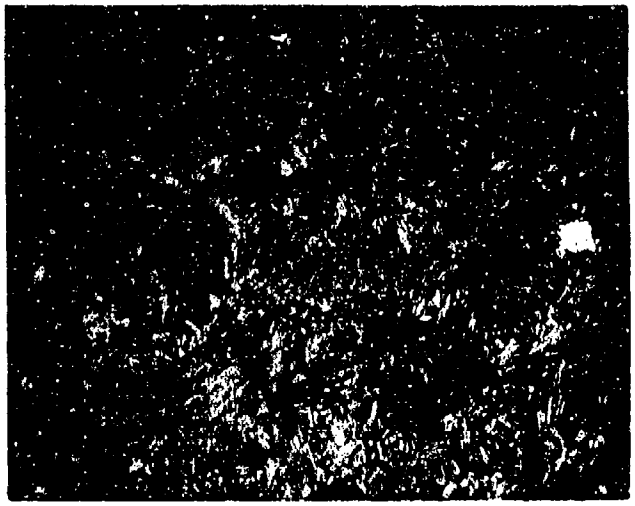

(a)

(b)

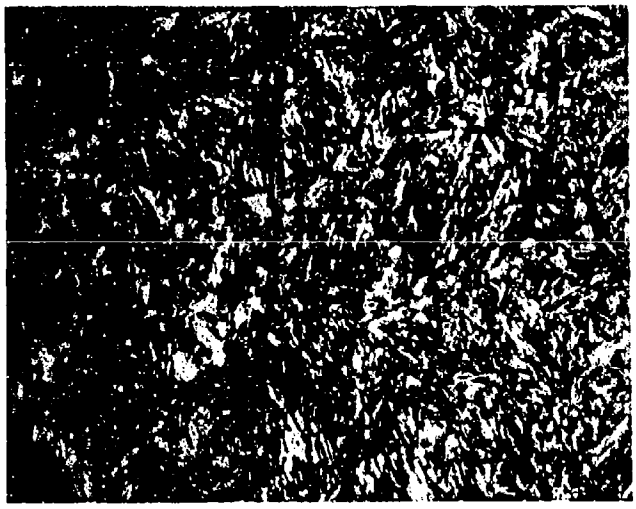

(c)

Fig. 50. Longitudinal Cross-Section of the Non-Leaded 4145 Steel Specimen Tested in the As Heat Treated Condition. Arrows C and F Point to Microcracks in the Terminus Indicated in Fig. 49(b), and Illustrate The Nature of Branching; 2% Nital Etch. (a) 500X, (b) 1000X, and (c) 1000X.

(a)

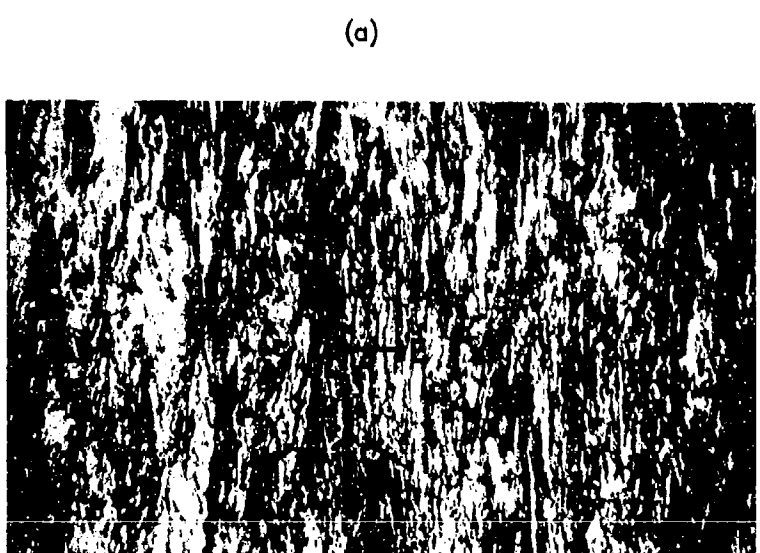

(b)

Fig. 51. Longitudinal Cross-Section of the Non-Leaded 4145 Steel Specimen, Heat Treated plus 50% Die Drawn Condition; 2% Nital Etch. Regions D and E in Fig. 49d are Shown at High Magnification of (a) 500X and (b) 1000X. The Microcrack Runs Parallel to the Drawing Direction.

(a)

(b)

Fig. 52. Photomacrographs of Internally Leaded 4145 Steel, Heat Treated and Cold Worked by Die Drawing Various Percentages (a) 0%, (b) 10%, (c) 20%, (d) 30% and (e) 50% to Achieve 200 ksi Nominal Strength, and Tested at 650°F; 10X.

(c)

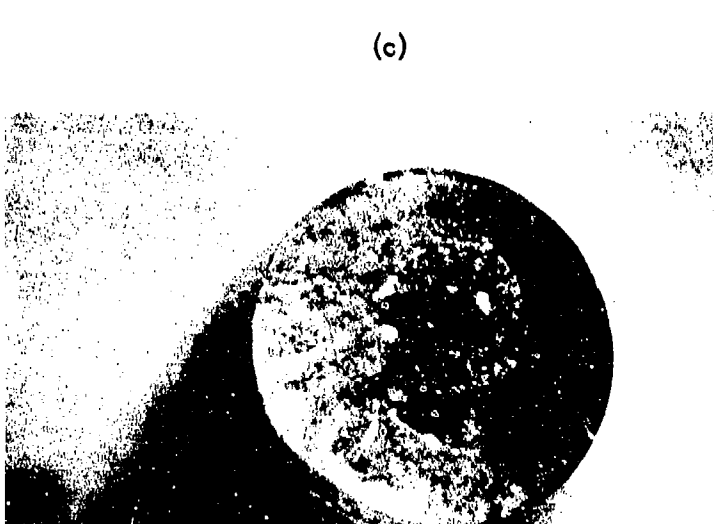

(d)

Fig. 52. (Continued)

(e)

Fig. 52. (Continued)

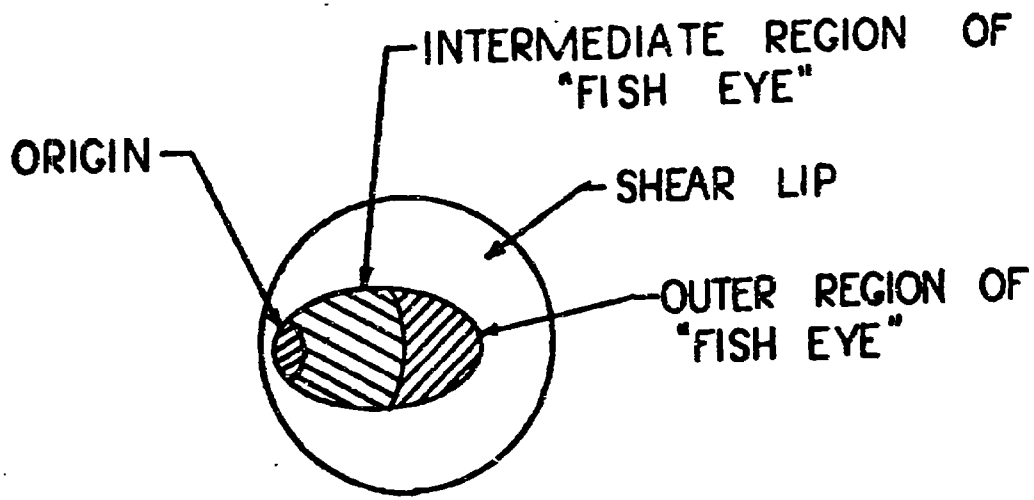

Fig. 53. Schematic Drawing of the "Fish Eye" Region of the Type D Fracture

(a)

(b)

Fig. 54. Surface Replicas of the Internally-Leaded 4145 Steel Specimen, Heat Treated to 200 ksi Nominal Strength, Showing the Intergranular Facets in the Origin Area of the "Fish Eye" Area of the Type D Fracture; 2400X

(a)

(b)

Fig. 55. Surface Replicas of the Internally-Leaded 4145 Steel Specimen Heat Treated to 185 ksi and Cold Worked 10% by Die Drawing to Achieve 200 ksi Nominal Strength, Showing the Intergranular Facets in the Origin Area of the "Fish Eye" in the Type D Fracture; 2400X

(a)

(b)

Fig. 56. Surface Replicas of the Internally-Leaded 4145 Steel Specimen Heat Treated to 180 ksi and Cold Worked 20% by Die Drawing to Achieve 200 ksi Nominal Strength, Showing the Intergranular Facets in the Origin Area of the "Fish Eye" in the Type D Fracture; 2400X

(a)

(b)

(c)

Fig. 57. Surface Replicas of the Internally-Leaded 4145 Steel Specimen Heat Treated to 162 ksi and Cold Worked 30% by Die Drawing to Achieve 200 ksi Nominal Strength, Showing (a) the Intergranular Facets (b) Quasi-Cleavage Facets, and (c) Transgranular Facets in the Origin Area of the Type E Fracture; 2400X.

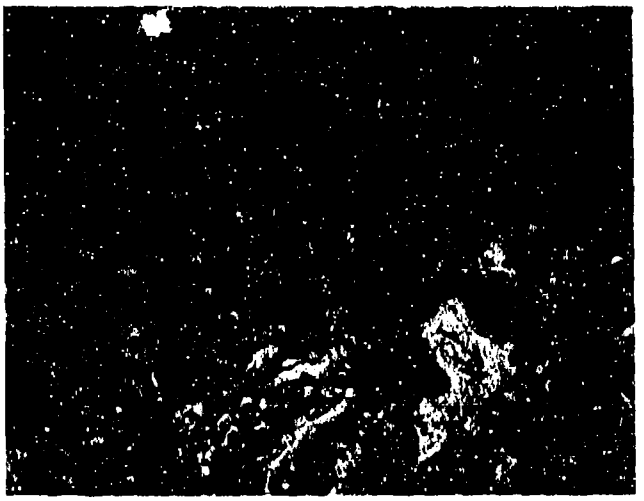

Fig. 58. Surface Replica of the Internally-Leaded 4145 Steel Specimen Heat Treated to 154 ksi and Cold Worked 50% by Die Drawing to Achieve 200 ksi Nominal Strength; Showing transgranular Facets in the Origin Area of the Type E Fracture; 2400X

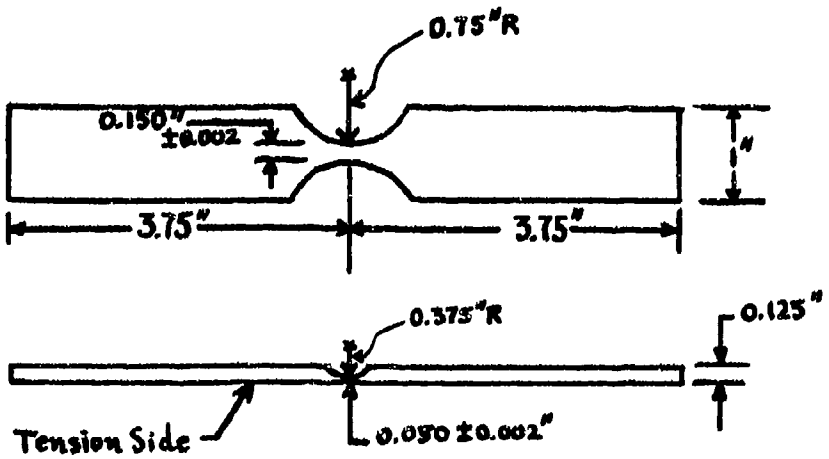

Fig. 59. Specimen Configuration

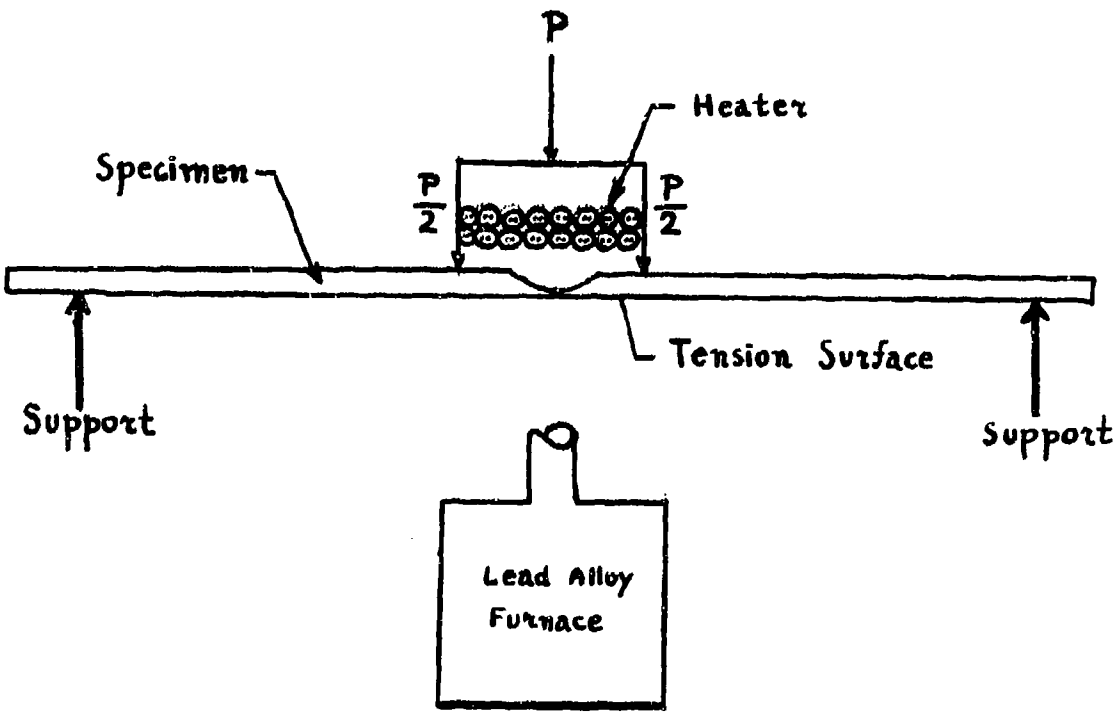

Fig. 60. Method of Specimen Loading

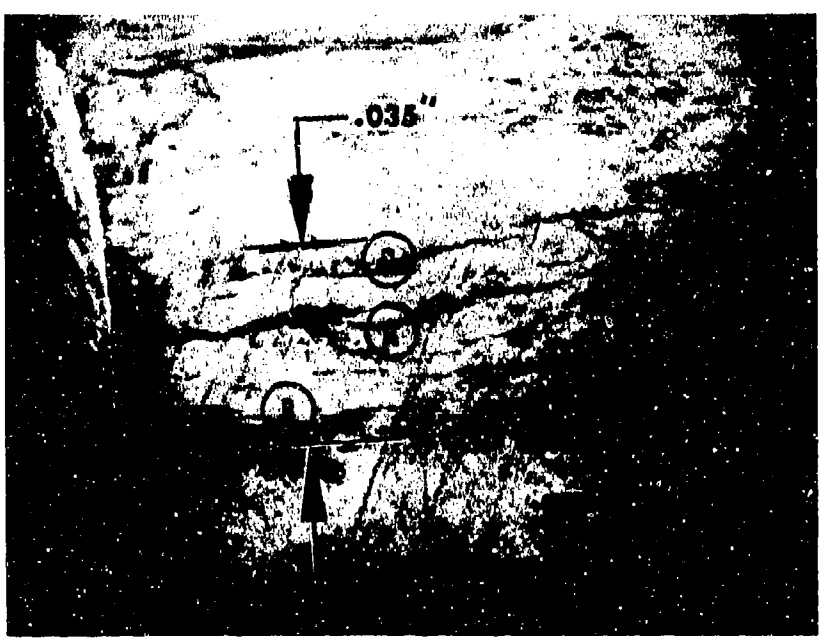

Fig. 61. Secondary Electron Photograph of the Tensile Surface of Specimen F-1

Magnification 22X. Encircled areas represent areas examined at higher magnifications. Area A is shown in Fig. 62.

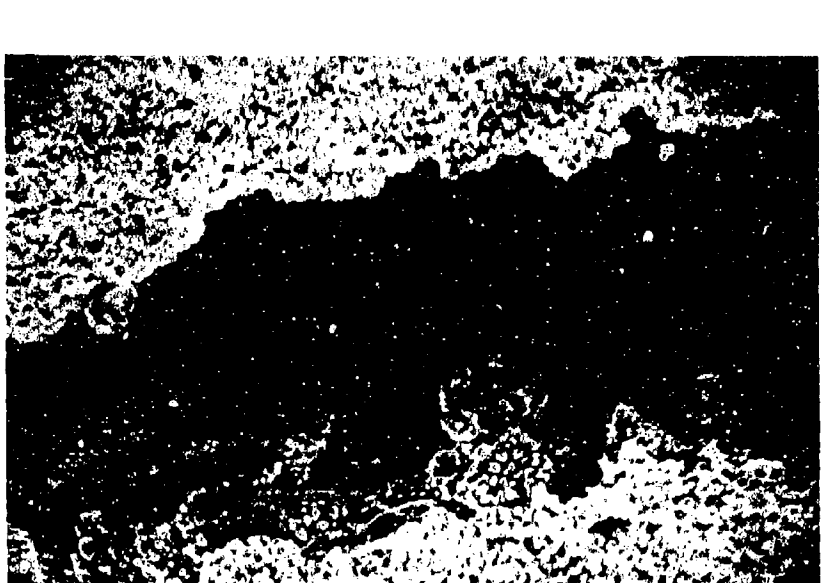

Fig. 62. Secondary Electron Photograph of Area A, shown in Fig. 61

Magnification 1100X. Globules represent condensed vapors that have overgrown. No evidence of a continuous liquid film is found. Average embryo size at the specimen surface is 7,000A°.

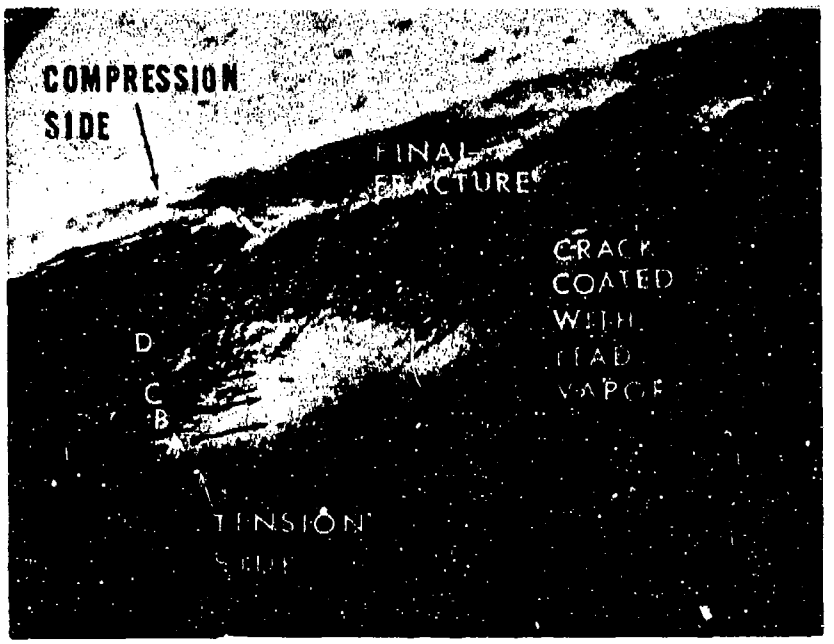

Fig. 63. Secondary Electron Photograph of Specimen G-3

Magnification 20X. Areas A, B, C, and D were further examined, see Figs. 64-68. They are located 40, 200, 400 and 600 microns below the tension side of the specimen. Note the thumbnail appearance of the crack front. Arrows pointing the location of areas A, B, C, and D are not to scale.

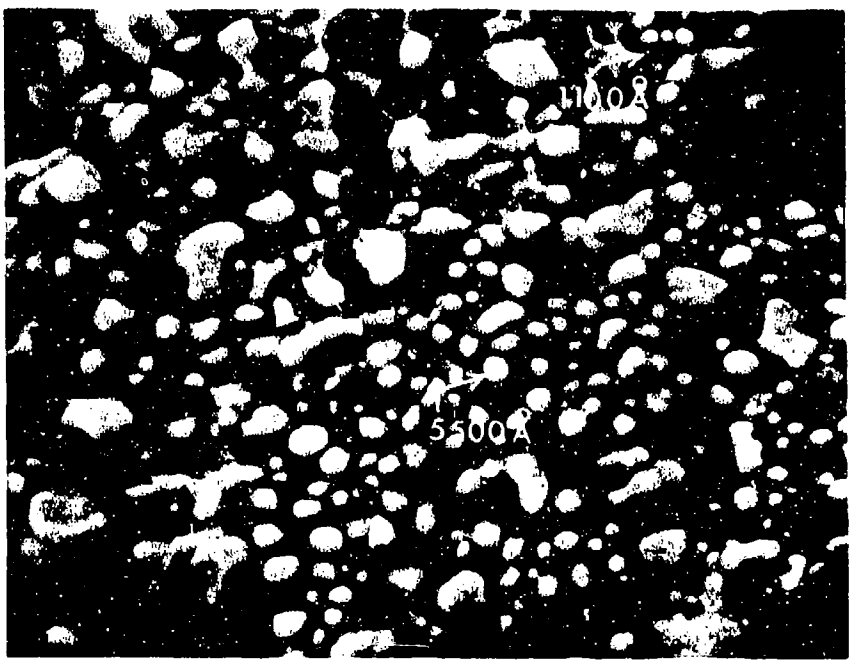

Fig. 64. Secondary Electron Photograph of Area A shown in Fig. 63

Magnification 2800X. Radii of a few embryo are indicated. Depth below tension surface; 40 microns.

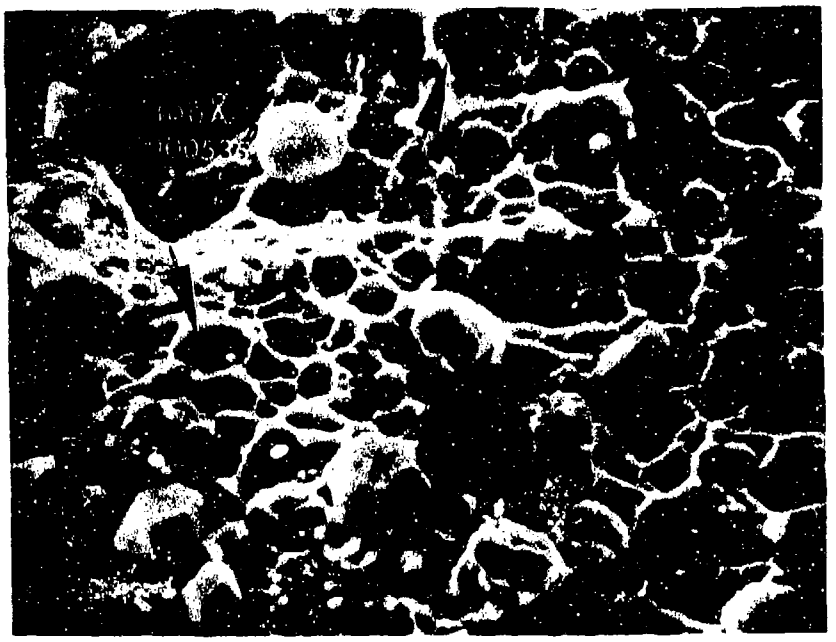

Fig. 65. Secondary Electron Photograph of Area B shown in Fig. 63

Magnification 2800X. Note the crystallographic appearance of the grown embryo and the appearance of a whisker texture. The large arrows point to the grain containing rather small embryo (500 Å) arranged in a hexagonal manner. Photograph was taken at a depth of 200 microns below the surface.

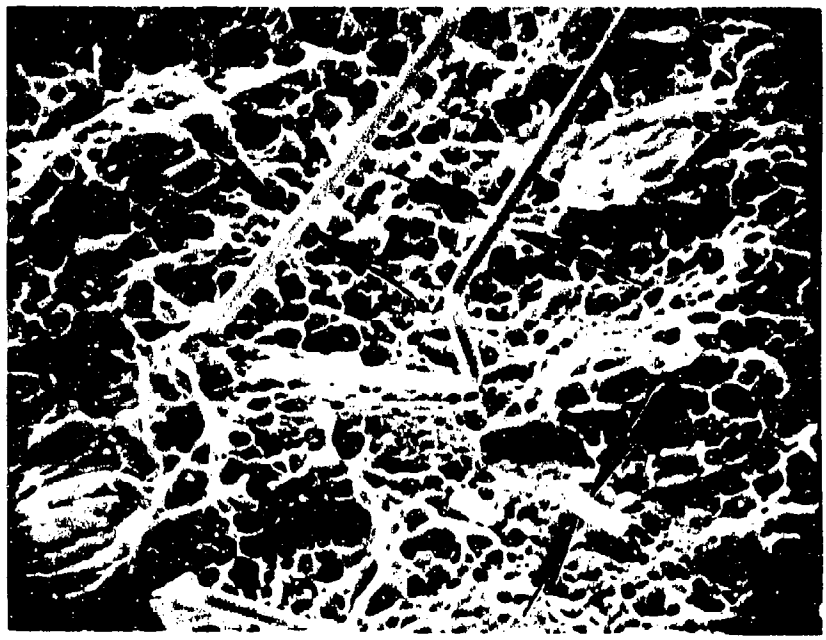

Fig. 66. Secondary Electron Photograph of Area C shown in Fig. 63

Magnification 1400X. A well developed whisker texture is observed. The width of the above whiskers is 15,000 to 18,000 Å or .00006" to .000072". Photograph was taken at 400 microns below the surface. Whiskers formed while crack was exposed to the vapors.

Fig. 67. Secondary Electron Photograph of a Whisker Located in Area C of Fig. 63

Magnification 7000X. Well developed characteristics can be noted. The size of the embryo at the upper left hand corner is approximately 700 to 1000Å radius.

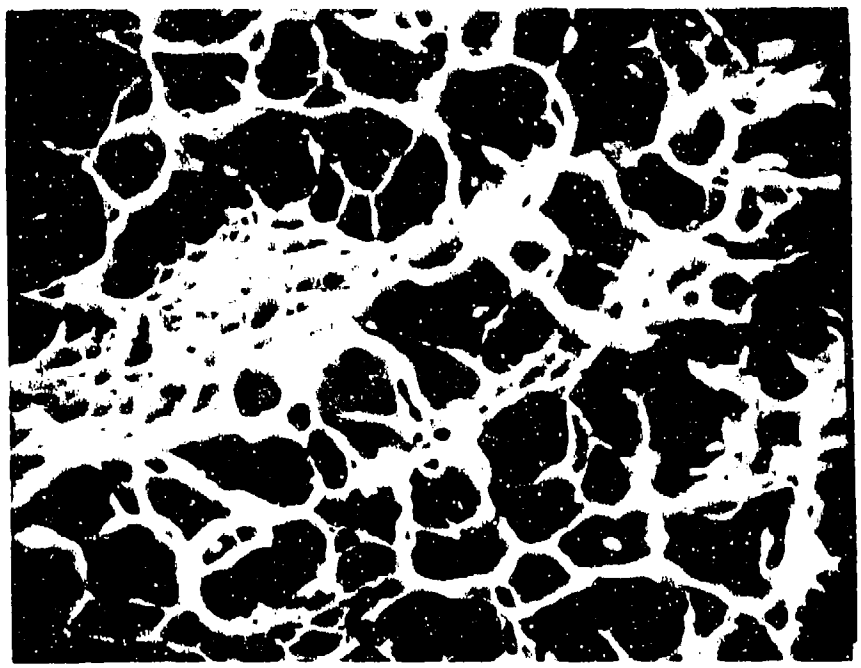

Fig. 68. Secondary Electron Photograph of Area D, Fig. 63

Magnification 2800X. Photograph taken at 600 microns below the specimen surface. A total of 14 embryo was resolved having a radius approximately 800 Å.

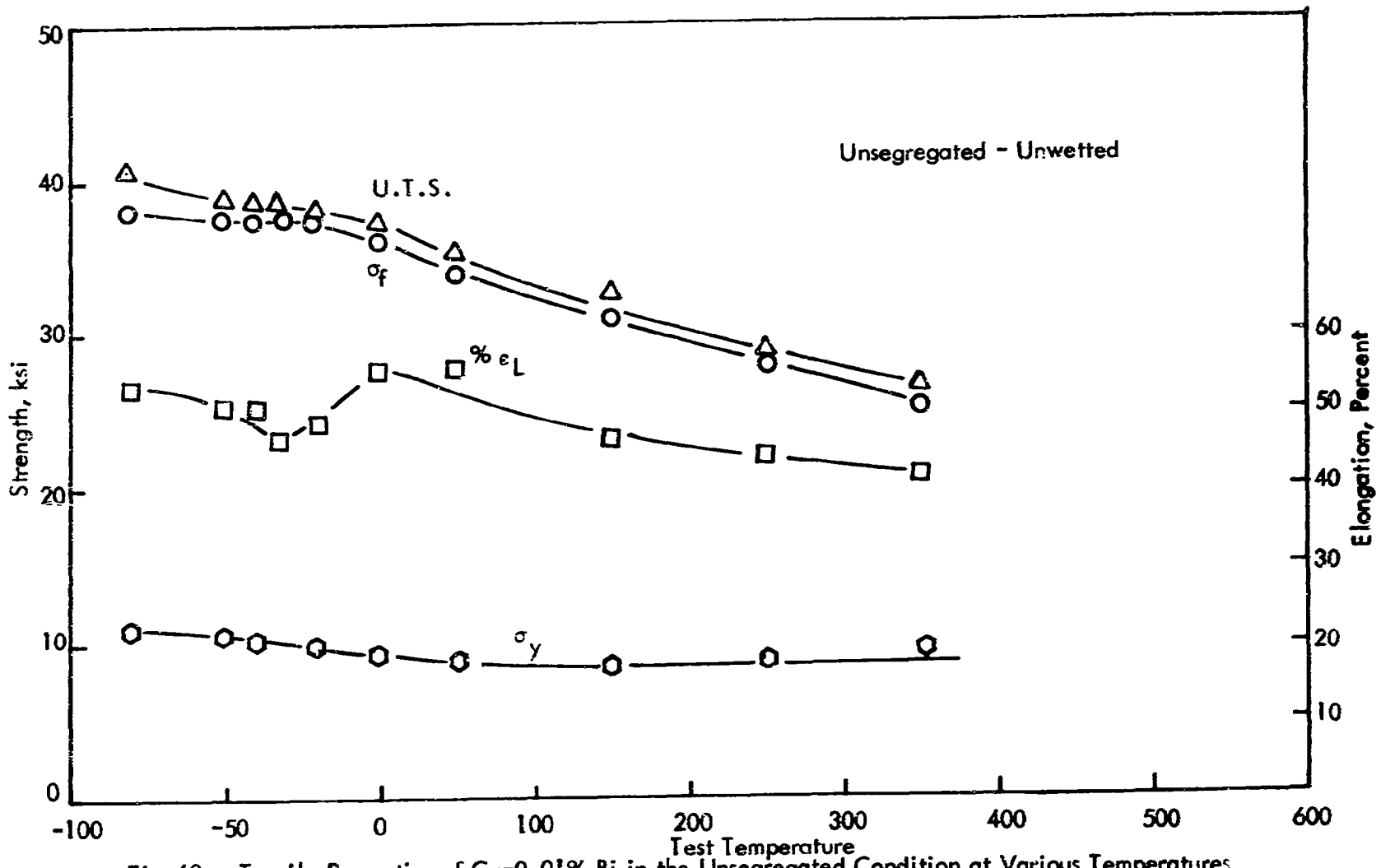

Fig.69 . Tensile Properties of Cu-0.01% Bi in the Unsegregated Condition at Various Temperatures

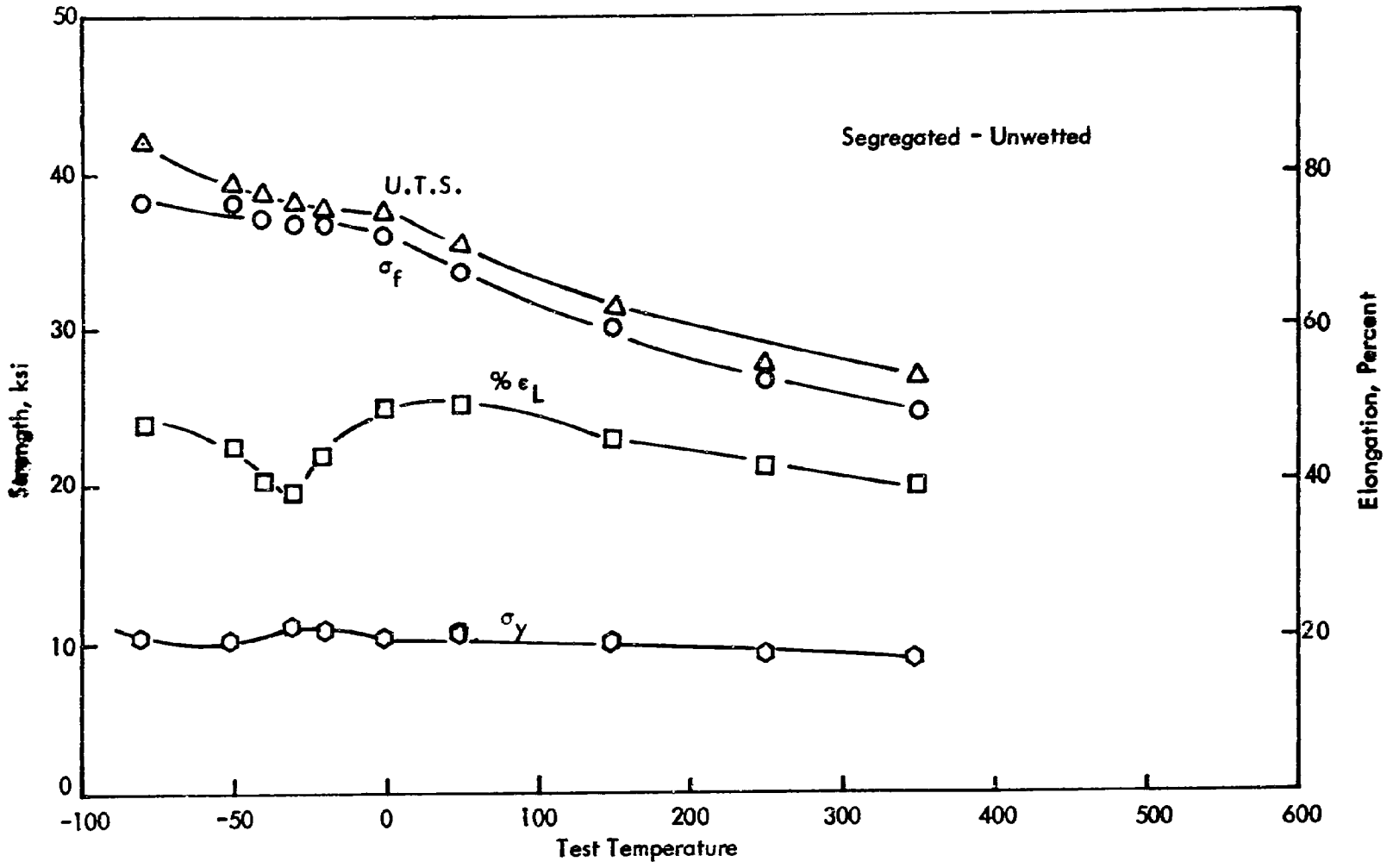

Fig. 70. Tensile Properties of Cu-0.01% Bi in the Segregated Condition at Various Temperatures

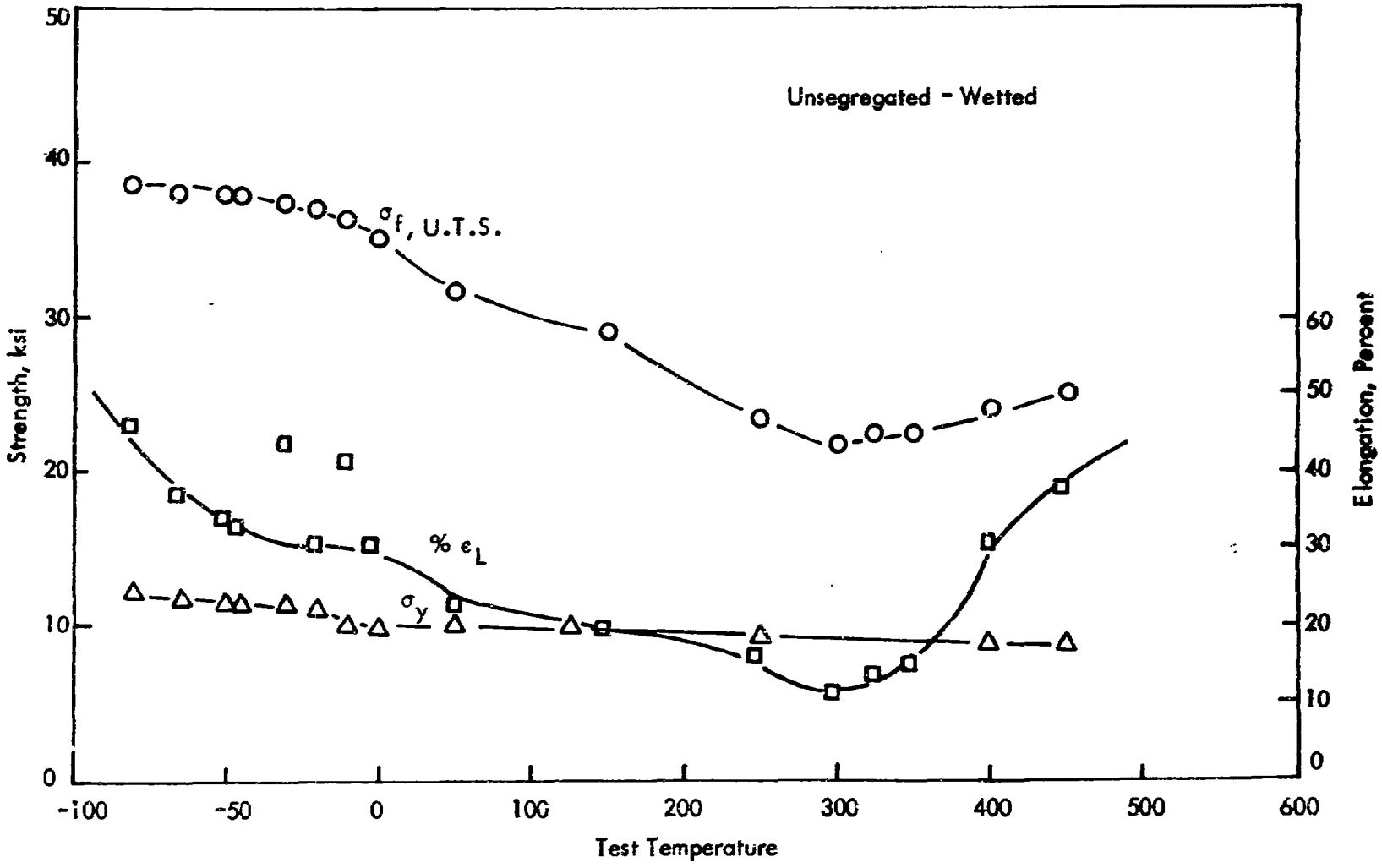

Fig. 71. Tensile Properties of Cu-0.01% Bi in the Unsegregated Condition with Mercury on the Surface at Various Temperatures

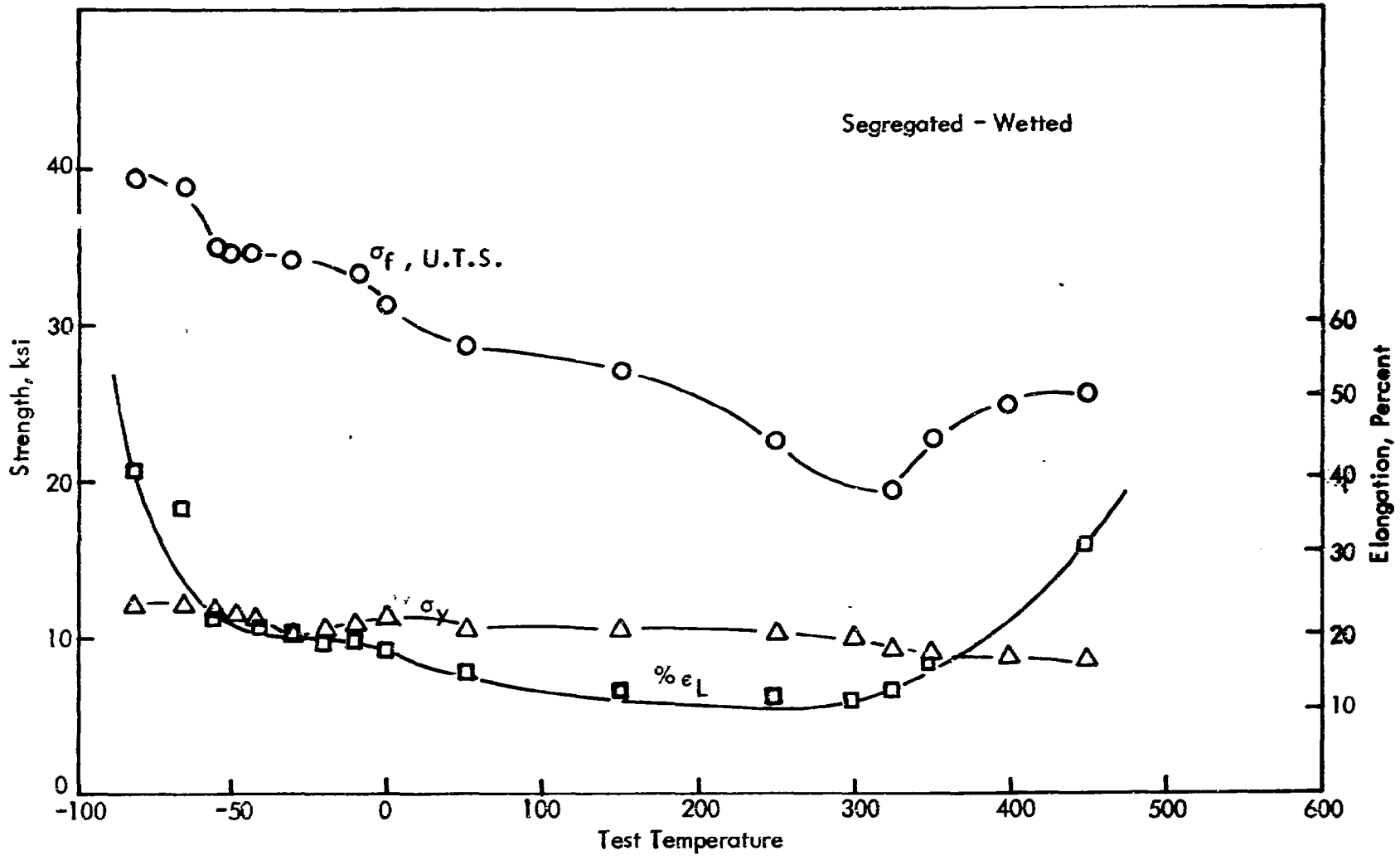

Fig. 72. Tensile Properties of Cu-0.01% Bi in the Segregated Condition with Mercury on the Surface at Various Temperatures

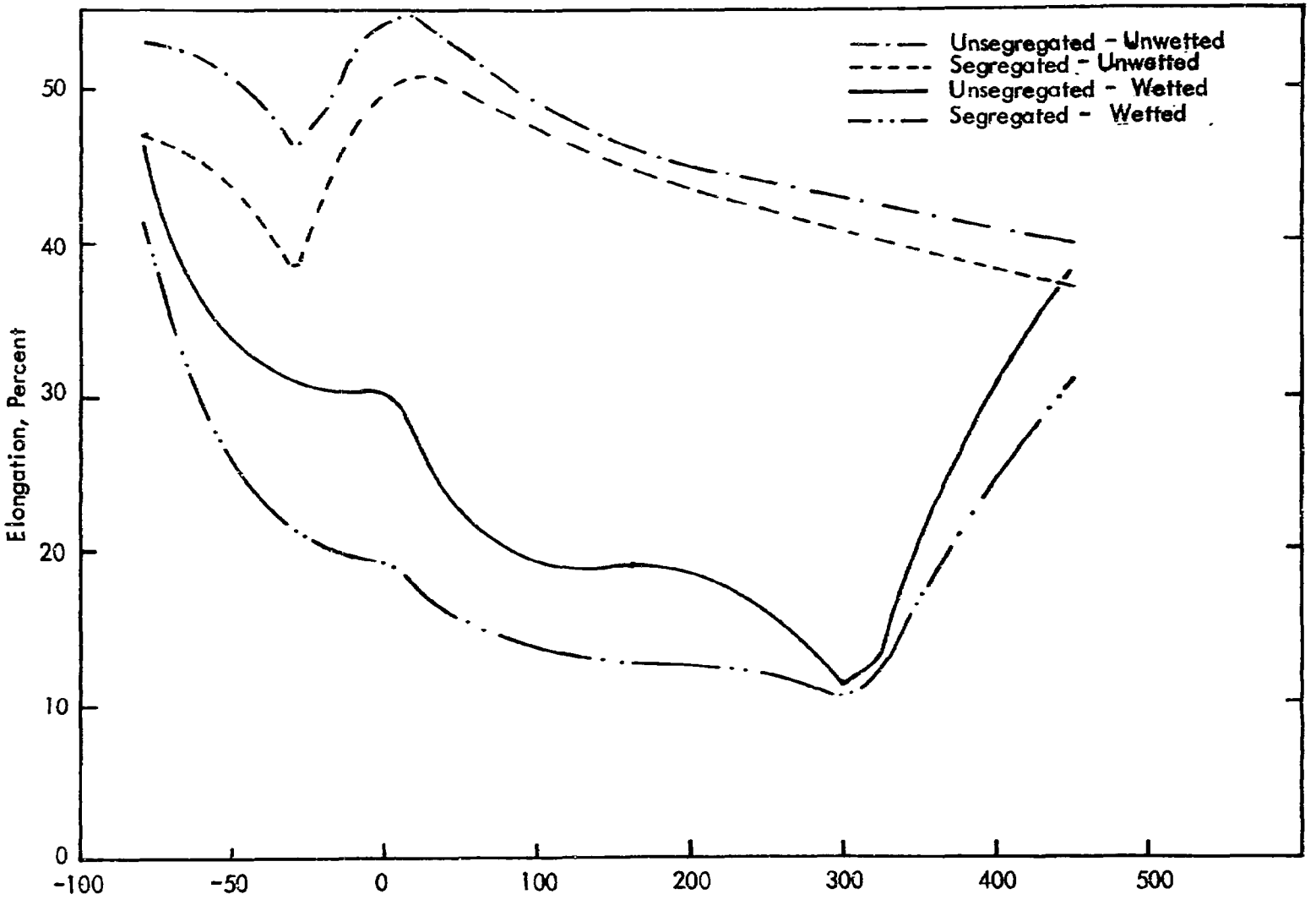

Fig. 73. Elongation vs Temperature for Cu-0.01% Bi in Segregated-Wetted, Unwetted and Unsegregated-Wetted, Unwetted Conditions

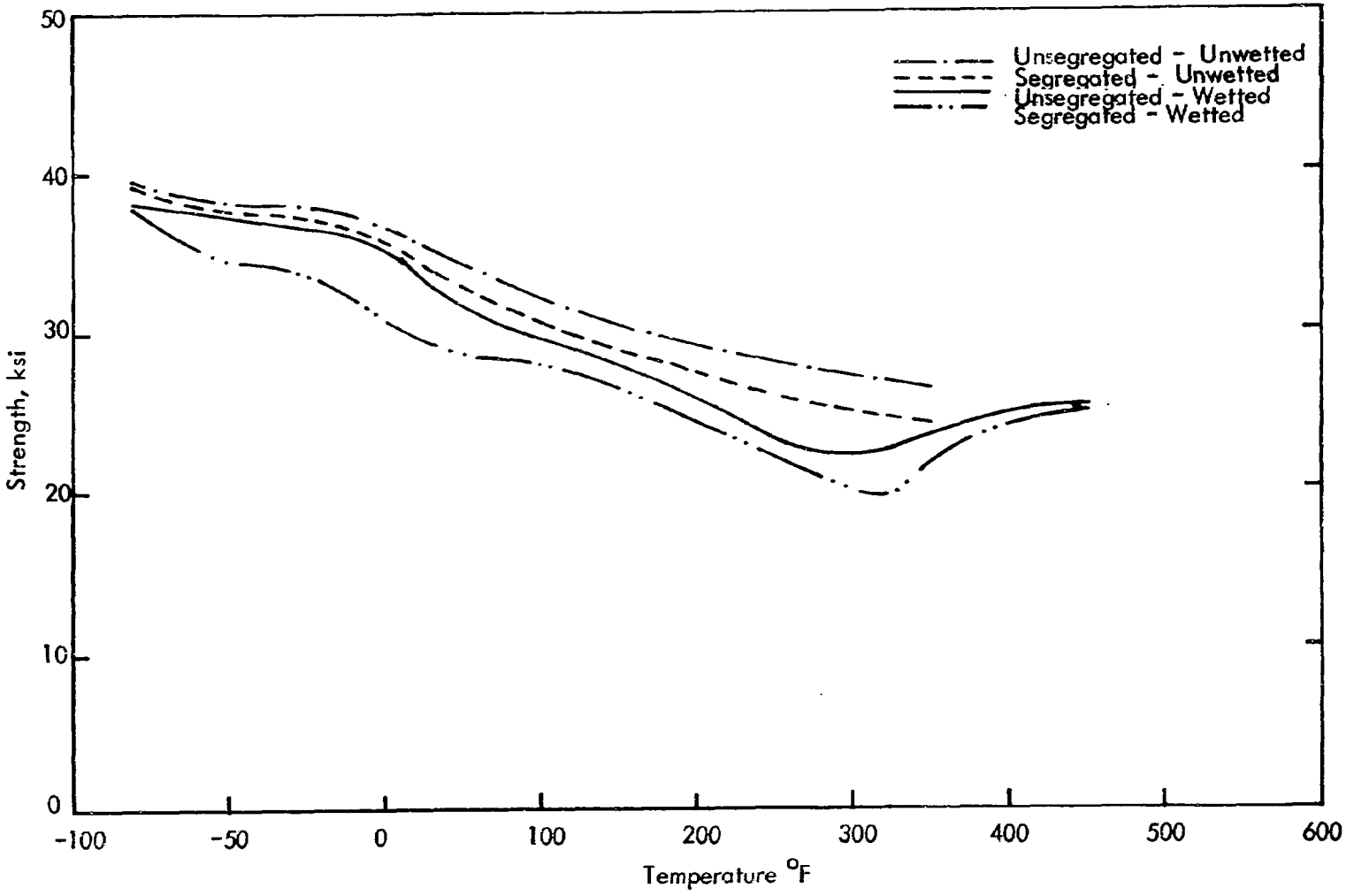

Fig. 74. Fracture Stress vs Temperature Relationship for Cu-0.01% Bi in Segregated-Wetted, Unwetted and Unsegregated-Wetted, Unwetted Conditions

Security Classification

DOCUMENT CONTROL DATA - R & D

(Security classification of title, body of abstract and indexing annotation must be entered when the overall report is classified)

1. ORIGINATING ACTIVITY (Corporate author)	2a. REPORT SECURITY CLASSIFICATION
Illinois Institute of Technology 3300 S. Federal St. Chicago, Illinois 60616	Unclassified
	2b. GROUP

3. REPORT TITLE

"ENVIRONMENTAL SENSITIVITY OF STRUCTURAL METALS: LIQUID METAL EMBRITTLEMENT"

4. DESCRIPTIVE NOTES *(Type of report and inclusive dates)*

Third Annual Technical Progress Report Period: June 1, 1971 to May 31, 1972

5. AUTHOR(S) *(First name, middle initial, last name)*

Paul Gordon, Darryl L. Albright, Earl Zwicker
Norman N. Breyer, Lawrence J. Broutman, Russell D. Larsen
James W. Dally, William R. Warke

6. REPORT DATE	7a. TOTAL NO. OF PAGES	7b. NO. OF REFS
June 1972	142	42

8a. CONTRACT OR GRANT NO.	9a. ORIGINATOR'S REPORT NUMBER(S)
DAAA25-69-C0608	55232-3ATPR
b. PROJECT NO.	
c.	9b. OTHER REPORT NO(S) *(Any other numbers that may be assigned this report)*
d.	

10. DISTRIBUTION STATEMENT

This publication or any portion thereof may not be reproduced without specific authorization from the Commanding Officer, Frankford Arsenal, ATTN: Chief Metallurgy Research Laboratory, Philadelphia, Pennsylvania 19137. However, DDC is authorized to reproduce the publication for U.S.*

11. SUPPLEMENTARY NOTES	12. SPONSORING MILITARY ACTIVITY
	U. S. Army, Frankford Arsenal Tacony and Bridge Streets Philadelphia, Pennsylvania 19137

13. ABSTRACT

This is the third annual technical progress report for the period June 1971 through May 1972 on a THEMIS research program on liquid metal embirttlement (LME). The phenomenon of LME is being investigated on levels from the atomic through bulk specimen and structural properties, and is being considered from both experimental and theoretical viewpoints. The research is aimed at elucidating the three important aspects of LME, namely, the mechanism by which embrittlement takes place at a crack, or potential crack, site, the mechanism by which the embrittling species is transported to this site, and various metallurgical, physical, and mechanical factors which have a significant influence on the severity of the embrittlement.

*10. Distribution Statement (Continued)

Government purposes. The information in this publication has not been cleared for release to the public. DDC AVAILABILITY NOTICE Qualified requestors may obtain copies of this publication directly from DDC. Foreign announcement and dissemination of this publication by DDC is limited.

14 KEY WORDS	LINK A		LINK B		LINK C	
	ROLE	WT	ROLE	WT	ROLE	WT